EFFECTS OF ENVIRONMENT ON CREEP BEHAVIOR OF NEXTEL 720/ALUMINA-MULLITE CERAMIC COMPOSITE AT 1200°C

THESIS

Christopher L. Genelin, Captain, USAF

AFIT/GAE/ENY/08-M11

DEPARTMENT OF THE AIR FORCE
AIR UNIVERSITY

AIR FORCE INSTITUTE OF TECHNOLOGY

Wright-Patterson Air Force Base, Ohio

APPROVED FOR PUBLIC RELEASE; DISTRIBUTION UNLIMITED

The views expressed in this thesis are those of the author and do not reflect the official policy or position of the United States Air Force, Department of Defense, or the United States Government.

AFIT/GAE/ENY/08-M11

EFFECTS OF ENVIRONMENT ON CREEP BEHAVIOR OF NEXTEL 720/ALUMINA-MULLITE CERAMIC COMPOSITE AT 1200°C

THESIS

Presented to the Faculty

Department of Aeronautical and Astronautical Engineering

Graduate School of Engineering and Management

Air Force Institute of Technology

Air University

Air Education and Training Command

In Partial Fulfillment of the Requirements for the

Degree of Master of Science in Aeronautical Engineering

Christopher L. Genelin, B.S.M.E

Captain, USAF

March 2008

APPROVED FOR PUBLIC RELEASE; DISTRIBUTION UNLIMITED

AFIT/GAE/ENY/08-M11

EFFECTS OF ENVIRONMENT ON CREEP BEHAVIOR OF NEXTEL 720/ALUMINA-MULLITE CERAMIC COMPOSITE AT 1200°C

Christopher L. Genelin, B.S.M.E.
Captain, USAF

Approved:

Dr. Marina B. Ruggles-Wrenn (Chairman)	3/12/08 Date
Dr. Robert Canfield (Member)	3/12/08 Date
Dr. Som Soni (Member)	3/12/08 Date

Abstract

The creep behavior of an oxide-oxide ceramic matrix composite (CMC) was investigated at 1200°C in laboratory air, in steam and in argon. The composite consisted of a porous alumina-mullite matrix reinforced with laminated, woven mullite/alumina (Nextel/720) fibers. The composite had no fiber coating and relied on its porous alumina/mullite matrix for flaw tolerance. Tensile stress-strain behavior was investigated and the tensile properties were measured at 1200°C in laboratory air. Tensile creep behavior of the CMC was examined for creep stress levels of 73, 91, 114 and 136 MPa. Creep run-out, set to 100 h, was achieved for stress levels ≤ 91 MPa in air. The presence of steam or argon accelerated the creep rates the N720/AM composite. Optical and scanning electron microscope (SEM) micrographs were used to examine fracture surfaces and to evaluate failure mechanisms. Fracture surfaces of the N720/AM composite were predominately planar. Limited areas of short fiber pull-out were observed for specimens tested at low creep stress levels in air.

Acknowledgments

I would like to thank my faculty advisor, Dr. Marina B. Ruggles-Wrenn for her direction and insight while guiding my through the thesis process. I would also like to thank Mr. Barry Paige, Chris Zickefoose and especially Sean Miller. Without their expertise in the laboratory, an experimental thesis such as this would not have been possible.

Christopher L. Genelin

Table of Contents

Page

List of Figures

List of Tables

EFFECTS OF ENVIRONMENT ON CREEP BEHAVIOR OF NEXTEL 720/ALUMINA-MULLITE CERAMIC COMPOSITE AT 1200°C

I. Introduction

A fiber-reinforced composite is a material system consisting of two or more visible phases whose mechanical performance and properties are designed to be superior to those of the constituent materials acting alone. Typically the strongest phase of the material system is referred to as the reinforcement, while the weaker phase is called the matrix. In some composites a third phase, or interphase, also exists. Each phase of the composite plays a unique role in the overall mechanical performance of the material system. In the case of high-performance structural composites, fibers bear the brunt of the loading. It follows that tensile strength and elastic modulus of the material system are a function of fiber volume fraction. While the matrix in low or medium performance composite can be designed to provide reinforcement to the overall material system, generally its purpose is limited to protecting the sensitive continuous fibers of high performance composites. The final phase, or interphase, acts as an interface between fibers and matrix. The purpose of the interphase is to enhance the stress-strain behavior of the material by hindering crack propagation from the matrix to the fiber reinforcement. Figure 1 shows a typical composite containing all three material phases [9, 5].

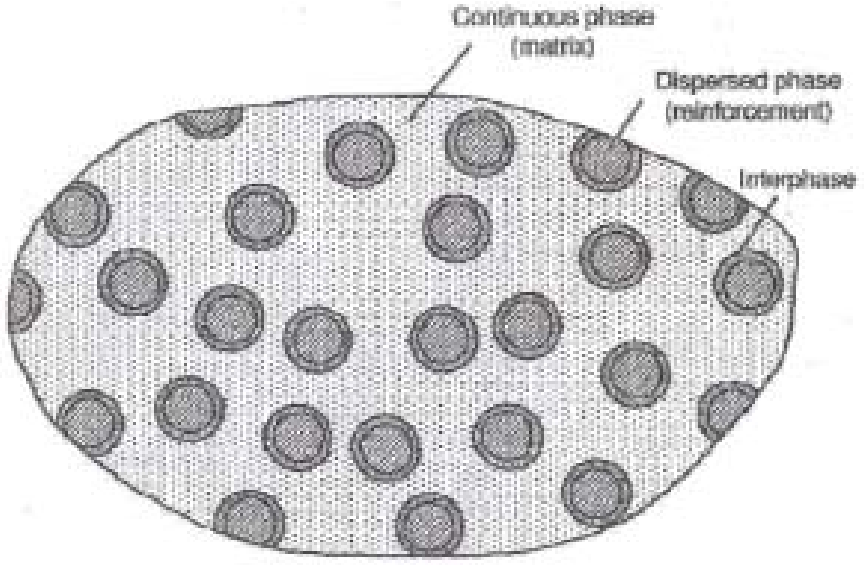

Figure 1. Three phases of a composite material system [9].

Composites have been in use for centuries wherever man needed one material with the properties of many. In modern day, nowhere is this more apparent than in the field of aeronautics where high-strength and low-weight is an ethos. Structural composites are now part of nearly all modern aircraft from wings and fuselages to engine cowlings. With increases in speed as well as advances in aerospace propulsion technologies, comes the need for materials that exhibit superior long-term mechanical properties under high pressure, high temperature and varying operational environments. To meet this requirement, engineers are now turning to high-performance structural ceramics [23].

Although resilient to the effects of high temperatures and oxidation, ceramics are often associated with brittleness and catastrophic failure. Recently, advances in the field of structural ceramics have begun to change this stereotype with the introduction of ceramic matrix composites (CMCs). Where traditional composites are strengthened by

fiber reinforcement protected by a weak matrix, both fiber and matrix in CMCs are of similar strength. By incorporating fibers into a ceramic matrix, material toughness and damage tolerance are increased and the risk of catastrophic failure is minimized [6]. Unlike monolithic ceramics, CMCs have been shown to exhibit fracture toughness five times that of their monolithic predecessors. Not only are these new composites tougher than monolithic ceramics, but they are also more tolerant to damage/cracking, and exhibit a non-catastrophic failure mode. For these reason, the importance of further research in the field of CMCs cannot be understated [5].

II. Applications and Background

2.1 Ceramic Matrix Composites

In the past few decades, the majority of research on continuous-fiber reinforced ceramic composites (CFCC) has been concentrated on a variety of SiC and Carbon based material systems. While these composites have been shown to effectively withstand the effects of high temperatures, they lack long term durability in oxidizing environments such as air and steam. To counter the persistent problem of oxidation, non-oxide composites require some form of protection, generally in the form of environmental barrier coatings. With recent advances in materials and manufacturing, focus is shifting toward oxide-oxide CMCs. As the name suggests, oxide-oxide CMCs consist of an oxide matrix and oxide fibers. Being oxides, these materials are not prone to oxidation and their mechanical properties have been shown to be unaffected by long term exposure to oxidizing environments at high temperatures [29].

Damage tolerance in continuous fiber-reinforced ceramic composites is generally achieved in one of two ways (see Figure 2). The first tolerance mechanism utilizes a fiber coating or interphase to mechanically separate the fiber reinforcement from the matrix. The weak interface between fiber and matrix allows cracks to propagate through the matrix, but around the fibers. Downsides of this approach include a relative short supply of the fiber coating materials themselves as well as the complexity of producing coated fibers. The second approach involves the use of a porous matrix with low fracture toughness to achieve the same effect. While porous matrix composites may be easier and

hence less costly to manufacture, they do pose unique challenges. Unlike CMCs that utilize fiber coatings for damage tolerance, the porous matrix composites must have a matrix that is weak enough to deflect cracking around the fiber reinforcement but strong enough to resist off-axis loading. This porosity optimization problem has resulted in numerous composites with a variety of matrix materials [31].

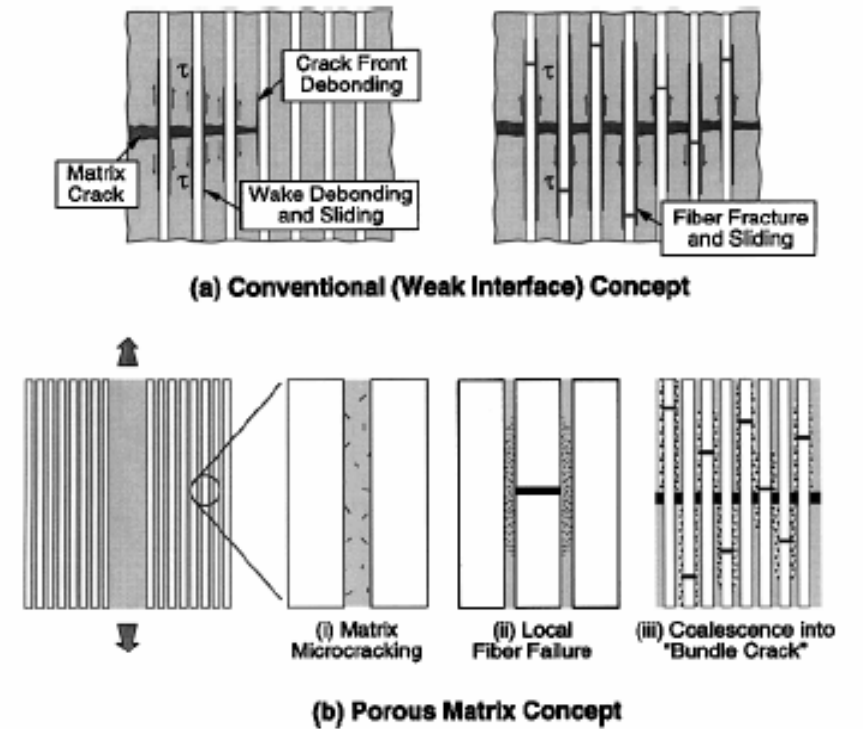

Figure 2. Common CMC damage tolerance mechanisms: (A) Weak fiber/matrix interface and (B) Porous matrix [31].

2.2 Applications

Although advances have been made to increase the high temperature performance of metallic super alloys, their cost is high and their resistance to the effects of environment is poor. In recent years, ceramic matrix composites have begun to attract the interest of the technical community. More specifically, oxide-oxide ceramics have

become of great interest not only for their long-term high-temperature performance, but also their inherent resistance to oxidizing environments [19].

Nowhere is the need for high-strength, high-temperature oxidization resistant materials more apparent than in the field of aerospace propulsion. Ceramic matrix composites are ideal candidate materials for components in turbine engines such as combustor walls where structural materials are required to withstand the effects of high temperature, pressure and moisture. By using CMCs in such applications, engine performance can be enhanced by a reduced need for cooling air and an overall reduction in weight when compared to engines utilizing metallic super alloys. Not only can high strength/low weight CMCs reduce engine weight, but they can also result in a much lower cost/weight aircraft. Many modern aircraft such as the F-22 have aft fuselages constructed almost entirely of titanium as temperatures around the engines exceed operational temperatures of aircraft aluminum and most conventional aircraft composites. Although the high-speed XB-70 was constructed entirely of temperature resistant stainless steel, it too required a complex system of cooling air around its six engines (see Figure 3) [21]. Research efforts on smaller combustors designed to operate at higher temperatures have expedited the need for advances in the field of CMCs and cemented their use in such future applications [16, 20].

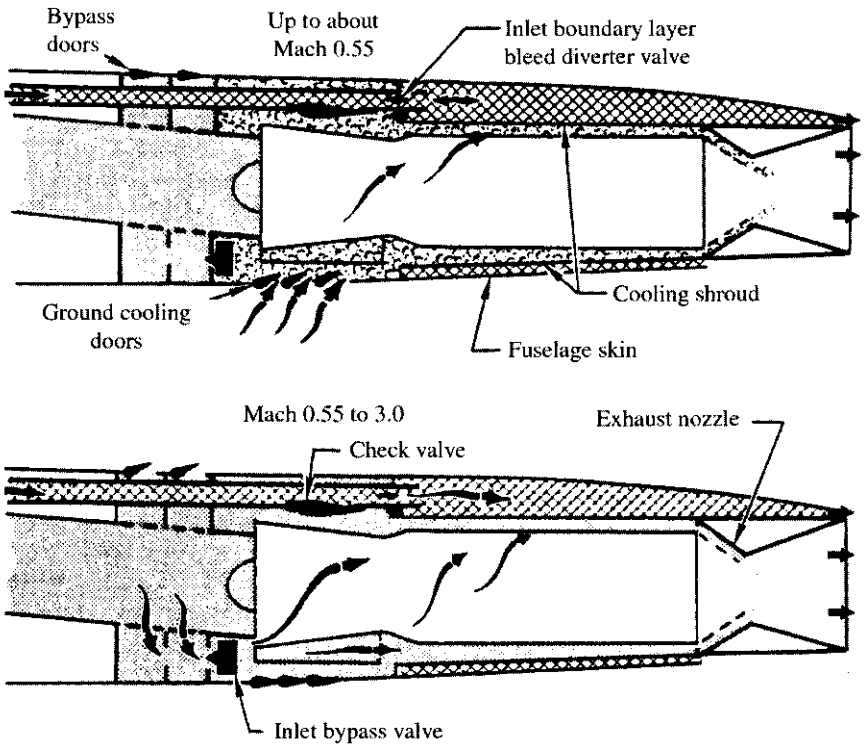

Figure 3. Cooling provisions needed for XB-70 without the use of CMCs [21].

2.3 Previous Research Efforts

Previous research efforts on ceramic matrix composites at AFIT focused largely on the N720/Alumina composite. The material consisted of Nextel 720 mullite-alumina fibers and relied on a porous alumina matrix for damage tolerance. Harlan [13] studied the creep-rupture behavior of the composite with 0/90° fiber orientation in both air and steam environments at 1200 and 1330°C. The results showed that while the material performed well during creep testing in air, creep performance in steam was severely degraded. Creep performance at 1330°C was poor in air and was further degraded by the presence of steam.

Braun [3] investigated the creep behavior of the N720/A composite in the 1000-1200°C range in laboratory air and in steam at creep stresses from 80-150 MPa. Braun found that creep rates increased with increasing temperature and creep stress. The presence of steam accelerated creep rates and significantly reduced creep life. This degradation increased with increasing temperatures. At 1000°, all specimens achieved creep run-out, defined as 100 h at creep stress. At 1100°C, all tests in air, but only the 100 MPa test in steam achieved creep run-out. Creep run-out was achieved only in the 80 MPa test in air at 1200°C. At 1000 and 1100°C, all creep strains accumulated in air were lower than failure strains obtained in tension tests. While at 1200°C, creep strains accumulated in air far exceeded failure strains obtained in tension tests [4].

Braun observed a clear correlation between the appearance of fracture surfaces and test temperature and environment. Specimens tested in steam had much flatter fracture surfaces and shorter damage zones than samples tested in air at the same temperature. Variations in temperature also affected the fracture surface appearance. Fracture surface obtained at lower temperatures exhibited more fiber pull-out than the fracture surfaces obtained at higher temperatures. Braun found longer creep lifetimes went along with brushy failure, extensive pull-out and longer damage zones. It was concluded that higher temperatures caused additional matrix sintering and decreased matrix porosity which in turn resulted in a less damage tolerant composite.

Siegert [25] studied the creep behavior of the N720/A composite, with ± 45° fiber orientation at 1200°C in air and steam, as well as argon, a non-oxidizing environment. Siegert's results showed that specimens tested in air produced lower creep rates than specimens tested at the same stress levels in argon and steam. Specimens tested in argon

had higher creep rates than in steam, but exhibited creep lifetimes similar to those obtained in steam.

2.4 The N720/AM Ceramic Matrix Composite

A new variant of the N720-based ceramic was studied in the current research effort. The N720/AM composite is a continuous fiber oxide-oxide ceramic matrix composite consisting of Nextel 720 mullite-alumina fibers and a porous alumina-mullite matrix with no fiber coating. The composite relies on the porous matrix for crack deflection and damage tolerance.

The Nextel 720 fiber is produced by Minnesota Mining and Manufacturing (3M) for use in high temperature composites. The two phase mullite-alumina fiber was designed to operate at temperatures in excess of 1100°C. The Nextel 720 fiber offers a reduction in creep rate by three orders of magnitude when compared to its predecessor, the Nextel 610 single alumina phase fiber. The fiber is manufactured using a sol-gel process and has a diameter of 12.5 μm. The fiber is made up of 85% Al_2O_3 and 15% SiO_2 by weight, has a single filament tensile strength of 2100 MPa and a Young's modulus of 260 GPa. Comprised of oxides, the Nextel 720 fibers have also been shown to be resistant to the effects of environment. Previous research also showed that the fibers exhibit brittle failure [10].

Previous research has shown that additional matrix sintering and loss of matrix porosity is among the main causes of performance degradation for porous matrix composites. Because of its slow sintering kinetics at temperatures up to 1300°C and excellent creep resistance, mullite was added to the matrix of the N720/AM composite as

a means of limiting shrinkage associated with the sintering of a pure alumina matrix [12, 17]. The low fracture toughness and elastic modulus make mullite ideal for crack deflection in a porous matrix, but these same properties hinder its effectiveness against shear, off-axis and compressive loading. As a result, a mixture of both alumina and mullite create a more operationally capable matrix [30].

Optical and scanning electron micrographs of the N720/AM composite tested during this research effort can be seen in Figures 4 and 5. The material was manufactured by Composite Optics Incorporated (COI) Ceramics, a division of Alliant Techsystems, in San Diego, CA. The composite consists of 12 Nextel 720 0°/90° woven layers in a mullite-alumina matrix. Physical properties of the composite tested over the course of this research were provided by COI and can be seen in Table 1. The volume percent of mullite in the matrix did not exceed 13%.

Table 1. Physical properties of the N720/AM CMC provided by COI.

Panel #	Thickness (mm)	Fabric (% Volume)	Matrix (% Volume)	Porosity (% Volume)	Density (g/cc)
7693-2	3.2	40.4	32.8	26.8	2.63

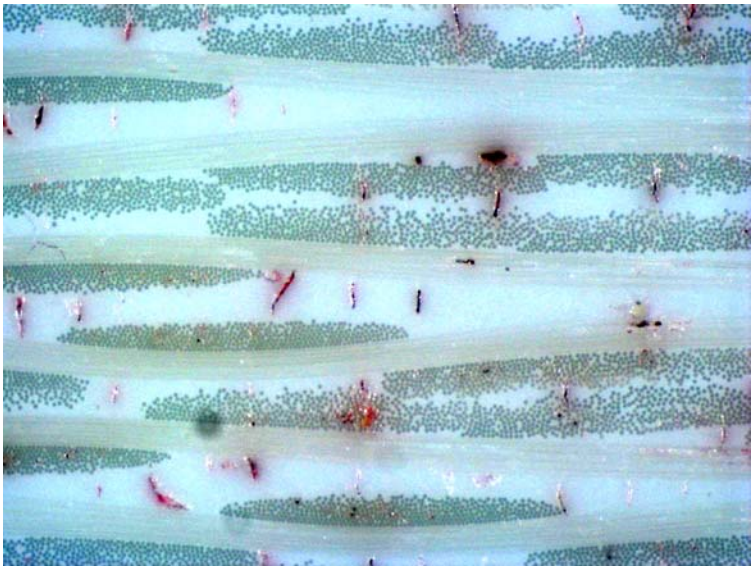

Figure 4. Optical micrograph of virgin N720/AM composite showing matrix rich areas and microcracking.

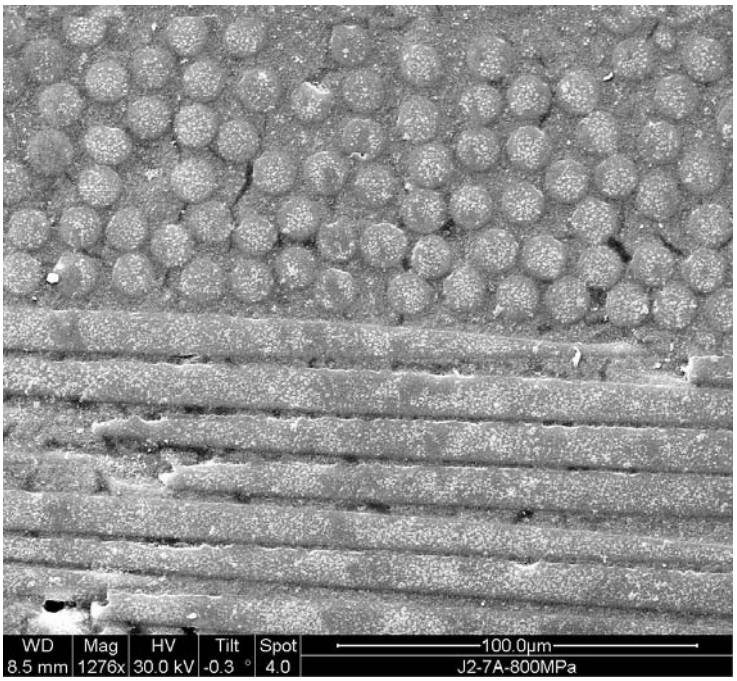

Figure 5. SEM micrograph of virgin N720/AM composite showing 0° and 90° fibers.

Figures 4 and 5 reveal numerous micro-cracks in the matrix of the composite. These cracks are a result of differences in thermal expansion coefficient of the fibers and are not a result of testing. The presence of matrix microcracks in an untested material is typical for porous matrix CMCs. The micrographs in Figures 4 and 5 also show good matrix infiltration between fibers as well as matrix rich areas between fiber tows.

2.5 Thesis Objective

The objective of this research was to assess the creep-rupture behavior of the Nextel 720/AM ceramic matrix composite at 1200°C in laboratory air, argon and steam. Multiple tests were conducted in all three environments at various levels of creep stress. The data obtained for the N720/AM composite are compared to the results for the N720/A CMC from previous work. As a result, the efficiency of adding mullite to the matrix in this material system can be assessed.

III. Experimental Setup

3.1 Specimen Preparation

The Nextel720/Alumina-Mulite specimens used for this research were cut from a 12 x 12 inch panel by the AFIT machine shop using a high pressure waterjet. To prevent edge fraying, the panel was sandwiched between two thin aluminum sheets with double sided adhesive tape. Average thickness of the panel was 3.2 mm. Standard dogbone-shaped specimens were used in all tests. Specimen geometry is shown in Figure 6.

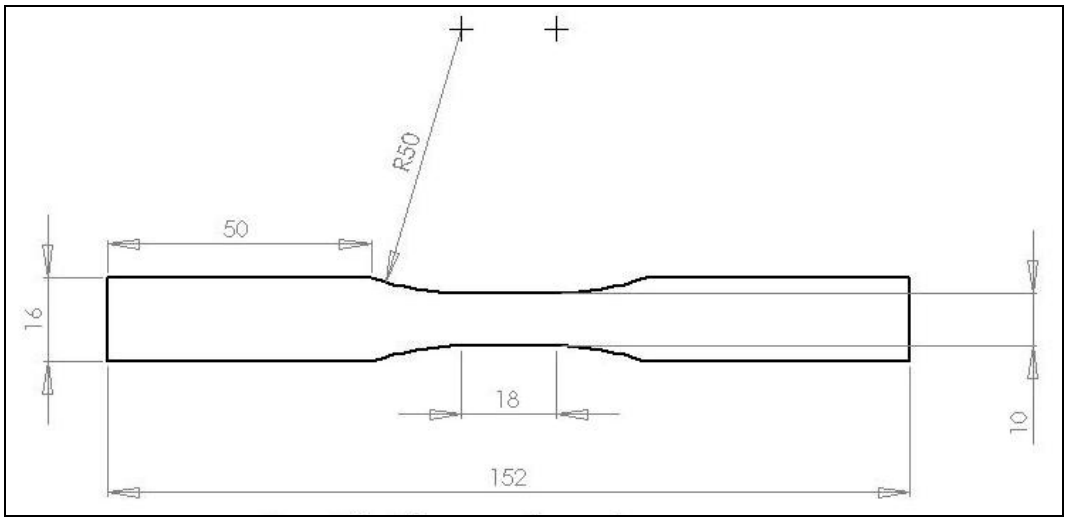

Figure 6. Test Specimen, dimensions in mm.

After machining, the specimens were cleaned to remove any debris created during the cutting process. The specimens were first rinsed with alcohol, and then placed in an ultrasonic cleaner for 15 min. Once removed from the ultrasonic bath, the specimens were soaked in alcohol for 20 min and finally dried in an oven for 1 h at 250°C.

The last step in preparing the specimens for testing was to attach fiberglass tabs to the gripping sections. The purpose of the tabs was to protect the specimen against possible surface cracks caused by the grips of the testing machine. The tabs were attached to the specimens using M-Bond 200 adhesive. A specimen with tabs can be seen in Figure 7.

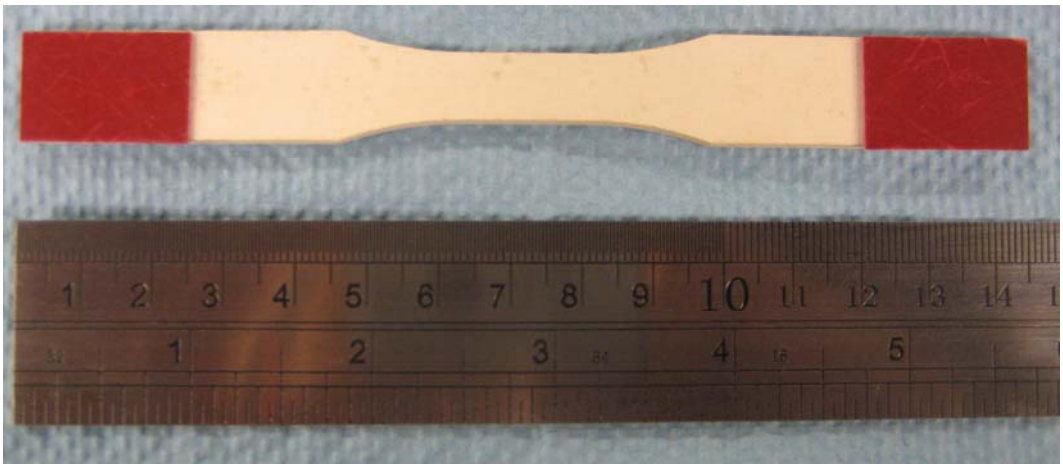

Figure 7. N720/AM tensile specimen with tabs.

3.2 Mechanical Testing Equipment

Two different MTS Corporation model 810 servo-hydraulic testing machines were used to carry out mechanical testing for this research. The first machine, intended for testing in laboratory air and steam, had a load cell of 5.5 kip (25 kN) capacity. The machine was equipped with MTS 647 hydraulic wedge grips. Surfalloy was applied to gripping surfaces to prevent the specimen from slipping. Grip pressure of 8 MPa was used in all tests conducted on the 5 kip machine. The grips were water cooled by a NESLAB model HX-75 chiller. The cooling water temperature was set to 15°C. An MTS Teststar II digital controller was used for input signal generation and data acquisition. The MTS Multipurpose Testware (MPT) software allowed for the

programming of automated test routines and data collection. In order to run concurrent tests, a second MTS machine was set up for testing in argon.

The second MTS machine had a load cell of 22 kip (98 kN) capacity, and also was equipped with MTS 647 water-cooled hydraulic wedge grips. However the grips used on the 22 kip machine were much larger than those on the 5 kip machine (see Figure 8). Therefore the grip pressure was reduced to 2.5 MPa. The grips were cooled by a NESLAB RTE7 water chiller with water temperature set to 15°C. The 5 kip and 22 kip mechanical testing stations can be seen in Figures 9 and 10, respectively.

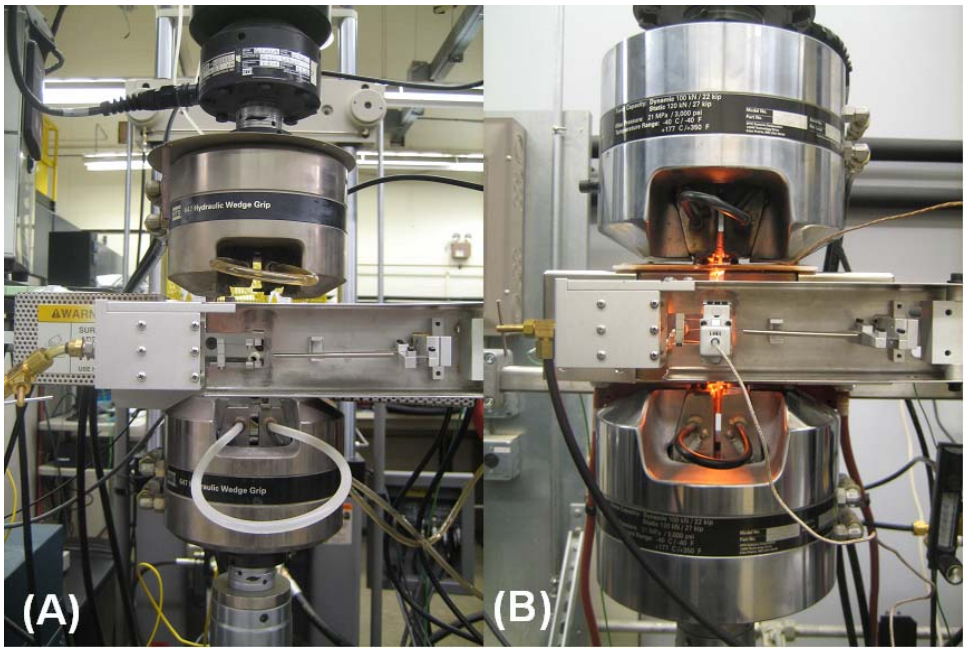

Figure 8. MTS mechanical testing machines: (a) 5 kip and (b) 22 kip.

Figure 9. 5 kip mechanical testing station.

Figure 10. 22 kip mechanical testing station.

Strain was measured using high temperature low contact force extensometers manufactured by MTS with a gauge section of 12.7 mm. The extensometer set-up incorporated a heat shield and air cooling system which protected the extensometer from the high temperatures required for this research. The extensometer was calibrated to measure tensile strains up to 20% (see Figure 11).

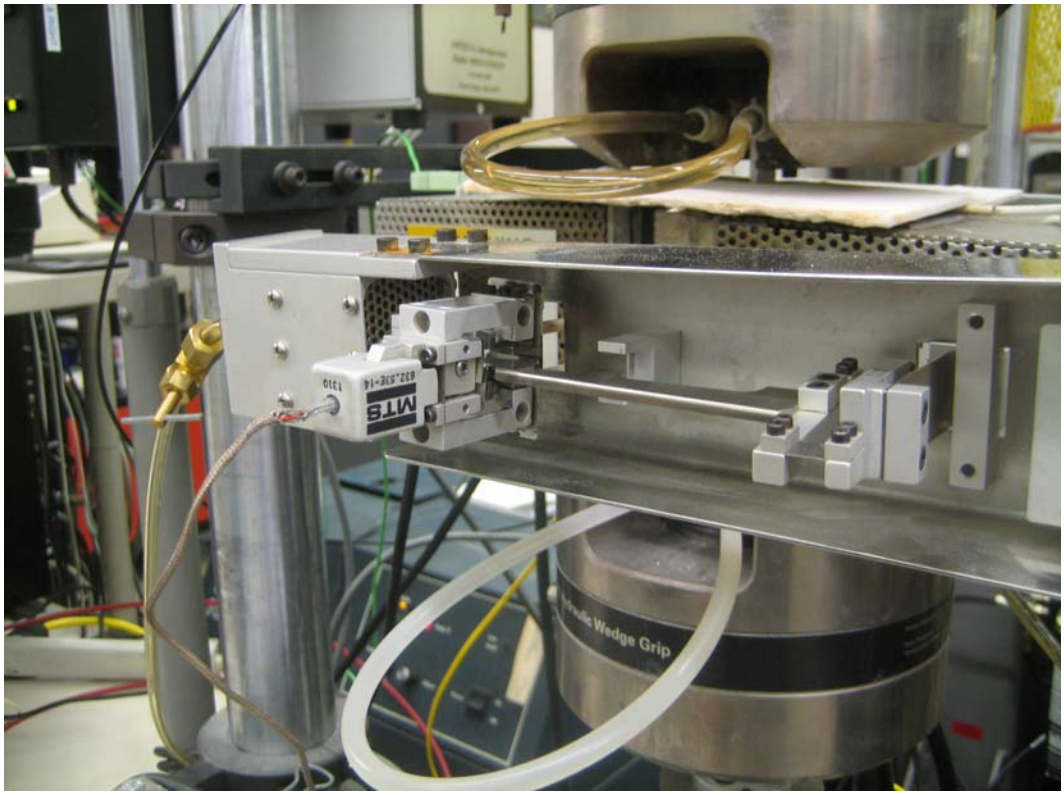

Figure 11. Extensometer platform with heat shield and cooling air.

3.3 Environmental Controls

To maintain a testing temperature of 1200°C, the 5 kip machine was equipped with a two zone Amteco Hot Rail Furnace System. The 22 kip machine was equipped with a two zone MTS 653 High Temperature Furnace. Each furnace contained two heating elements per zone and was internally insulated with alumina. The insulation was customized to allow the oven to close around the specimen without interference. A small hole was made in the back of the insulation to allow for gas feeding tubes and a slot was cut in the front for the extensometer rods. These openings were kept as small as possible in order to avoid heat loss, yet large enough not to interfere with mechanical testing (see Figure 12). To provide additional shielding to the upper grips, a clamshell of ceramic board insulation was fabricated to wrap around the top of the specimen and was placed

on top of the furnaces (see Figure 13). The furnaces were controlled using MTS 409 Temperature Controllers. Two non-contact internal R-type thermocouples provided feedback to the controller which needed to maintain the desired temperature of the test specimen.

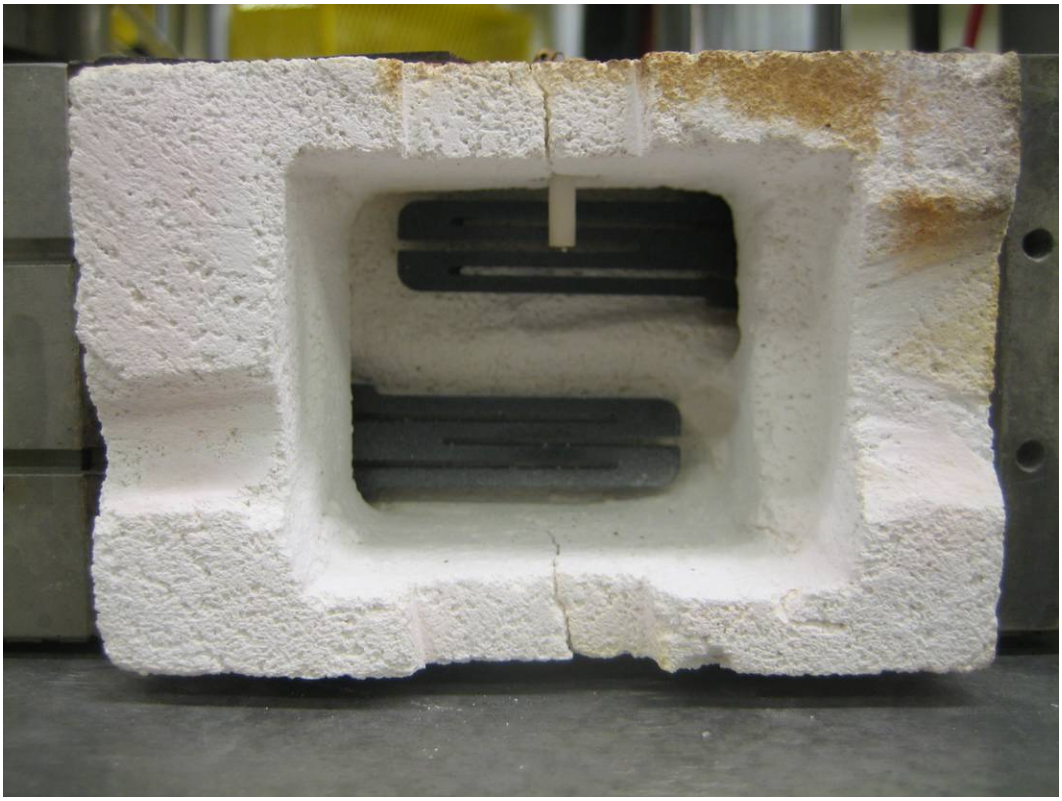

Figure 12. Interior view of modified furnace insulation where heating elements and control thermocouple are visible.

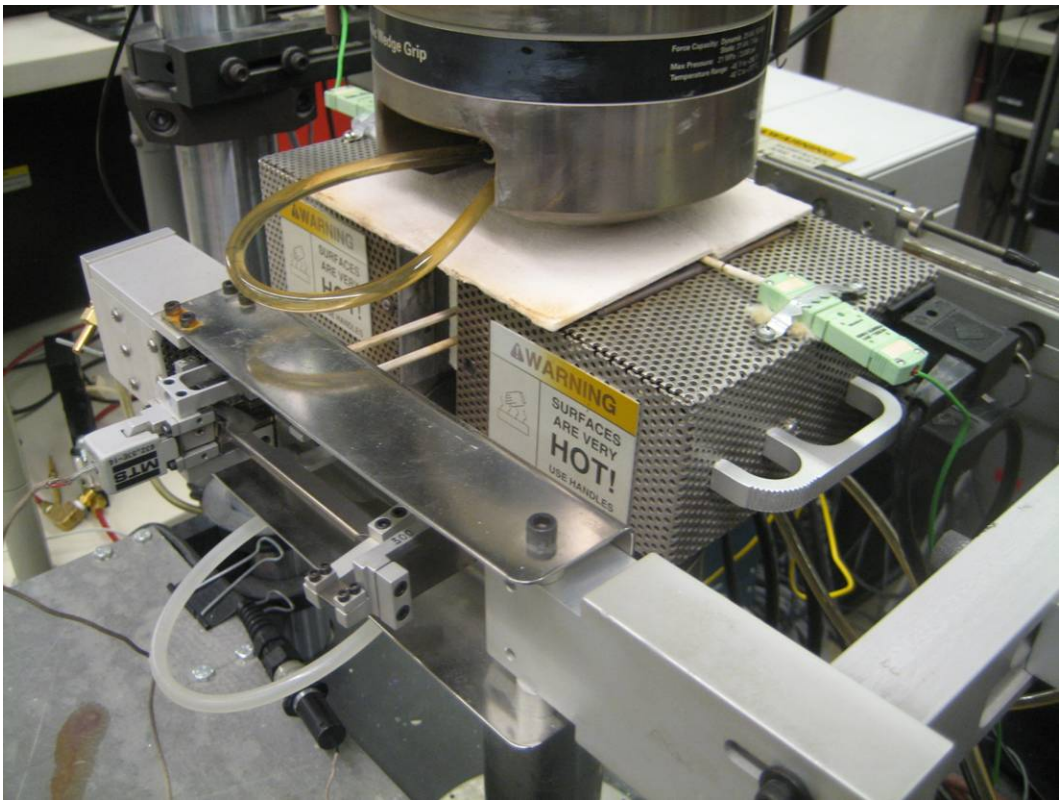

Figure 13. Protective clamshell insulation on the 5 kip machine.

An alumina susceptor was employed for testing in both argon and steam environments. The steam was generated by an AMTECO HRFS-STMGEN steam generation system using deionized water. The steam was pumped through a feeding tube into the back of the susceptor at approximately 30 mL/h. Temperature control on the steam generator was set to 300°F. Testing in argon also required the use of the susceptor. In this case high purity argon was pumped into the susceptor. Flow was regulated using an Omega Mass Flow Controller set to 41 mL/hr. This flow rate ensured all air would be evacuated from the susceptor creating a near 100% argon environment around the gauge section of the specimen. The specimen with a susceptor and gas feeding tube can be seen in Figure 14.

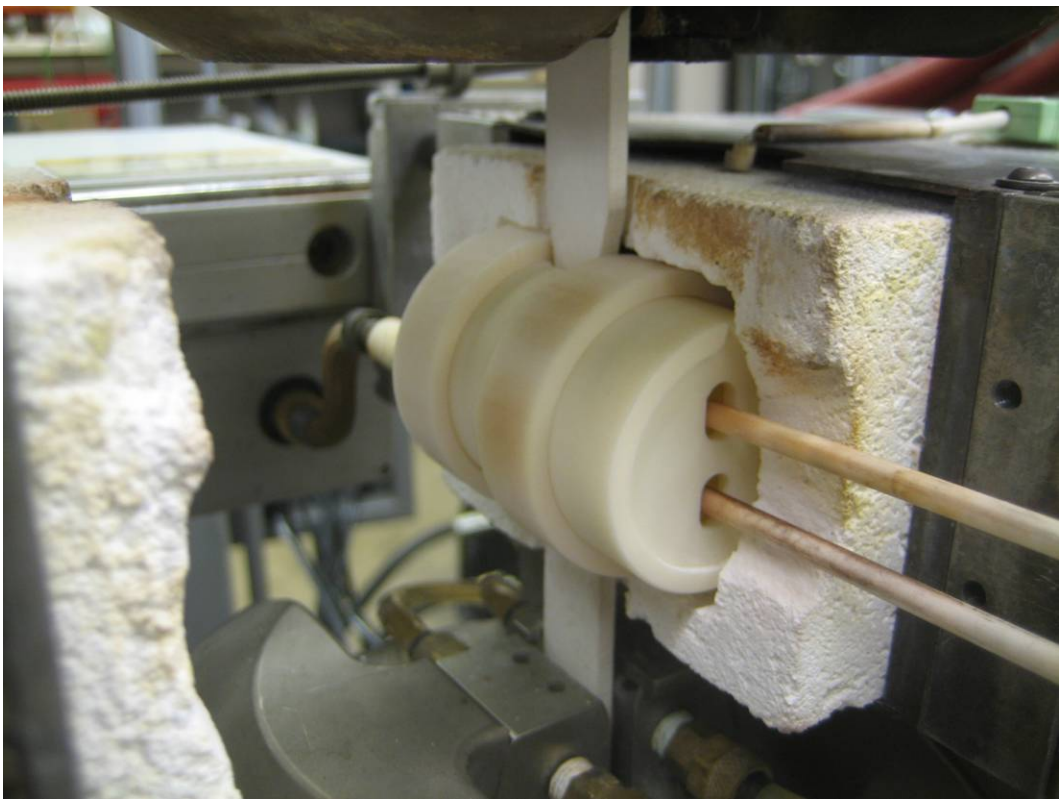

Figure 14. Alumina susceptor and steam feeding tube on the 5 kip machine.

3.4 Microstructural Characterization

After the completion of mechanical testing, fracture surfaces were examined using both an optical microscope and a scanning electron microscope (SEM). A Zeiss Stemi SV II optical microscope equipped with a Zeiss AxioCam HRc digital camera and Axiovision version 4.4 software (see Figure 15) was employed. The specimens were also examined using an FEI Quanta 200 SEM shown in Figure 16.

Figure 15. Zeiss Stemi SV II optical microscope.

The N720/AM CMC is a non-conductive material. Therefore in order to view the fracture surfaces of the samples under the SEM, they were first coated with a thin layer of carbon using an SPI-Module Sputter Coater. Micrographs were taken at several different magnifications in order to examine the details of microstructure and fracture surfaces.

Figure 16. FEI Quanta 200 Scanning Electron Microscope.

3.5 Test Procedures

3.5.1 Preparation of Mechanical Testing Equipment.

Prior to mechanical testing, the servo-hydraulic testing machine was warmed up to ensure the hydraulic fluid was at operating temperature. The MTS function generator was used to cycle the actuator in displacement control for a minimum of 30 min. The actuator was positioned a location operationally representative of testing height. Per the manufacturer's recommendation, the function generator was programmed to deliver a cyclic command in displacement control using a square waveform at a frequency of 3 Hz and amplitude of .002 inches. As the machine was warming up, the cooling water chiller for the grips was turned on and its temperature set to 15°C. Cooling air for the extensometer was also turned on.

3.5.2 Temperature Calibration

All tests were conducted at 1200°C. To calibrate the furnace controllers, a sample was instrumented with two R-type thermocouples. The thermocouples were attached to the specimen by sandwiching them between the specimen and scrap pieces of N720/A on each side. The assembly was then wired together with piano wire to secure the thermocouples in place. This instrumented sample could then be placed in the MTS machine in order to calibrate the ovens to achieve specimen temperature of 1200°C (see Figure 17).

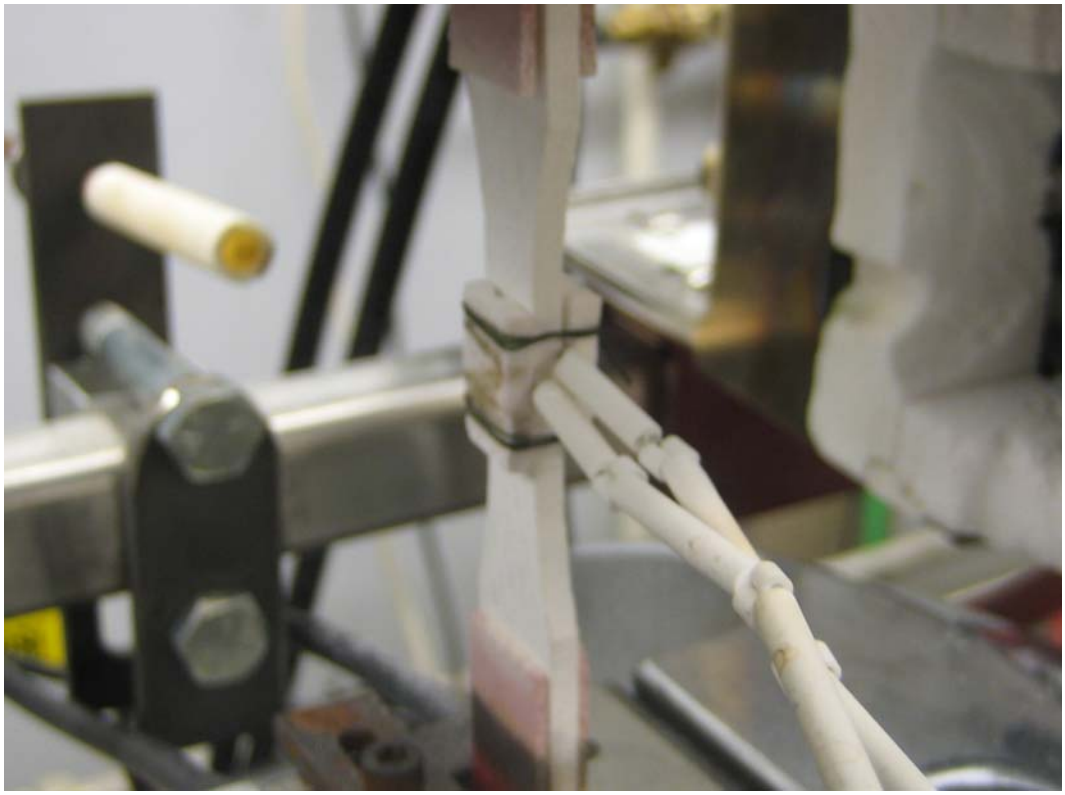

Figure 17. Test specimen instrumented with thermocouples.

The sample was first placed in the top grip and gripped under displacement control. The force on the load cell was zeroed and control mode was switched to force before the bottom of the specimen was gripped. The ovens were then closed around the sample with the thermocouples protruding through a small hole in the front of the oven. Finally, the clamshell of ceramic sheet insulation was placed around the specimen on top of the oven to provide additional shielding to the grips. The temperature was then raised to 1000°C at a rate of 1°C/s. At this point, the thermocouple temperature readings were closely monitored while the oven temperatures were manually increased to achieve the desired temperature of the test specimen.

After both thermocouples were within ±5°C of the desired temperature of the test specimen, the oven temperatures were held constant for 2 h to ensure they could maintain the 1200°C on the specimen. This procedure was repeated after every oven element replacement to ensure the temperature of the test specimen was consistently at 1200°C.

3.5.3 Monotonic Tensile Test.

Four monotonic tensile tests to failure were conducted for this research. These tests were carried out at 1200°C in laboratory air. The first two tests were conducted on the 5 kip machine.

The specimens were heated under zero load from room temperature to 1200°C at 1°C/s and held at 1200°C for 20 minutes. During testing, load, strain, displacement, oven temperature and time were measured and recorded every second. After the 20 minutes of dwell time, the sample was loaded in displacement control at a constant rate of 0.05mm/s until failure. For this portion of the tensile test, data was recorded every 0.01 s. The remaining two tests were conducted on the 22 kip machine using the same procedure.

3.5.4 Creep Test.

Creep tests were conducted at 1200°C in air, steam and argon environments at four different stress levels. A test matrix is presented in Table 2.

Table 2. Summary of creep tests conducted at 1200°C.

Specimen #	Test Environment	Creep Stress (MPa)
1	Air	73
2	Air	91
3	Air	114
4	Air	136
5	Argon	73
6	Argon	91
7	Argon	114
8	Argon	136
9	Steam	73
10	Steam	91
11	Steam	114
12	Steam	136

Creep tests were conducted in load control. Specimens were loaded to creep stress at the rate of 15 MPa/s. During load up to creep stress, data was recorded every 0.01 s. After the desired stress level was reached, the data acquisition rate was decreased exponentially from 1200 Hz for the first 5 minutes to 0.5 Hz for the remainder of the test. Creep run-out stress was set to 100 h. If the specimen achieved a run-out, the load was ramped down to zero at 15 MPa/s. A tensile test to failure was then conducted at 1200°C to measure retained properties. As in the case of the monotonic tensile test, the test for retained properties was conducted under displacement control at a rate of 0.05 mm/s. In the event of specimen failure, the computer was programmed to stop the test, shut off hydraulic power, shut down the ovens and stop recording data.

Creep tests in argon and steam employed similar procedures, but with the addition of an alumina susceptor. Argon and steam were pumped through a feeding tube into the

back of the susceptor at a rate of 30 mL/minute in the case of steam and at 40 mL/minute in the case of argon expelling the dry air from the susceptor and creating a near 100% steam or a near 100% argon environment inside the susceptor. An example of a typical creep test procedure is shown in Figure 18.

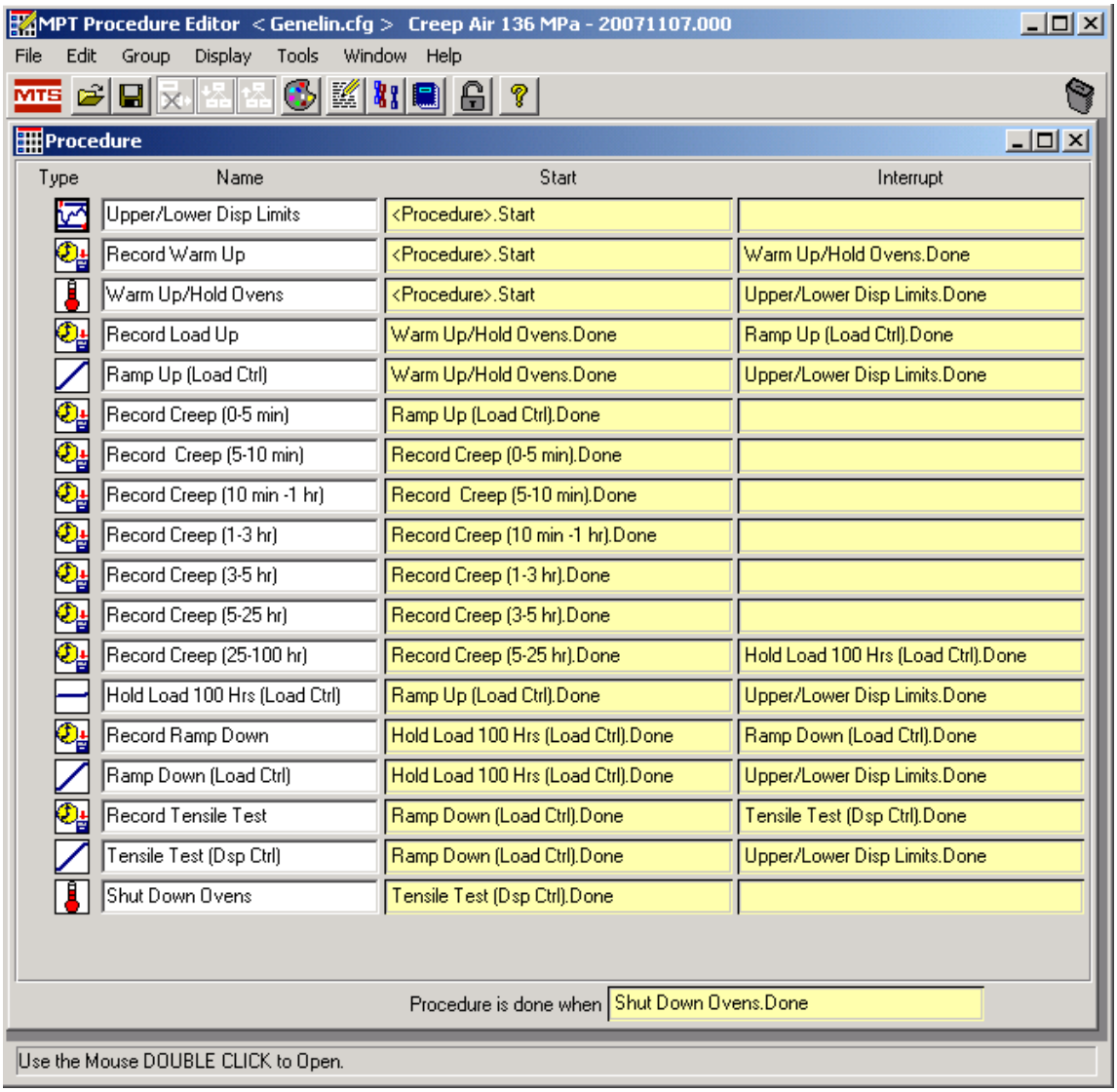

Figure 18. Typical creep test procedure.

3.5.5 Tensile Tests at 0.0025 and 25 MPa/s

To explore the hypothesis that slow crack growth is the primary failure mechanism for the N720/AM CMC, two additional tensile tests were conducted in force control at 1200°C in steam. The tests were conducted at constant stress rates of 0.0025 and 25 MPa/s.

IV. Results and Discussion

4.1 Section Summary

This chapter reports the experimental results obtained during the course of this research. Complete summaries of experimental data are given in Tables 3-5 below. The section begins with a discussion of thermal properties of the N720/AM composite. Results of the monotonic tensile tests and creep rupture tests are then presented and compared to results for the N720/A composite from earlier studies. Microstructure of the N720/AM composite is discussed. A slow crack growth discussion is also presented.

Table 3. Summary of N720/AM tensile data.

Sample	Environment	Control Method	Thermal Strain (%)	E (GPa)	UTS (MPa)
CG-1	Air	0.05 mm/s	N/A	75.5	147.4
CG-2	Air	0.05 mm/s	0.73	77.4	153.3
CG-4	Air	0.05 mm/s	0.73	71.9	161.2
CG-5	Air	0.05 mm/s	0.73	73.1	150.8
Average			0.73	74.5	153.2
CG-25*	Steam	25 MPa/s	0.72	N/A	150.7
CG-26	Steam	0.0025 MPa/s	0.81	27.64	93.6
CG-27	Steam	25 MPa/s	0.77	60.4	150.4

* Unreliable strain measurement

Table 4. Summary of N720/AM creep data.

Sample	Environment	Thermal Strain (%)	E (GPa)	Creep Stress (MPa)	Creep Life (h)	Creep Strain (%)	Secondary Creep Rate (s^{-1})
CG-11*	Air	0.65	61	73	>100	0.6	9.0E-09
CG-9*	Air	0.72	68.5	91	>100	0.6	9.0E-09
CG-8	Air	0.69	60	114	22.28	0.44	4.0E-08
CG-6	Air	0.69	N/A	125	0.43	0.19	7.0E-07
CG-7**	Air	0.75	67.7	136	0.0025	0.037	3.0E-05
CG-10	Air	0.65	70	136	0.59	0.27	8.0E-07
CG-18**	Argon	0.84	71.7	73	39.57	1.8	1.0E-07
CG-24	Argon	0.84	75.7	73	92.8	5.86	1.0E-07
CG-21	Argon	0.83	60.2	91	18.77	2.94	4.0E-07
CG-22	Argon	0.84	61.4	114	0.45	0.66	3.0E-06
CG-17**	Argon	0.76	58.8	136	0	0	0.0E+00
CG-23	Argon	0.8	N/A	136	0.071	0.62	2.0E-05
CG-16	Steam	0.82	62.8	73	37	2.49	2.0E-07
CG-15	Steam	0.78	86.4	91	4.18	1.6	9.0E-07
CG-14	Steam	0.76	63.8	114	0.49	0.48	3.0E-06
CG-12	Steam	0.8	66	136	0.012	0.105	2.0E-05
Average		0.76	66.7				

* Run-out

** Failure in grips

Table 5. Summary of N720/AM retained properties for samples achieving creep run-out of 100 h.

Sample	Environment	Prior Creep Stress (MPa)	Control Method	Retained E (GPa)	Retained UTS (MPa)
CG-9	Air	73	0.05 mm/s	67.5	169.4
CG-11	Air	91	0.05 mm/s	70.1	167.1
Average				68.8	168.25

4.2 Thermal Expansion

Thermal strain was measured while heating to test temperature and was used to calculate the coefficient of linear thermal expansion, α_t, for the N720/AM composite using the following equation:

$$\alpha_t = \frac{\varepsilon_t}{\Delta T} \quad (1)$$

where ε_t is the *thermal strain* in m/m, and ΔT is the *change in temperature* in degrees Kelvin. For the 22 specimens tested, thermal strains varied between 0.65 and 0.84% with a standard deviation of 0.0607%. The calculated coefficient of linear thermal expansion for the N720/AM CMC was 6.45 $10^{-6}K^{-1}$, which was slightly lower than that for the N720/A composite which utilized the same fibers, but had a pure alumina matrix. Thermal strain measurements and coefficients of linear thermal expansion are summarized in Table 6.

Table 6. Thermal strains produced by N720/A and N720/AM CMCs due to temperature rise from 23 to 1200°C [13, 18, 14].

Author	Material	Specimens	Mean Thermal Strain (%)	Thermal Strain Standard Deviation (%)	Coefficient of Linear Thermal Expansion ($10^{-6}K^{-1}$)
Harlan [13]	N720/A	12	0.867	0.174	7.43
Mehrman [18]	N720/A	16	0.902	0.0717	7.66
Hetrick [14]	N720/A	7	0.891	0.0294	7.57
Current Research	N720/AM	22	0.759	0.0607	6.45

4.3 Monotonic Tension

Four monotonic tensile tests were performed at 1200°C in laboratory air. For the N720/AM composite, the average ultimate tensile strength (UTS) was 153.2 MPa, the average elastic modulus, 74.5 GPa, and failure strain, 0.34%. Note that for the N720/A composite, the average UTS was 192 MPa, the average elastic modulus, 75 GPa, and failure strain, 0.38% [13, 23, 18]. Representative stress-strain curves for both composites are shown in Figure 19, where data for N720/A composite is from references [13, 23].

Table 7. Average tensile properties for N720/A and N720/AM at 1200°C in laboratory air.

N720/A			N720/AM		
UTS (MPa)	E (GPa)	ε_f (%)	UTS (MPa)	E (GPa)	ε_f (%)
192	75	0.38	153.2	74.5	0.34

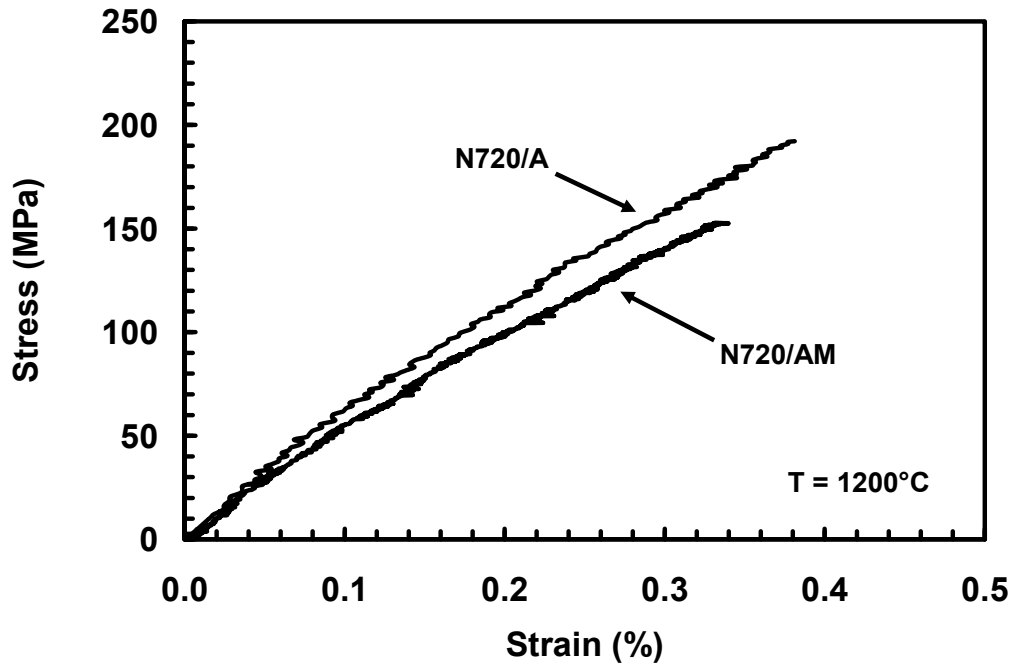

Figure 19. Tensile stress-strain curves for N720/A and N720/AM at 1200°C in laboratory air.

In the case of composites with 0°/90° fiber orientations, failure in tension is controlled almost entirely by the fibers oriented in the direction of the load. Consequently, fiber volume fraction, V_f, becomes a critical parameter when comparing results obtained for two different materials. The average fiber volume fraction of the N720/A specimens investigated in previous research was 44% [13, 23, 24, 15]. In contrast, the fiber volume fraction of the N720/AM composite investigated in this effort was 40%. Once the UTS of 153.2 MPa obtained for the N720/AM specimens is normalized to the fiber volume fraction of 44%, the adjusted UTS value of 168.52 MPa is calculated, which is within 13% of the average value obtained fro the N/720A composite. (see Equation 2).

$$UTS_{Adjusted} = \left(\frac{44}{40}\right) * UTS \quad (2)$$

Two N720/AM specimens were also tested in tension to failure at 1200°C in steam. To investigate the effect of stress rate on tensile properties, the stress-controlled tensile tests were conducted at constant stress rates of 0.0025 and 25 MPa/s. Modulus, ultimate tensile strength, failure strain and time to failure are presented in Table 8. Stress-strain curves produced at each stress rate can be seen in Figure 20.

Table 8. Summary of tensile properties of N720/AM composite at 1200°C in steam.

Stress Rate (MPa/s)	E (GPa)	UTS (MPa)	Failure Strain (%)	Time-to-Failure (h)
0.0025	27.64	93.63	1.26	10.38
25	60.4	150.4	0.55	0.0016

In steam at 25 MPa/s, the tensile modulus was 60.4 GPa, a 19% reduction from the modulus observed from displacement-controlled tensile tests in air. The ultimate tensile strength of the material was 150.4 MPa which is similar to the average UTS measured observed in air (153.2 MPa). Failure strain increased by 62% when compared to displacement-controlled tensile tests in air and the specimen failed after just 0.0016 h.

When tested at 0.0025 MPa/s, the appearance of the stress-strain curve changes dramatically. The stress-strain curve consists of two distinct sections. From 0-40 MPa the curve is linear with a 54% reduction in modulus when compared to the 25 MPa/s test. As stress levels increase, the slope of the stress-strain curve drops significantly and considerable inelastic strain develops. It is at this point that the porous matrix can no longer tolerate the damage brought upon by the increase in stress and the fibers are forced to bear the entire load. After 10.38 h the load reaches 93.63 MPa and the sample fails in

tension at a load 38% lower than the 25 MPa/s test. Failure strain for the 0.0025 MPa/s tensile test increased by 130% when compared to the 25 MPa/s test.

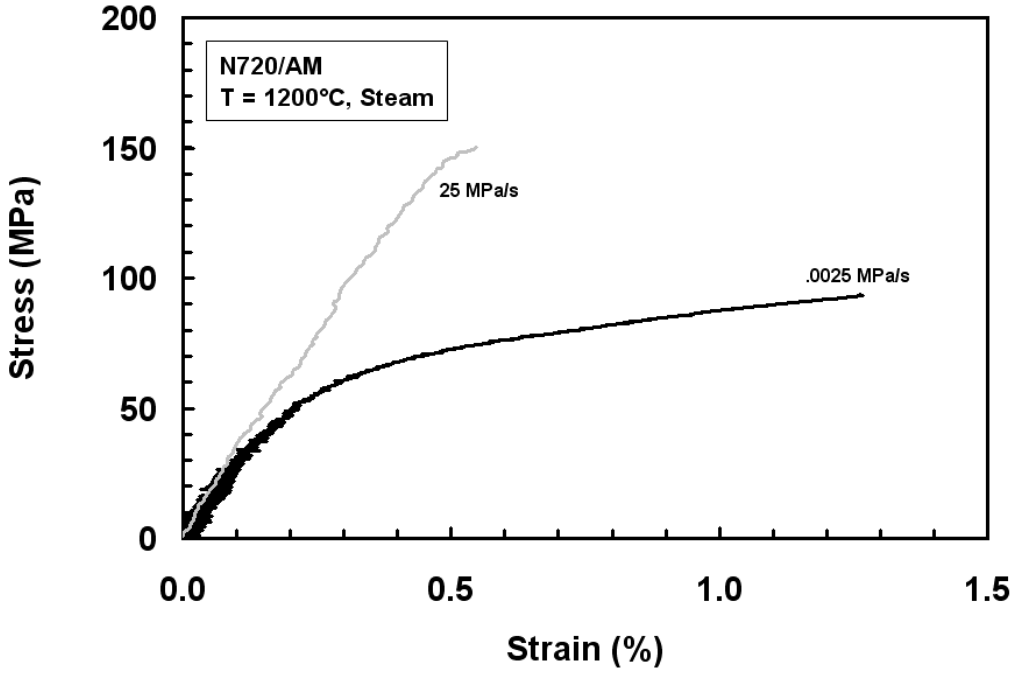

Figure 20. Tensile stress-strain curves for N720/A composite at 1200°C in steam. Dependence of stress-strain behavior and tensile properties on stress rate is evident.

4.4 Creep-Rupture

Creep tests of N720/A specimens with an average fiber volume fraction of 44% were carried out at creep stress levels of 80, 100, 125 and 150 MPa which is equivalent to 42, 52, 65 and 78% of the material's UTS, respectively. In order to make a valid comparison of creep behaviors of the N720/A and N720/AM composites, equivalent creep stress levels must be used. In the case of the N720/AM CMC, the creep stress levels used for the N720/A composite need to be adjusted for the lower fiber volume fraction using the following relation:

$$\sigma_{N720/AM} = \left(\frac{40}{44}\right) * \sigma_{N720/A} \quad (3)$$

where $\sigma_{N720/AM}$ is the *equivalent creep stress level for N720/AM* with a fiber volume fraction of 40% and $\sigma_{N720/A}$ is the *creep stress level for N720/A* with a fiber volume fraction of 44%. The following creep stress levels were used in this study: 73 MPa (equivalent to 80 MPa for $V_f = 0.44$), 91 MPa (equivalent to 100 MPa for $V_f = 0.44$), 114 MPa (equivalent to 125 MPa for $V_f = 0.44$), and 136 MPa (equivalent to 150 MPa for $V_f = 0.44$). A table of creep results produced in air, in argon and in steam for the N720/A and N720/AM composites is presented in Table 9.

Table 9. Creep results for the N720/A and N720/AM composites tested in air, steam and argon. N720/A creep data from references [13, 23, 24, 15].

Creep Results Produced in Laboratory Air				
Material	**Creep Stress (MPa)**	**Creep Life (h)**	**Creep Strain (%)**	**Secondary Creep Rate (s^{-1})**
N720/A	80	>100	0.798	1.5E-08
N720/A	100	41	1.520	8.6E-08
N720/A	125	18.14	1.259	1.2E-07
N720/A	150	0.27	0.581	6.0E-06
N720/AM	80*	>100	0.6	9.0E-09
N720/AM	100*	>100	0.6	9.0E-09
N720/AM	125*	22.28	0.44	4.0E-08
N720/AM	150*	0.59	0.27	8.0E-07
Creep Results Produced in Argon				
N720/A	80	>100	0.656	1.0E-08
N720/A	100	>100	0.962	1.8E-08
N720/A	125	36.3	1.889	8.9E-08
N720/A	150	0.878	0.326	1.0E-06
N720/AM	80*	92.8	5.86	1.0E-07
N720/AM	100*	18.77	2.94	4.0E-07
N720/AM	125*	0.45	0.66	3.0E-06
N720/AM	150*	0.071	0.62	2.0E-05
Creep Results Produced in Steam				
N720/A	80	46	2.957	4.2E-07
N720/A	100	2.49	0.040	2.0E-06
N720/A	125	0.241	0.713	8.3E-06
N720/A	150	0.027	0.399	2.5E-05
N720/AM	80*	37	2.49	2.0E-07
N720/AM	100*	4.18	1.6	9.0E-07
N720/AM	125*	0.49	0.48	3.0E-06
N720/AM	150*	0.012	0.105	2.0E-05

* Equivalent creep stress at $V_f = 0.44$

All creep curves obtained for the N720/A composite at 1200°C in air environment (Figure 21) exhibit primary and secondary creep regimes. For all stress levels, transitions from primary to secondary creep occur at one third of the creep life. Secondary creep continues to failure (or until a 100 h run-out is achieved in the case of the of the 80 MPa test). Although creep curves for the N720/AM composite also exhibit both primary and secondary creep regimes, the transition from primary to secondary creep occurs much earlier in creep life for stress levels ≤100 MPa (see Figure 22). For stress levels of 125

and 150 MPa, the transition occurs after 25% of creep lifetime had elapsed. The N720/AM specimens tested at 80 and 100 MPa achieved the 100 h run-out. For the other two specimens, secondary creep persists to failure [23].

Creep vs. time curves obtained for N720/AM at 1200°C in air are shown in Figure 22. It is seen that creep run-out was achieved at 73 and 91 MPa. Furthermore, similar creep strains were accumulated at 73 and 91 MPa after 100 h of creep. Creep strain accumulation increased as the applied stress increased to 114 MPa and then decreased as the creep stress increased to 136 MPa. For the N720/AM CMC, creep strains produced at the 73 and 91 MPa levels are nearly double the failure strain obtained in the tension tests. Creep strains at the two higher stress levels were approximately equal to failure strain obtained in tension tests. All creep strains produced in air for the N720/AM composite were ≤ 0.6%. In contrast, creep strains for the N720/A composite accumulated in air significantly exceed the failure strain obtained in tensile testing. It is noteworthy that for creep stress levels equivalent to 100 MPa for $V_f = 0.44$, larger creep strains were accumulated by N720/A than by the N720/AM composite [23].

In creep rupture testing, total strain is a sum of the strain accumulated during load-up to creep stress and that accumulated during the actual creep test. For the N720/AM composite tested in air, creep strain ranges from 65 to 85% of the total strain and decreases with increasing applied stress. For the N720/A composite tested at stress levels ≤ 125 MPa, creep strain accounted for nearly 90% of total strain. However at the 150 MPa stress level, creep strain made up only 33% of the total strain.

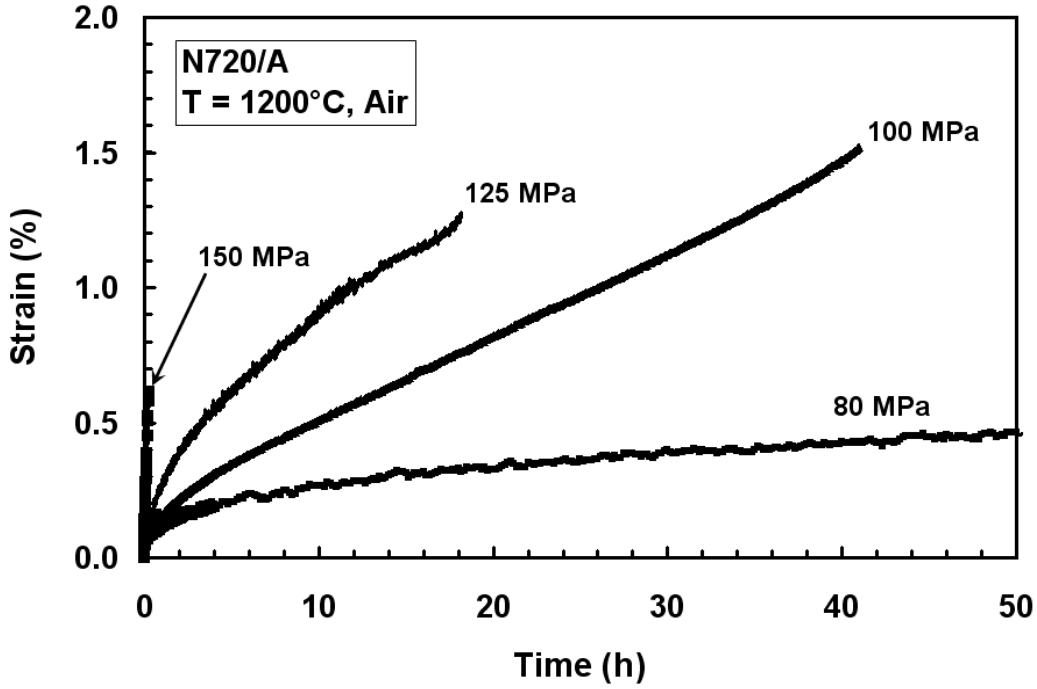

Figure 21. Creep vs. time curves for N720/A composite obtained at 1200°C in air. Data from references [13, 23].

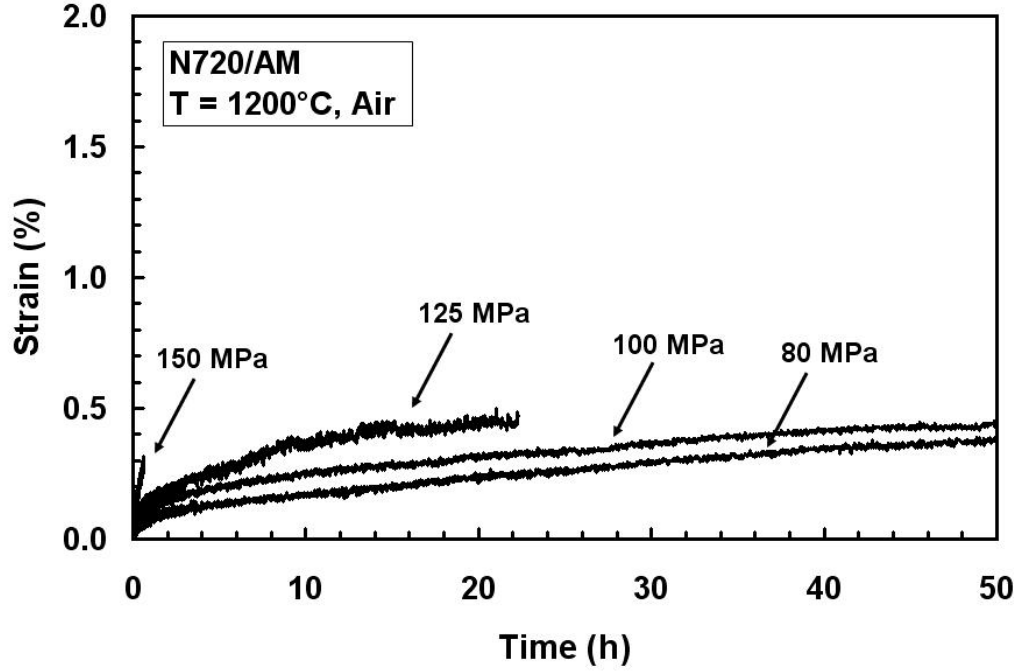

Figure 22. Creep vs. time curves for N720/AM composite obtained at 1200°C in laboratory air. Stress levels equivalent to $V_f = 0.44$ are shown on labels.

Figures 23 and 25 show that test environment has little effect on the appearance of the creep curves obtained for the N720/A composite. Creep curves and creep strains obtained in air are comparable to those produced in argon and in steam. However, this was not the case for the N720/AM CMC. While creep curves produced in argon did exhibit both primary and secondary creep regimes, in argon the transition from primary to secondary creep occurred much earlier in creep life at the two lowest stress levels. At 114 and 136 MPa, transitions from primary to secondary creep occurred after ~ 23 and 36% of the creep life, respectively. For all stress levels in argon, secondary creep continued until failure. Creep strains for N720/AM obtained in argon were 2 to 9 times higher than those obtained in air. Moreover, in argon creep strains decreased with increasing creep stress. For creep stress levels of 73 and 91 MPa, creep strain made up approximately 95% of the total strain. For 114 MPa, creep strain accounted for nearly 75% of total strain. For 136 MPa, creep strain approached 53% of the total strain. Creep curves for N720/AM produced at 1200°C in argon are presented in Figure 24.

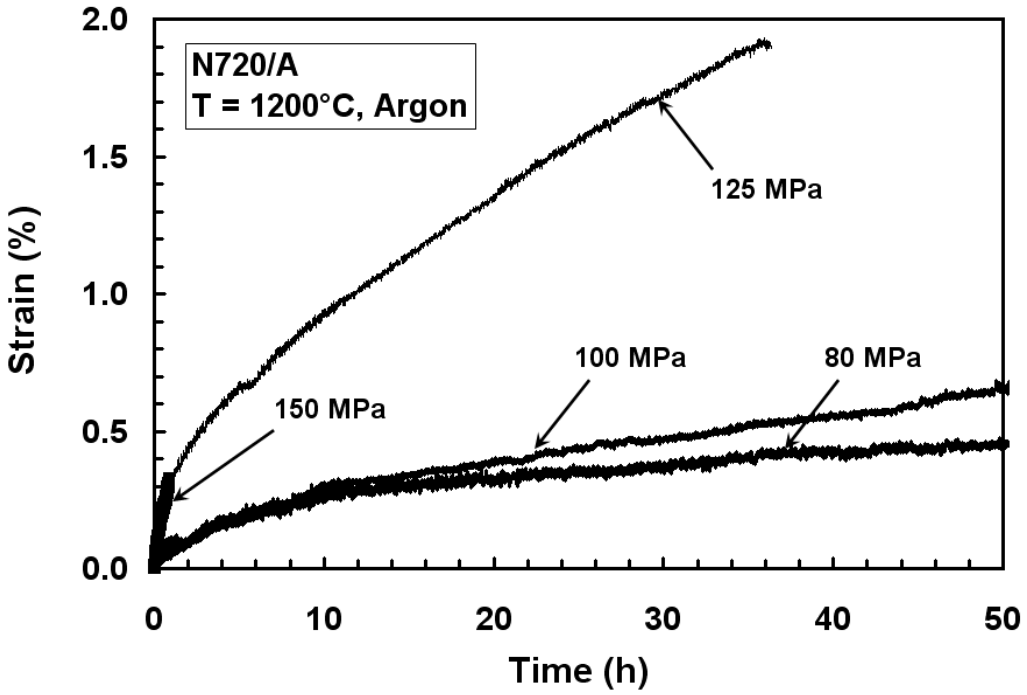

Figure 23. Creep vs. time curves for N720/A composite obtained at 1200°C in argon. Data from references [24, 15].

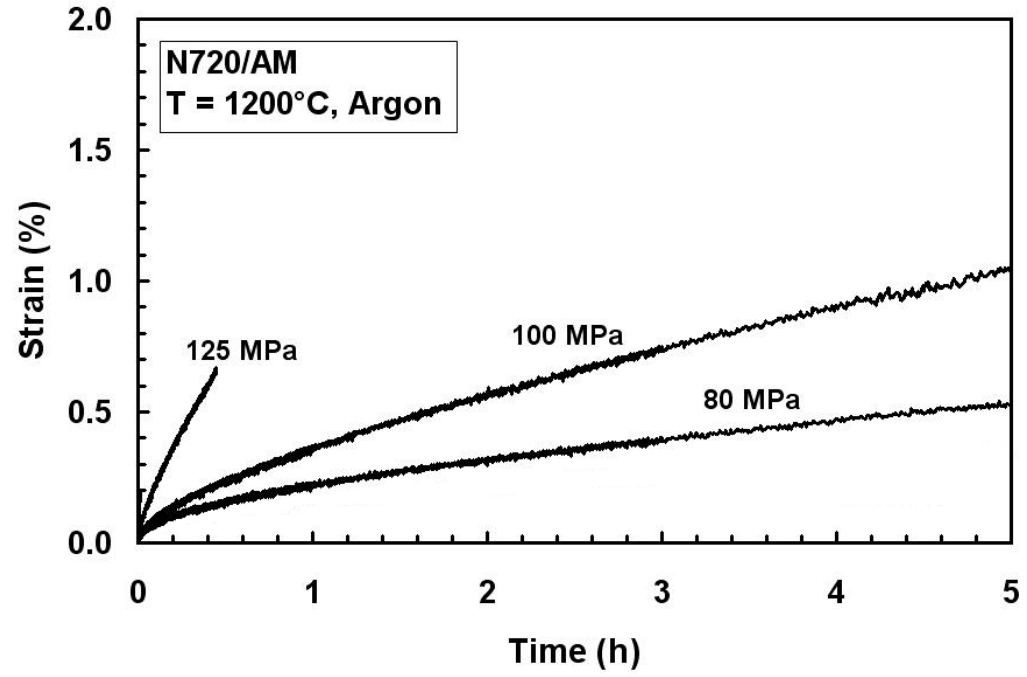

Figure 24. Creep vs. time curves for N720/AM composite obtained at 1200°C in argon. Stress levels equivalent to $V_f = 0.44$ are shown on labels.

Creep curves for the N720/AM obtained at 1200°C in steam also differ significantly from those produced at 1200°C in air (see Figure 26). Primary and secondary creep regimes were obtained in all tests. Primary, secondary and tertiary creep were observed at 73 MPa (see Figure 27). At 73 and 91 MPa primary creep transitioned into secondary creep after approximately 5% of creep life. At 114 MPa transition occurred after 15 % and at 136 MPA the transition was almost immediate. The transition for the 150 MPa case was almost immediate. In the case of the 73 MPa creep test in steam, the N720/AM composite transitions to tertiary creep fairly early in creep life. Creep strains account for 25 to 95% of total strain and decrease with increasing creep stress. Creep strains produced in steam are approximately two times those produced in argon.

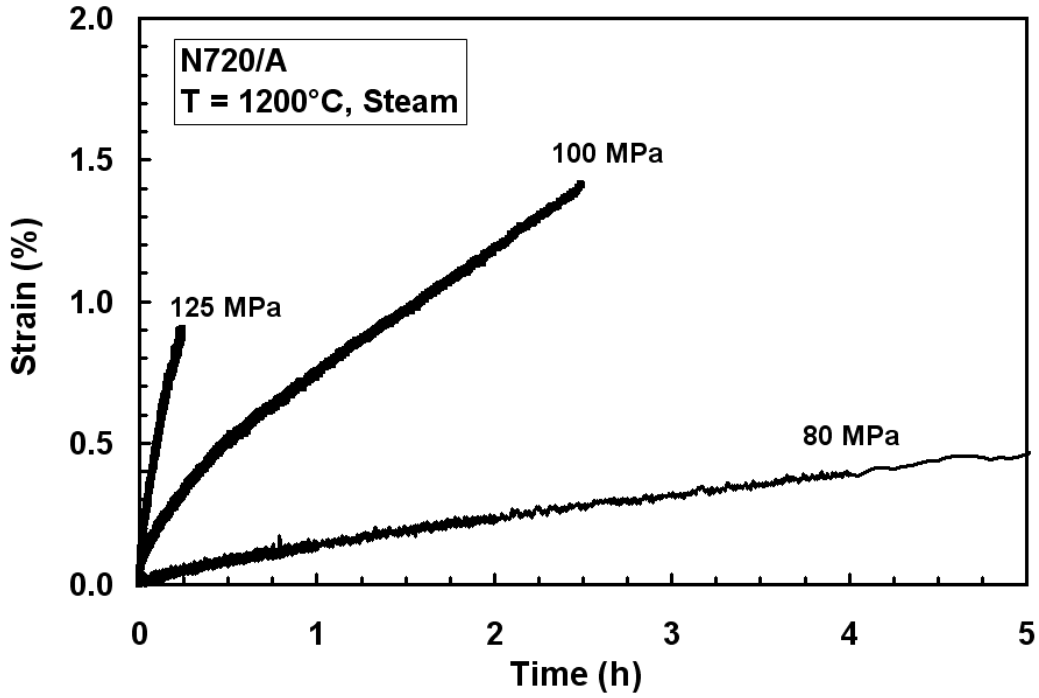

Figure 25. Creep vs. time curves for N720/A composite obtained at 1200°C in steam. Data from Reference [13, 23].

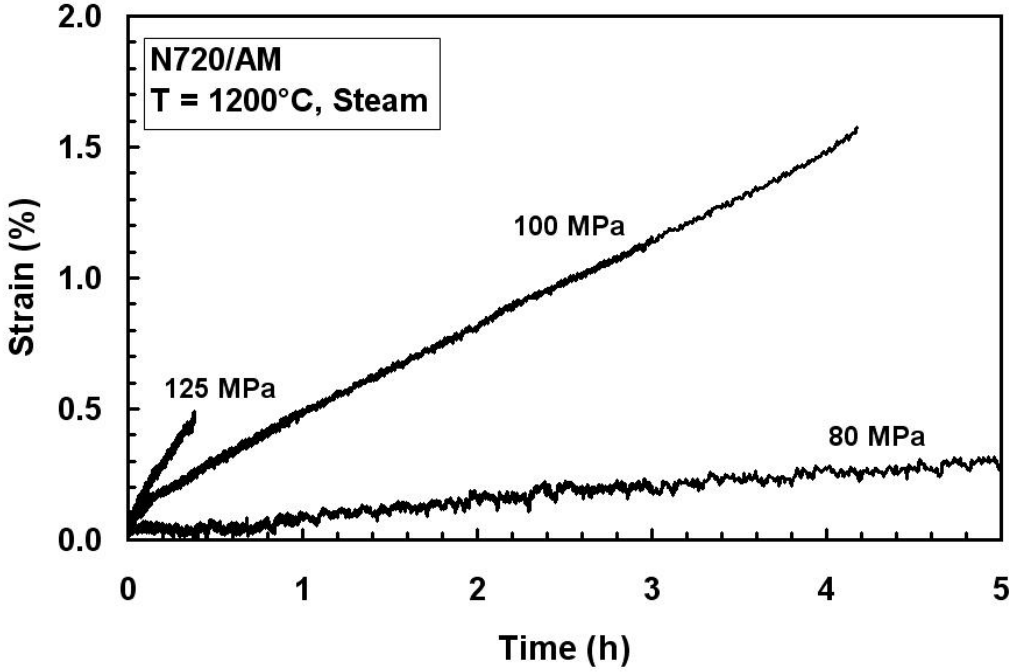

Figure 26. Creep vs. time curves for N720/AM composite obtained at 1200°C in steam. Stress levels equivalent to $V_f = 0.44$ are shown on labels.

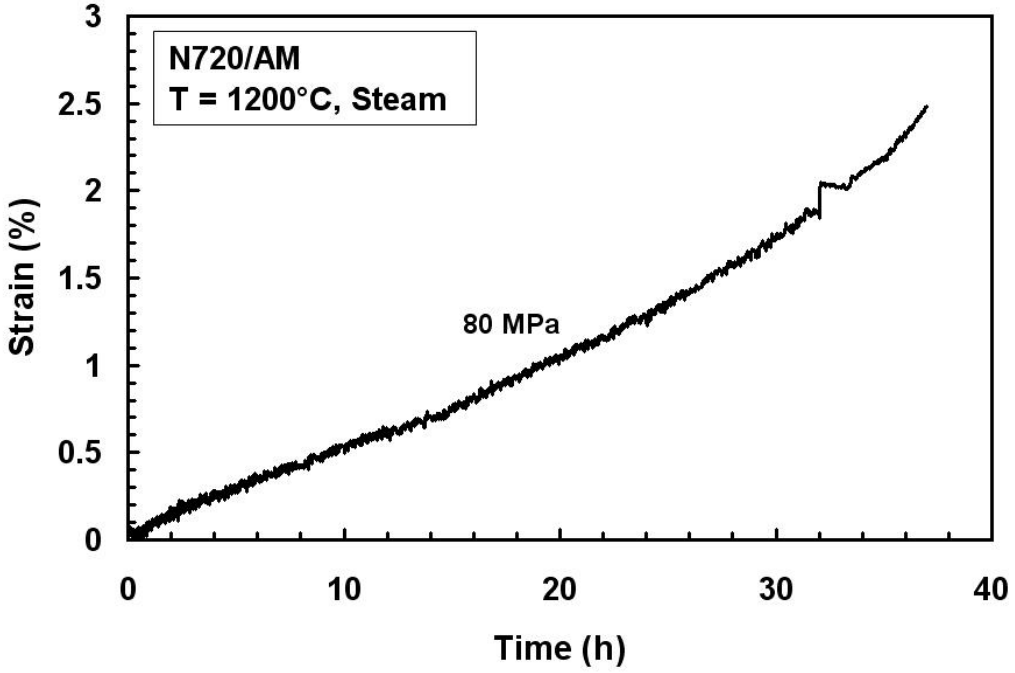

Figure 27. Creep vs. time curve for N720/AM composite obtained at 1200°C in steam. Stress level equivalent to $V_f = 0.44$ is shown on label.

Minimum creep rate was reached in all tests. Creep rate as a function of applied stress for both the N720/A and N720/AM composites is presented in Figures 28 and 29, respectively. Data for the N720/A composite from references [13, 23, 24, 15] are included for comparison. In air, secondary creep rates for the N720/A can be nearly 10 times those of the N720/AM CMC. In steam, the secondary creep rates of N720/A are two times those of the N720/AM composite. However in argon, secondary creep rates of the N720/A composite are similar to those produced in air, while creep rates produced by the N720/AM CMC are similar to those produced in steam. At 80 MPa (equivalent to 73 MPa for $V_f = 0.40$), creep strain produced in steam for the N720/A was 5 times that obtained in air. For the N720/AM composite creep strain accumulated at 73 MPA in steam was also nearly 5 times that obtained in air. However for N720/AM creep strain produced in argon was nearly 10 times produced in air. At 91 MPa (equivalent to 100 MPa for $V_f = 0.40$), creep strain in argon remained 5 times that obtained in air at the same stress level. While both composites achieved runout in air at the two lowest stress levels, only the N720/A CMC achieved a 100 h run-out in argon (80 and 100 MPa). Neither material achieved runout in steam [23].

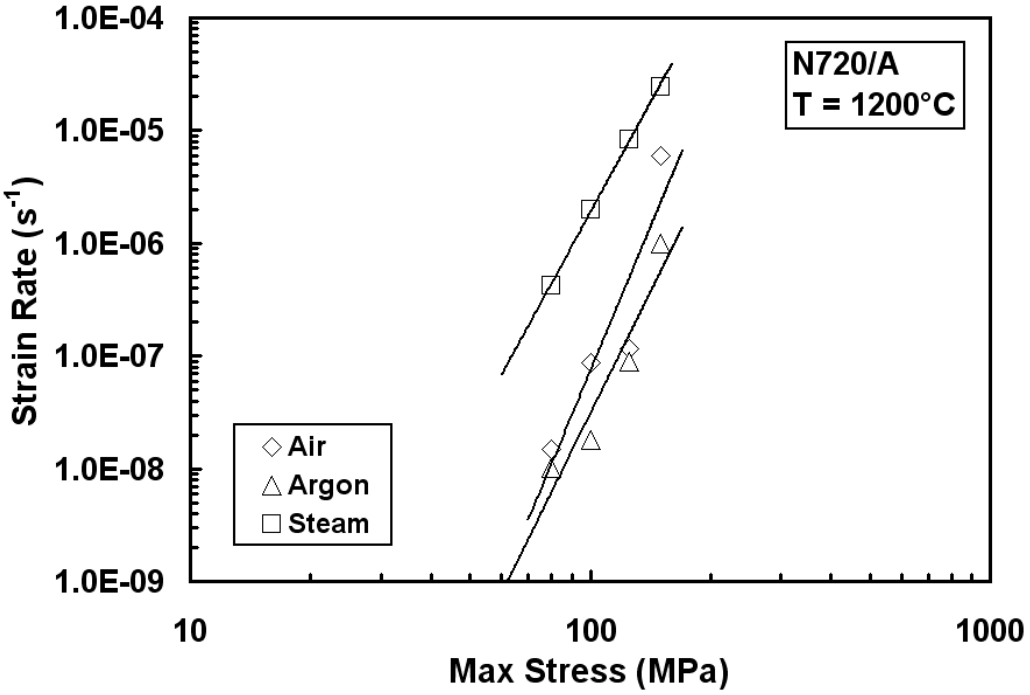

Figure 28. Secondary creep rate as a function of applied stress for N720/A composite at 1200°C in air, argon and steam. Data from references [13, 23, 24, 15].

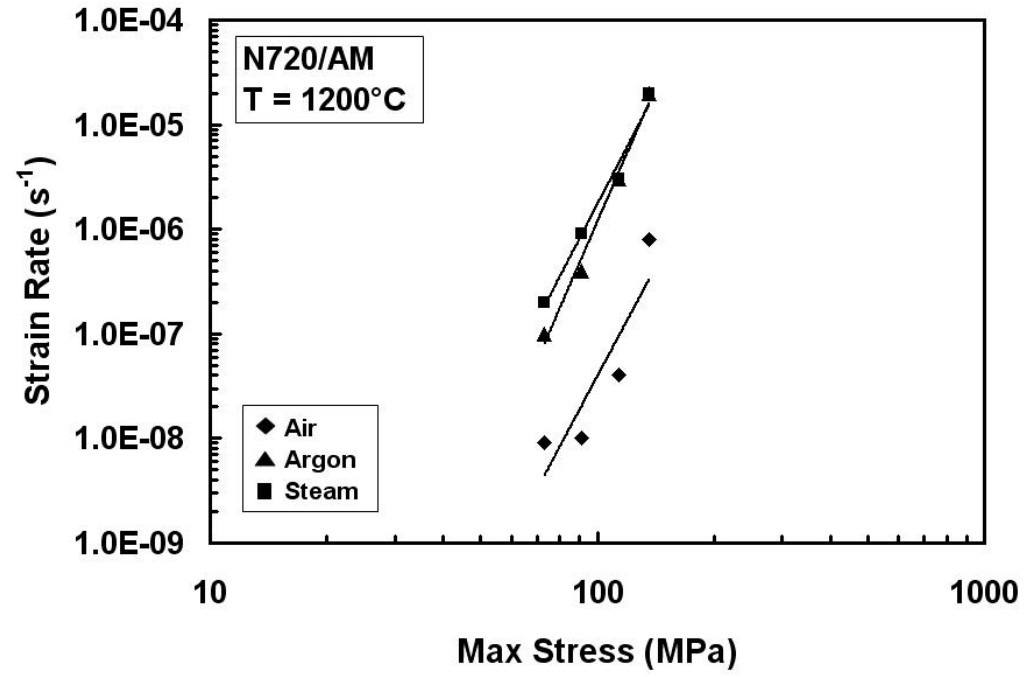

Figure 29. Secondary creep rate as a function of applied stress for N720/AM composite at 1200°C in air, argon and steam. Stress adjusted to $V_f = 0.44$.

Stress-rupture behaviors of both composites are summarized in Figure 30. It is seen that creep life of both composites decreases with applied stress. While the presence of argon had a beneficial effect on creep lifetimes for the N720/A composite, it degraded the creep lifetimes of the N720/AM composite. For stress levels ≥100 MPa (equivalent to 91 MPa for $V_f = 0.40$), creep lifetimes of the N720/A in argon were nearly double the lifetimes in laboratory air. For stress levels ≥125 MPa (equivalent to 114 MPa for $V_f = 0.40$), creep life in argon for the N720/AM was nearly as short as that in steam. Only at the lowest stress level did the N720/AM composite come close to achieving a run out at 1200°C in argon. The reduction in creep life due to steam was at least 90% for applied stress levels ≥100 MPa, and 54% for the applied stress of 80 MPa for N720/A [23]. For N720/AM, the loss of creep life due to steam was greater than 95% for stress levels ≥ 91 MPa (equivalent to 100 MPa for $V_f = 0.44$) and 63% at a stress level of 73 MPa (equivalent to 80 MPa for $V_f = 0.44$).

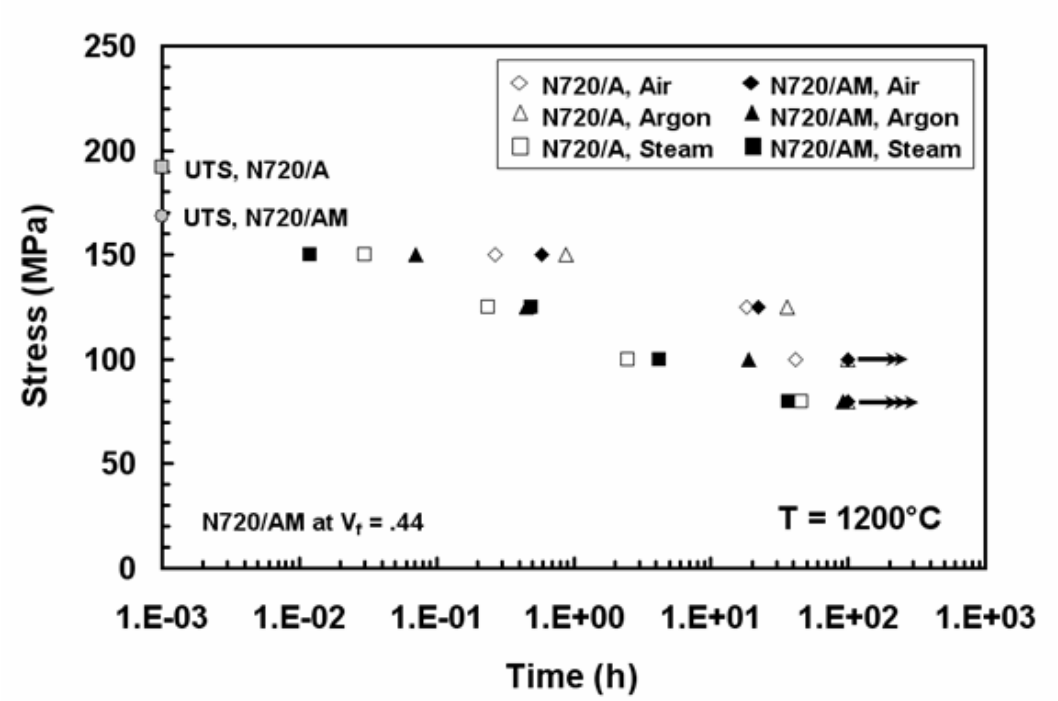

Figure 30. Applied stress vs. time to failure for N720/A and N720/AM ceramic composites at 1200°C in air, argon and steam. Data for N720/A from references [13, 23, 24, 15]. Stress adjusted for V_f = 0.44.

Retained strength and modulus of the specimens that achieved run-out are summarized in Table 10. Stress-strain curves obtained for N720/A and N720/AM specimens subjected to prior creep are shown in Figures 31 and 32, respectively. Stress-strain curves for the as-processed materials are included for comparison. Data for N720/A CMC obtained from references [13, 23, 24, 15].

Table 10. Retained properties of the N720/A and N720/AM specimens subjected to prior creep at 1200°C in laboratory air and argon environments. Data for N720/A composite from references [13, 23, 24, 15].

Material	Environment	Creep Stress (MPa)	Retained Strength (MPa)	Retained Modulus (GPa)	Failure Strain (%)
N720/A	Air	80	174	64.5	0.31
N720/A	Argon	80	180	54.7	0.38
N720/A	Argon	100	161	53.8	0.31
N720/AM	Air	80	167	70.1	0.36
N720/AM	Air	100	169	67.5	0.34

The N720/A material subjected to 100 h of prior creep at 80 MPa in air retained over 90% of its tensile strength. Loss in elastic modulus was limited to 14%. For the specimens subjected to prior creep in argon, tensile strength retention reached 83% while loss in elastic modulus was 20% [23]. After 100 h of prior creep in air at 73 MPa (equivalent to 80 MPa for $V_f = 0.44$), the tensile strength of the N720/AM composite is increased by 9% and the elastic modulus is reduced by 6%. Following prior creep at 91 MPa (equivalent to 100 MPa for $V_f = 0.44$), the strength of the N720/AM CMC is increased by 10% while the modulus is decreased 10%. Failure strain of the N720/AM composite was not significantly affected by prior creep.

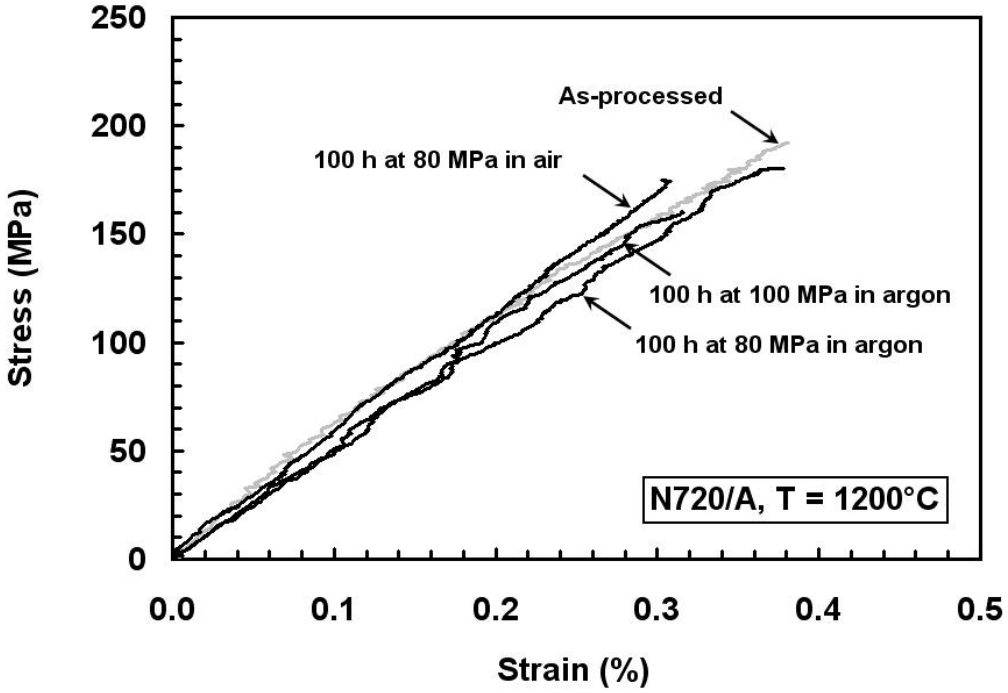

Figure 31. Effect of prior creep at 1200°C in air and in argon on tensile stress-strain behavior of N720/A composite. Data from references [13, 23, 24, 15].

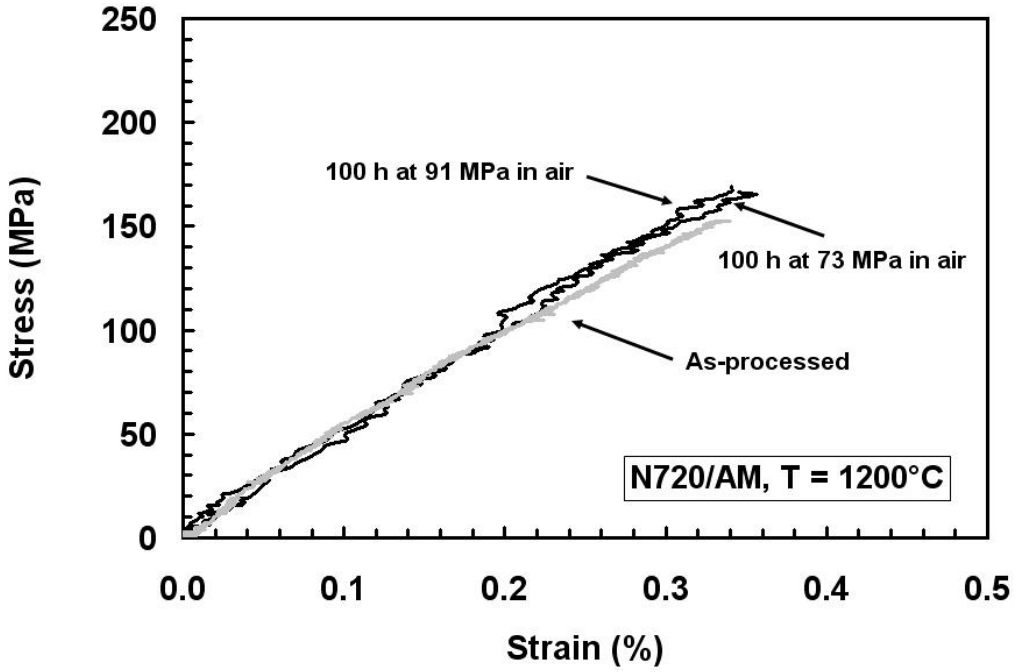

Figure 32. Effect of prior creep at 1200°C in air and in argon on tensile stress-strain behavior of N720/AM composite.

4.5 Prediction of Time to Failure Under Constant Stress

The stress-rate dependence of the tensile strength exhibited by the N720/AM composite at 1200 °C in steam is similar to that exhibited by monolithic ceramics at elevated temperatures [7, 8]. In the case of monolithic ceramics, the time (rate)-dependence of strength (also known as delayed failure) has been shown to proceed by subcritical crack growth due to stress corrosion [26-28]. The slow crack growth rate can be described by the empirical power law [11, 1, 2]:

$$\frac{da}{dt} = A\left[\frac{K_I}{K_{IC}}\right]^n \tag{4}$$

where a is the crack size, t is time, K_I is the mode I stress intensity factor, K_{IC} is the

critical stress intensity factor (or fracture toughness) under mode I loading, and *A* and *n* are the slow crack growth parameters. Under constant stress rate loading, the fracture strength σ_f can be derived as a function of applied stress rate $\dot{\sigma}$ as follows [11, 1, 2]:

$$\sigma_f = D\left(\dot{\sigma}\right)^{\frac{1}{n+1}} \tag{5}$$

Here *D* is a crack growth parameter associated with inert strength σ_i, *n* and crack geometry, and given by:

$$D = \left[\frac{2(n+1)K_{IC}^2\sigma_i^{n-2}}{AY^2(n-2)}\right]^{\frac{1}{n+1}} \tag{6}$$

By taking logarithms of both sides Eq. (5) can be expressed in the following form:

$$\log\sigma_f = \frac{1}{n+1}\log\dot{\sigma} + \log D \tag{7}$$

Following the procedure in [1, 2], the experimental data were plotted as log (compressive strength) vs. log (applied stress rate), then the parameters n = 18 and D = 128 were determined by a linear regression analysis from the slope and intercept, respectively.

For many glass and ceramic materials that exhibit subcritical (slow) crack growth as the predominant failure mechanism, time to failure under constant stress can be predicted from constant stress-rate test data by using the linear elastic crack growth model [7, 8]. Using the empirical power-law crack-velocity formulation in Eq. (4) the time to failure under constant stress can be derived in the form [22]:

$$t_f = \left[\frac{2K_{IC}^2\sigma_i^{n-2}}{AY^2(n-2)}\right]\sigma^{-n} \tag{8}$$

Combining equations (8) and (6), creep lifetime can be expressed in terms of the crack

growth parameters obtained from constant stress-rate data as:

$$t_f = \left[\frac{D^{n+1}}{(n+1)}\right]\sigma^{-n} \tag{9}$$

where t_f and σ are time to failure and applied creep stress, respectively. The predicted creep lifetimes in steam are shown in Figure 33 as a solid line. A good agreement between the predictions and the experimental results indicates that in both tensile creep tests and in constant stress-rate tension tests at 1200 °C in steam, the slow crack growth is indeed the governing failure mechanism for N720/AM CMC. The dependence of tensile strength on loading rate together with the reasonable prediction of creep lifetimes from constant stress-rate test data suggest that delayed failure of the N720/A CMC at 1200 °C in steam is governed by the power-law type subcritical crack growth. These results point to stress-corrosion as the mechanism behind the degraded tensile creep performance in steam.

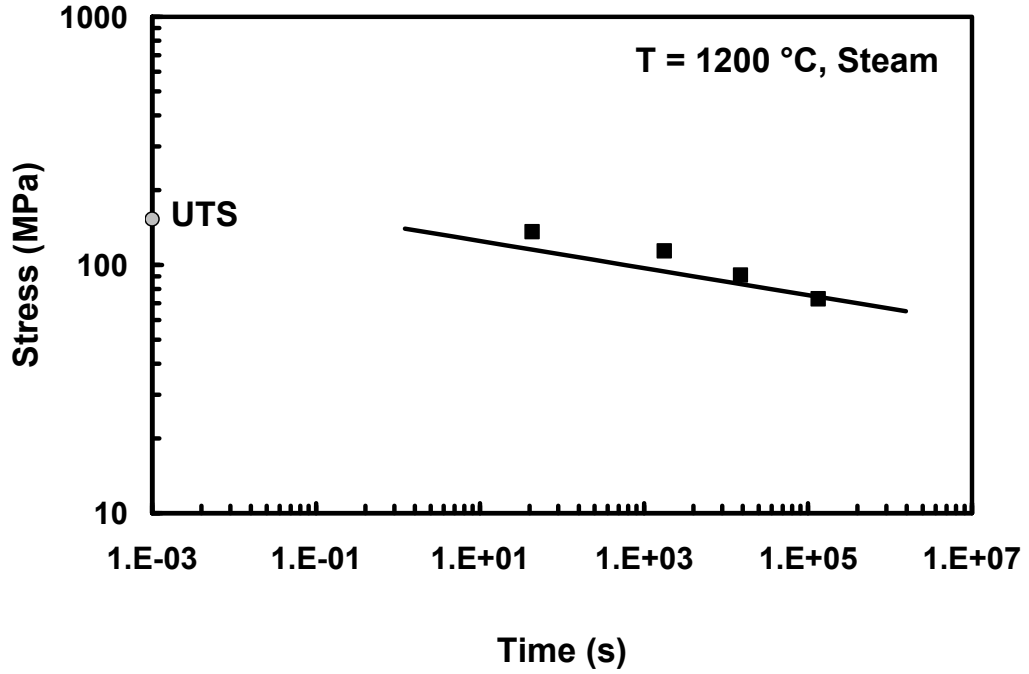

Figure 33. Creep stress vs. time to rupture for N720/AM ceramic composite at 1200°C in steam. The solid line represents prediction made based on Eq. (9) from the results of constant stress-rate tests.

4.6 Composite Microstructure

Optical micrographs of the N720/AM specimens tested in creep at 1200°C are presented in Figures 34 through 37 and are organized by creep stress level. It is seen that the fracture zones on all specimens are fibrous and brushy. However, no clear correlation between creep stress level or environment and length of damage zones is apparent. Previous research on N720/A invariably showed a correlation between time-to-failure (t_f) and length of damage zone [23]. This again is not the case for the N720/AM composite. For example, Figure 35 shows optical micrographs of specimens tested at a creep stress of 91 MPa (equivalent to 100 MPa for $V_f = 0.44$). The specimen in Figure 35(a) was tested in air and achieved run-out before being subjected to a displacement-controlled tensile test. The specimens in Figures 35(b) and 35(c) failed after 18.8 and 4.17 h of

creep, respectively. The damage zones for these specimens are slightly longer than that of the specimen that achieved run-out.

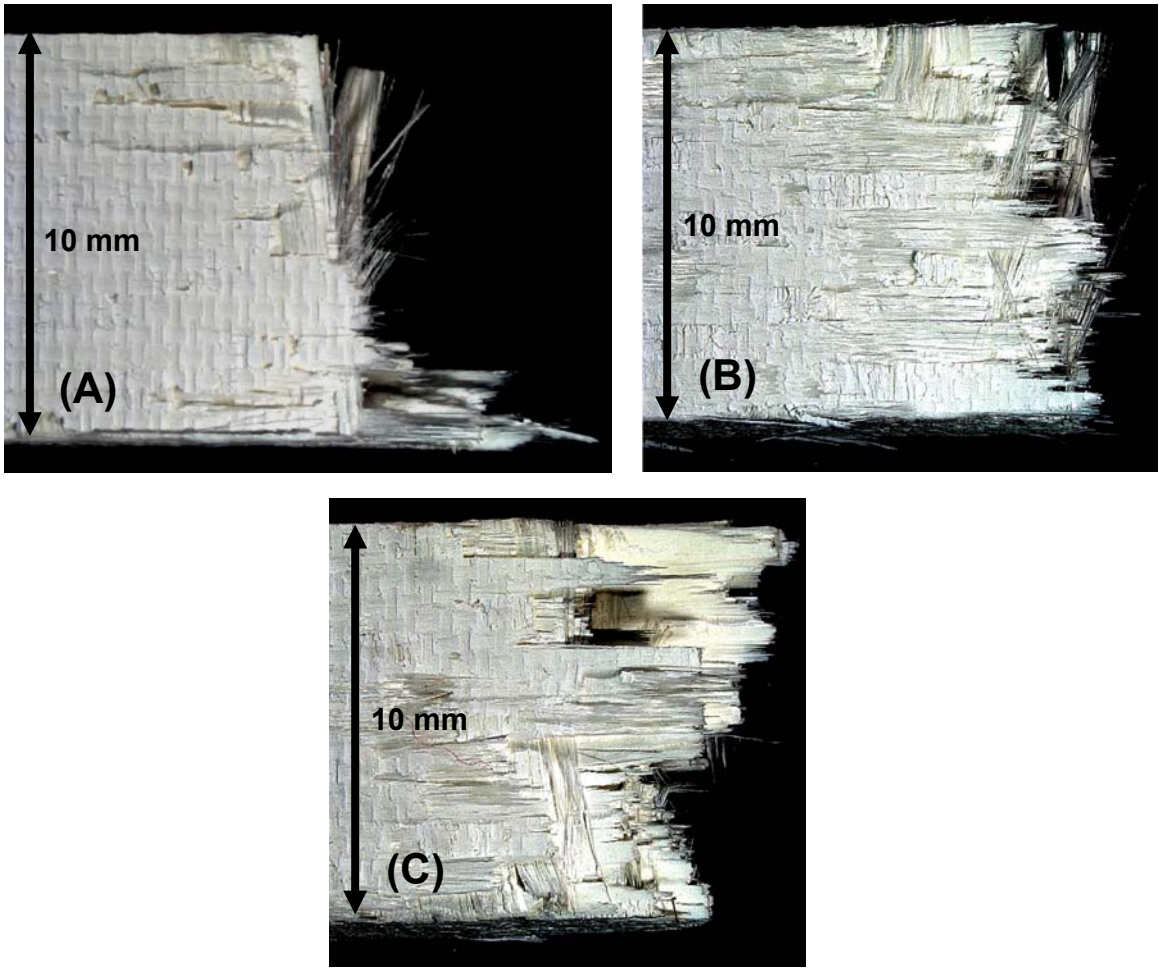

Figure 34. Fracture surfaces of the N720/AM specimens obtained in creep tests conducted at 73 MPa (equivalent to 80 MPa for $V_f = 0.44$) at 1200°C in: (a) air, $t_f >$ 100h, (b) argon, $t_f = 92.8$ h. (c) steam, $t_f = 37$ h.

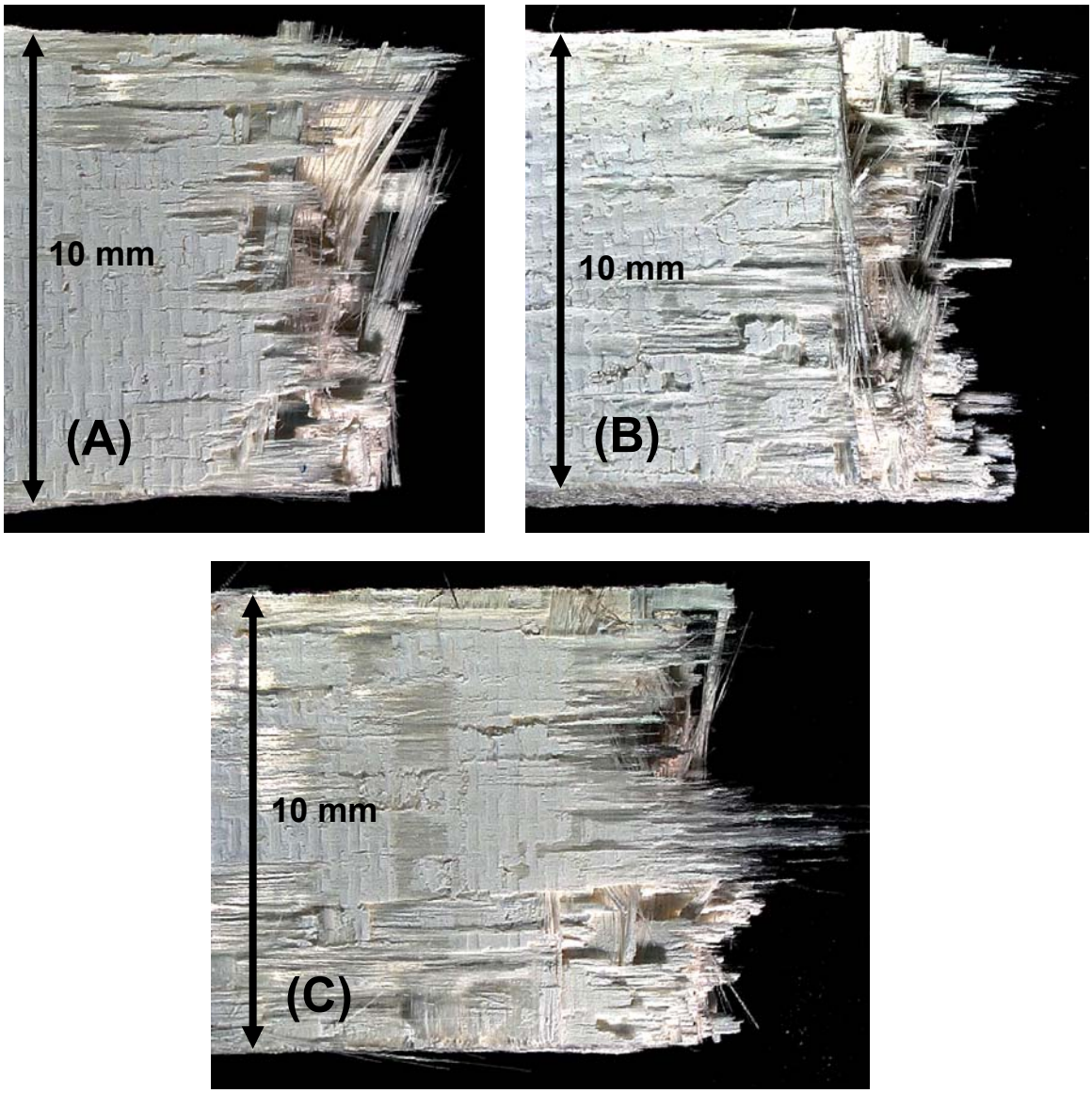

Figure 35. Fracture surfaces of the N720/AM specimens obtained in creep tests conducted at 91 MPa (equivalent to 100 MPa for $V_f = 0.44$) at 1200°C in: (a) air, t_f = > 100 h, (b) argon, $t_f = 18.8$ h; (c) steam, $t_f = 4.17$ h.

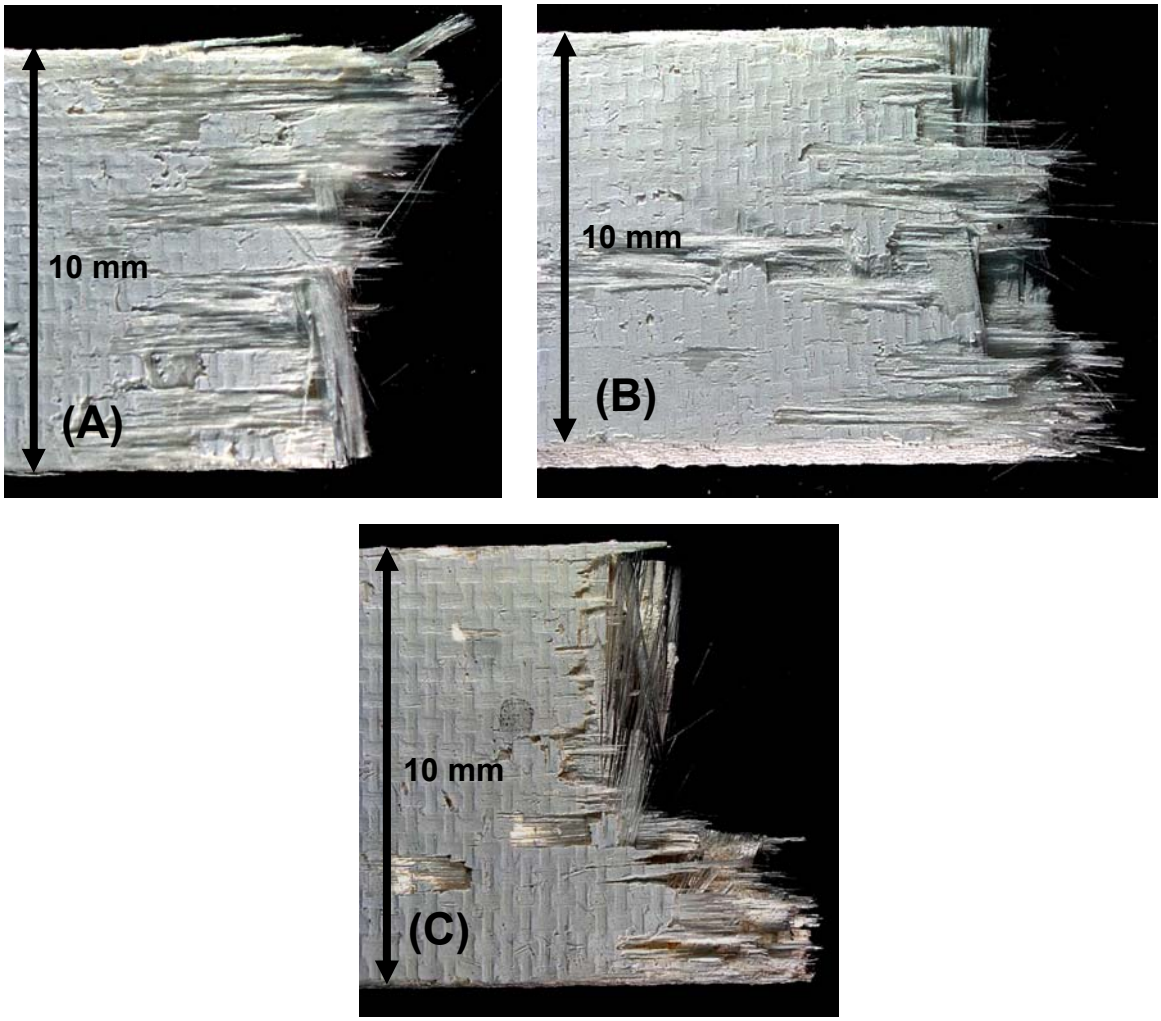

Figure 36. Fracture surfaces of the N720/AM specimens obtained in creep tests conducted at 114 MPa (equivalent to 125 MPa for $V_f = 0.44$) at 1200°C in: (a) air, $t_f = 22.3$, (b) argon, $t_f = .45$ h; (c) steam, $t_f = .38$ h.

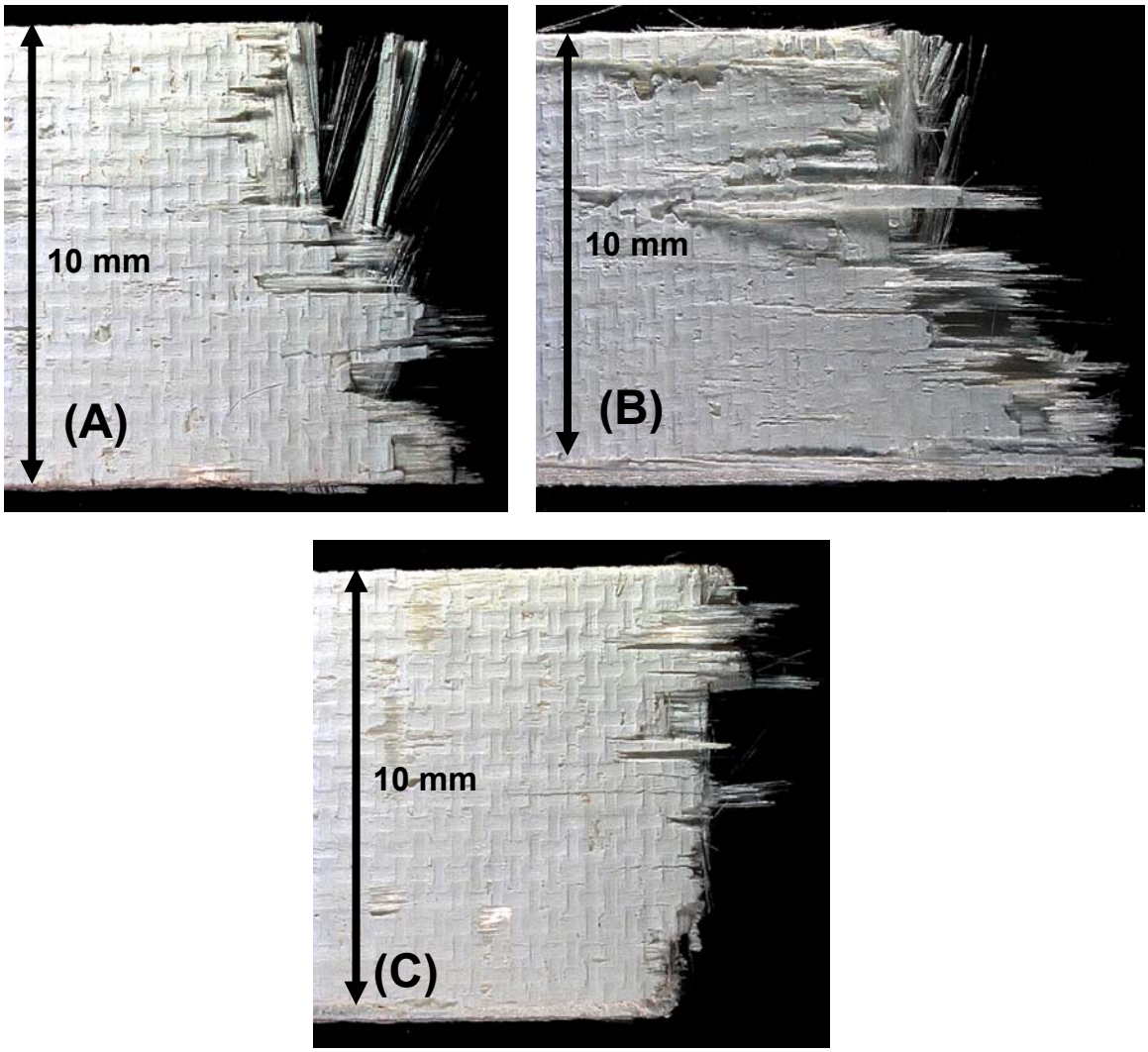

Figure 37. Fracture surfaces of the N720/AM specimens obtained in creep tests conducted at 136 MPa (equivalent to 150 MPa for $V_f = 0.44$) at 1200°C in: (a) air, $t_f = 0.59$, (b) argon, $t_f = 0.07$ h; (c) steam, $t_f = 0.01$ h.

Figure 38 shows optical micrographs of the two N720/AM specimens subjected to load controlled monotonic tensile testing in steam at 1200°C. The specimen in Figure 38 (a) was tested at a stress rate of 25 MPa/s. The damage zone appears to be relatively short and small amounts of fiber pull-out can be seen. In contrast, Figure 38 (b) shows the fracture surface of a specimen tested at a stress rate of 0.0025 MPa/s, which is four orders of magnitude lower. The damage zone is much larger than the specimen subjected

to the higher stress rate and shows large sections of fiber pull out. The sample in Figure 38 (b) failed after 10.4 h while the sample in Figure 38 (b) failed after just .0016h or 5.8 seconds.

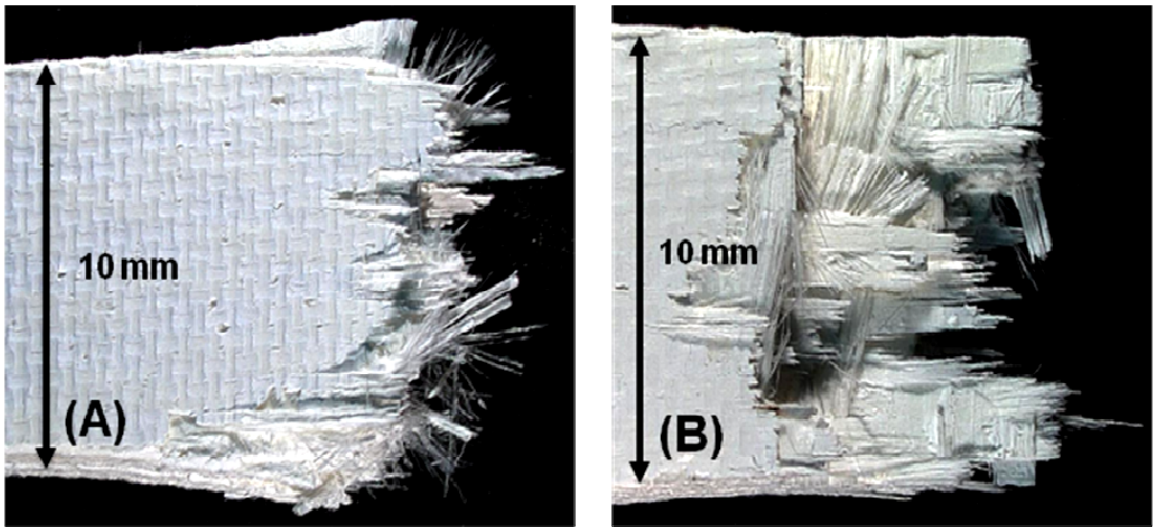

Figure 38. Fracture surfaces of the N720/AM specimens obtained from load controlled tensile tests at 1200°C at: (a) 25 MPa/s, t_f = 0.0017 h, (b) .0025 MPa/s, tf = 10.4 h.

SEM micrographs of the N720/AM fracture surfaces are shown in Figures 39-41. Additional SEM micrographs can be found in the appendix. Figures 39 (a), (b) and (c) show the fracture surface of the N720/AM specimen subjected to creep-rupture test at 73 MPa in air. The specimen achieved run-out and was subsequently subjected to a displacement controlled, monotonic tensile test to failure. It is apparent that the fracture surface is dominated by areas of planar fracture with small areas of very short 0° fiber pull-out. The fracture surface produced at 136 MPa, Figures 39 (d), (e) and (f), is almost entirely dominated by correlated fractures of the 0° fibers. Large amounts of fiber-matrix bonding on the 90° fibers were also observed.

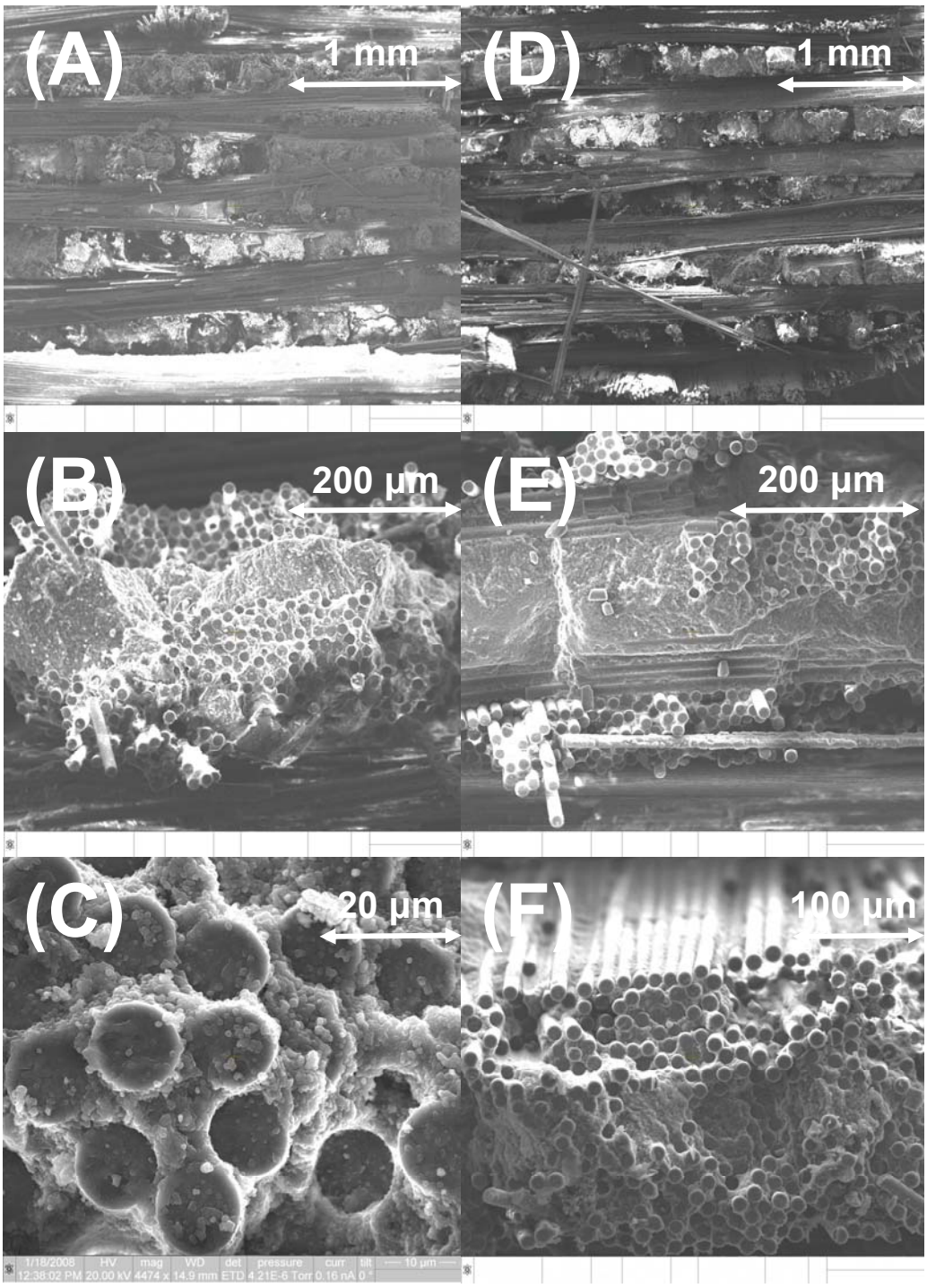

Figure 39. SEM micrographs of N720/AM fracture surfaces produced in creep tests conducted in air at 1200°C at stress levels of: (a)-(c) 73 MPa, (d)-(f) 136 MPa.

Figures 40 (a), (b) and (c) show the fracture surface of the N720/AM specimen subjected to a creep test at 73 MPa in argon. The specimen nearly achieved a run-out, the time to failure was 92.8 h. The fracture surface again is dominated by areas of planar failure, but also seen are small areas of short fiber pull-out, as was the case with the specimen tested in air at 73 MPa. The fracture surface also contains large amounts of brushy 90° fibers. Figures 40 (d), (e) and (f) show the N720/AM fracture surfaces obtained in creep-rupture tests in argon at 136 MPa. The fracture surface exhibits no signs of 0° fiber pull-out and is almost entirely planar.

Fracture surfaces of the N720/AM composite obtained in steam at both 73 and 136 MPa are dominated by planar areas of correlated failure of the 0° fibers (see Figure 41). Large matrix rich areas were observed in the specimen tested at 136 MPa.

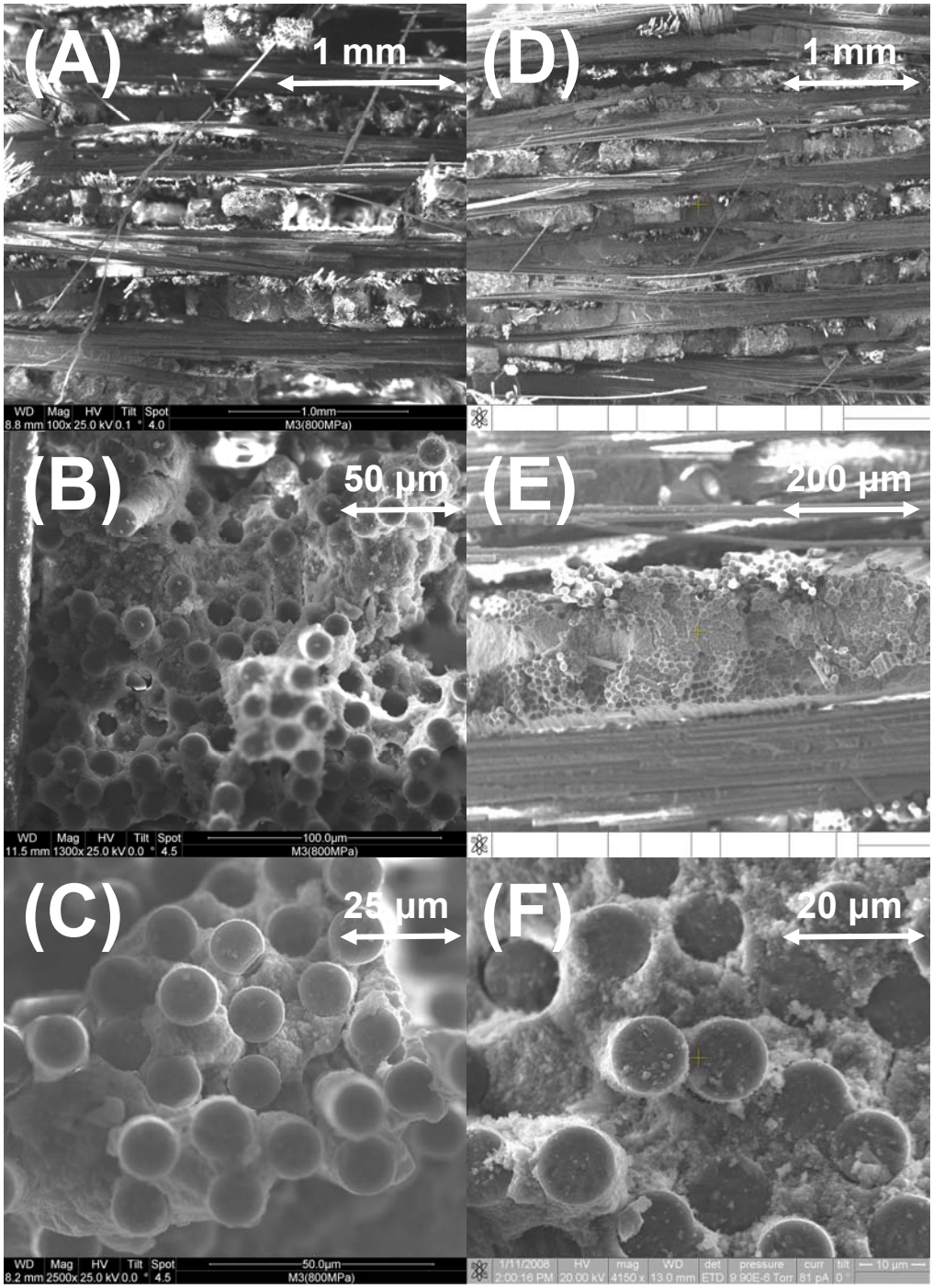

Figure 40. SEM micrographs of N720/AM fracture surfaces produced in creep tests conducted in argon at 1200°C at stress levels of: (a)-(c) 73 MPa, (d)-(f) 136 MPa.

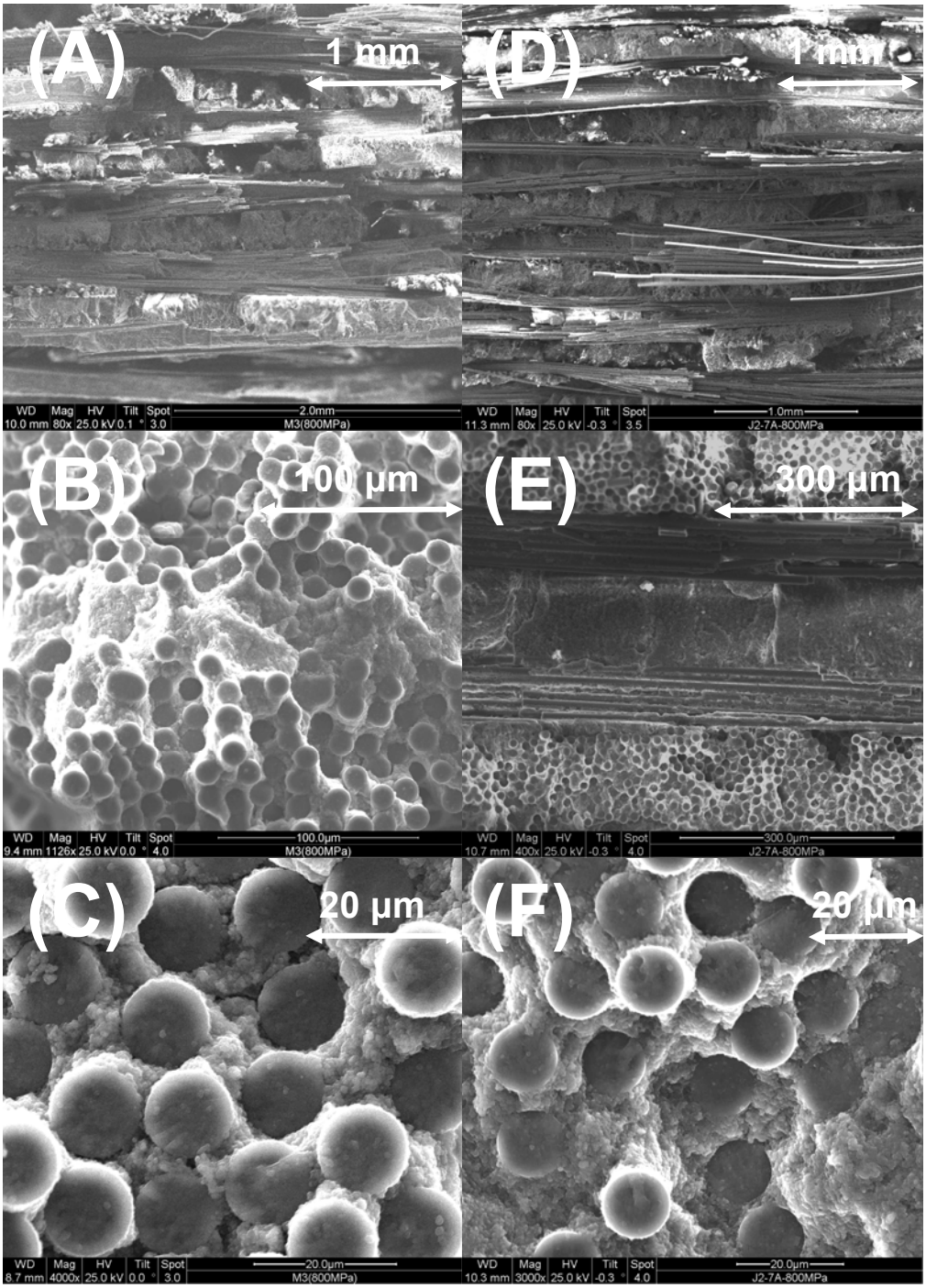

Figure 41. SEM micrographs of N720/AM fracture surfaces produced in creep tests conducted in steam at 1200°C at stress levels of: (a)-(c) 73 MPa, (d)-(f) 136 MPa.

Figures 42 (a), (b) and (c) show fracture surfaces of the N720/AM specimen subjected to a displacement controlled monotonic tensile test to failure in air at 1200°C. When compared to the fracture surface of the specimen subjected to 100 h of prior creep in air, the microstructures are nearly identical (see Figures 39 (a), (b) and (c)). Again the surface is dominated by planar areas of correlated fiber fracture, with minimal fiber pull-out. Recall that the 100 h of prior creep had little effect on the retained tensile strength of the specimen tested in air at 73 MPa. The similarities in microstructures of the two fracture surfaces further support this finding.

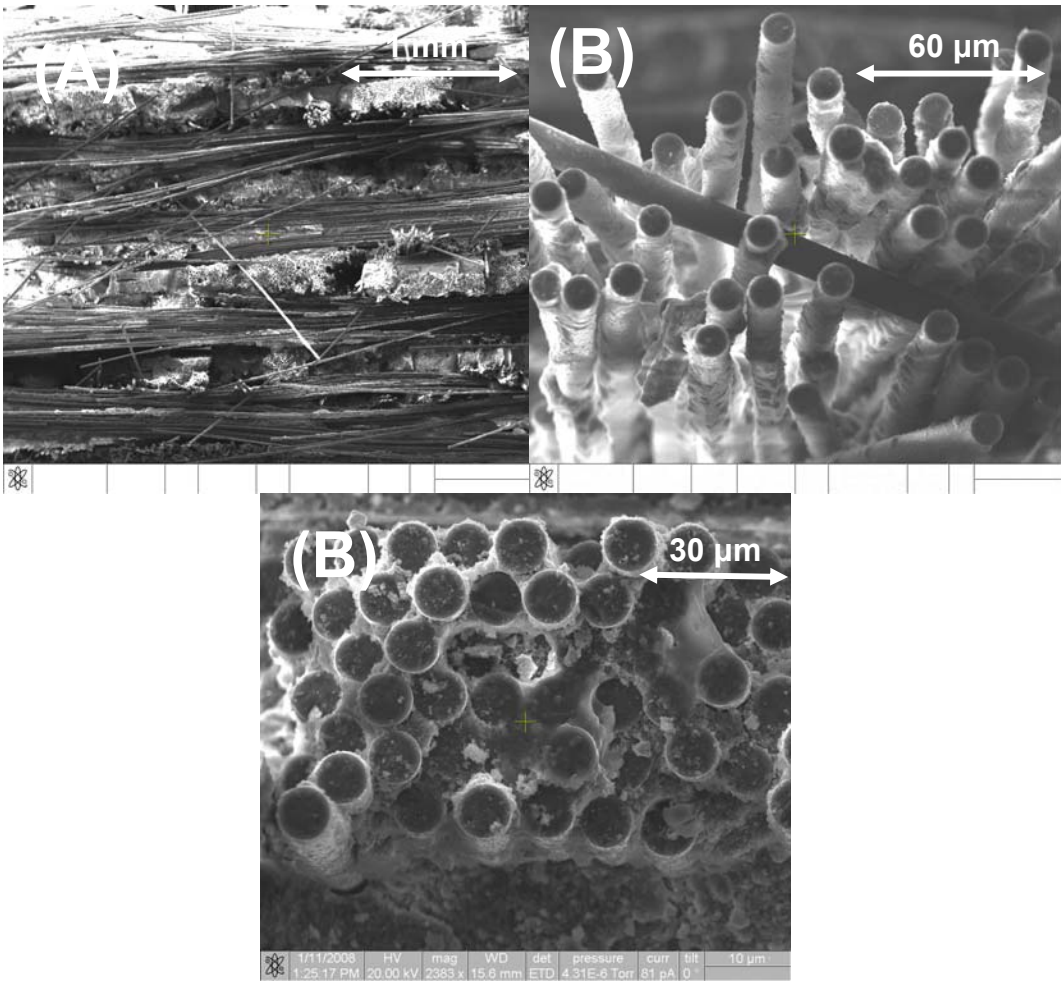

Figure 42. SEM micrographs of N720/AM fracture surfaces obtained in monotonic tensile tests in air at 1200°C, various magnifications.

V. Conclusions and Recommendations

5.1 Tensile Stress-Strain Behavior and Properties, Influence of Loading Rate

The tensile stress-strain behavior of N720/AM composite was investigated and the compressive properties measured at 1200 °C in laboratory air and in steam. The average tensile modulus was 74.5 GPa (equivalent to 82.0 GPa for $V_f = 0.44$) and the average tensile strength was 153.2 MPa (equivalent to 168.5 MPa for $V_f = 0.44$). Note that the tensile modulus of N720/AM CMC is slightly higher, while the UTS is somewhat below the corresponding values for the N720/A composite [13, 23, 24, 15]. The tensile stress-strain curve departs from linearity at the stresses between 20 and 30 MPa. However, the nonlinearity is not strongly pronounced. Such stress-strain behavior is qualitatively similar to that exhibited by the N720/A composite at 1200 °C [13, 23, 24, 15].

The influence of the loading rate on tensile behavior and properties was explored in constant stress-rate tests conducted at 25 and 0.0025 MPa/s at 1200 °C in steam. Tensile strength and modulus are influenced by the loading rate. As the loading rate decreases by four orders of magnitude, tensile modulus drops by 54% and tensile strength by 38%. At 0.0025 MPa/s in steam the tensile stress-strain behavior becomes distinctly nonlinear. Considerable inelastic strains develop as the stress exceeds 40 MPa.

5.2 Creep-Rupture

The creep-rupture behavior was evaluated for stress levels ranging from 73 MPa (equivalent to 80 MPa for $V_f = 0.44$) to 136 MPa (equivalent to 150 MPa for $V_f = 0.44$) at 1200 °C in air, argon and steam. In air and in steam the N720/AM composite exhibits

primary and secondary creep regimes. In argon, primary, secondary and tertiary creep regimes were observed. The creep strains accumulated at the two lower stress levels were higher than the failure strain obtained in tensile tests. The largest creep strains were accumulated at 73 and 91 MPa in argon and in steam. Conversely, all creep strains accumulated by the N720/A CMC exceeded the failure strain obtained in tension tests. In the case of the N720/A composite, the largest creep strains were accumulated in steam, while creep strains accumulated in argon were similar to those produced in air.

Minimum creep rate was reached in all tests. At 1200 °C, creep rates of N720/AM ranged from 9.0×10^{-9} to 8.0×10^{-7} s^{-1} in air, from 1.0×10^{-7} to 2.0×10^{-5} s^{-1} in argon, and from 2.0×10^{-7} to 2.0×10^{-5} s^{-1} in steam. In air, the creep rates of N720/AM were five times lower than those of the N720/A composite. However, in steam the creep rates produced by N720/AM CMC were two times those obtained for the N720/A. While the presence of argon had a minimal effect on the creep rate of N720/A, in the case of the N720/AM composite the effect of argon on the secondary creep rate was nearly as degrading as that of the steam environment. The creep rates of the N720/AM in argon were at least an order of magnitude higher than those in air and similar to those obtained in steam.

The N720/AM composite achieved creep run-out of 100 h at 73 MPa (equivalent to 80 MPa for $V_f = 0.44$) and 91 MPa (equivalent to 100 MPa for $V_f = 0.44$) at 1200 °C in air. In argon, creep lifetime of 92.8 h (approaching a 100-h run-out condition) was achieved at 73 MPa (equivalent to 80 MPa for $V_f = 0.44$). The presence of steam dramatically reduced creep lifetimes of N720/AM. Reductions in creep life due to steam were 63 to 98%. The presence of argon also had a detrimental effect on the creep

performance of N720/AM, reducing the creep lifetimes by 81 to 98%. The N720/AM specimens which achieved creep run-out in air retained over 100% of their tensile strength, whereas their modulus decreased by 10%.

Linear elastic crack growth model was employed to predict the time to failure under constant stress at 1200 °C in steam from the constant stress-rate data. A good agreement between the predicted lifetimes and the experimental results indicates that the power-law type subcritical (slow) crack growth due to stress corrosion is the governing failure mechanism at 1200 °C in steam.

Appendix: Additional SEM Micrographs

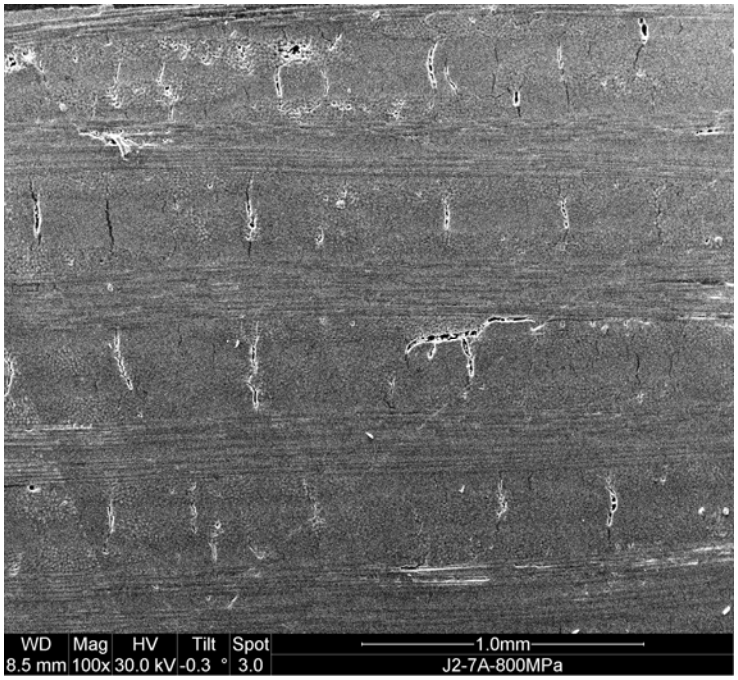

Figure 43. Virgin N720/AM specimen, 100X

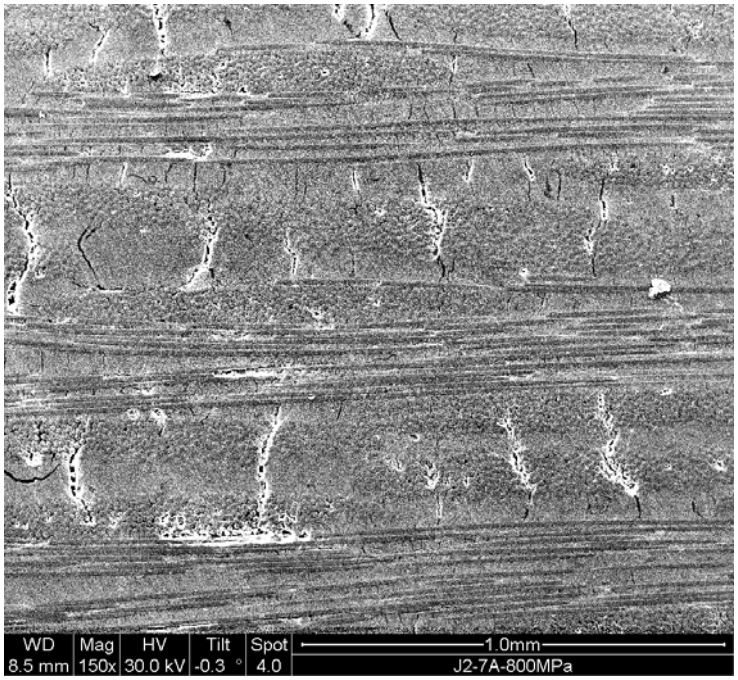

Figure 44. Virgin N720/AM specimen, 150X

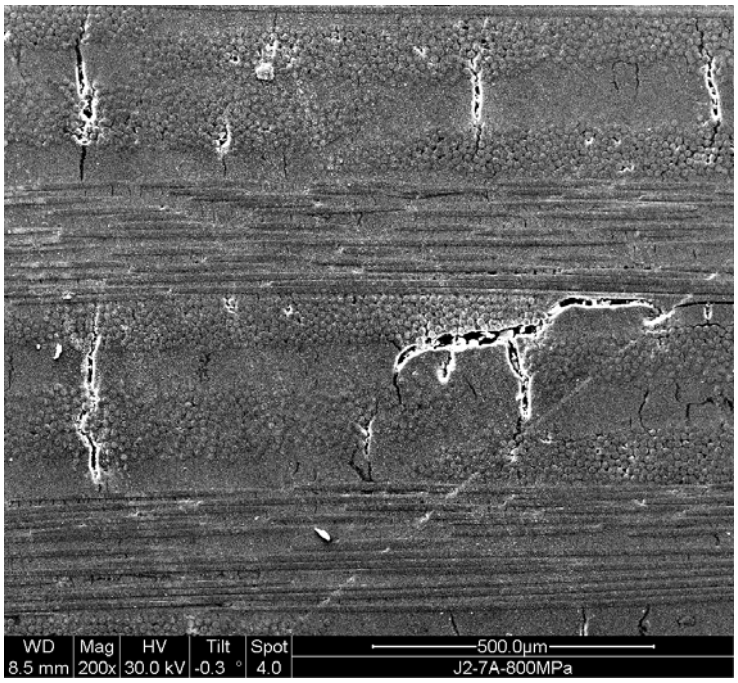

Figure 45. Virgin N720/AM specimen, 200X

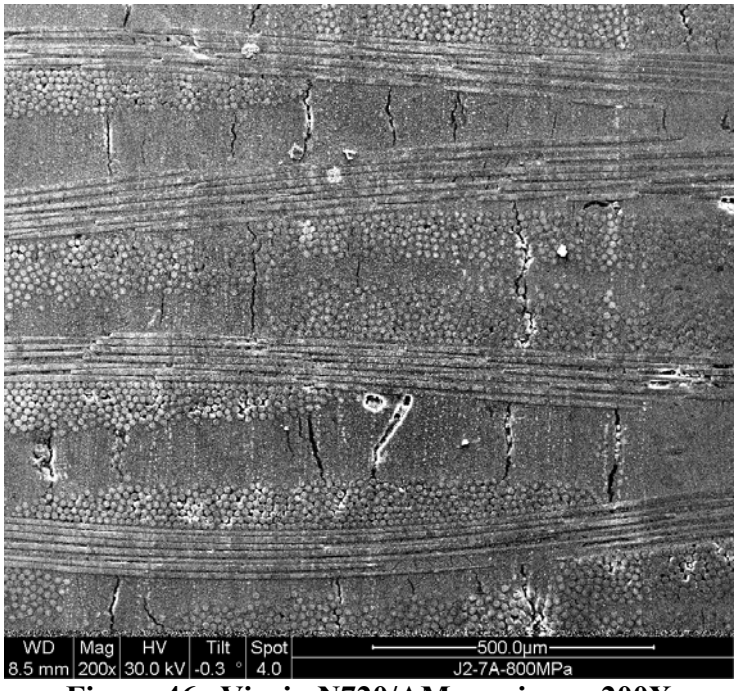

Figure 46. Virgin N720/AM specimen, 200X

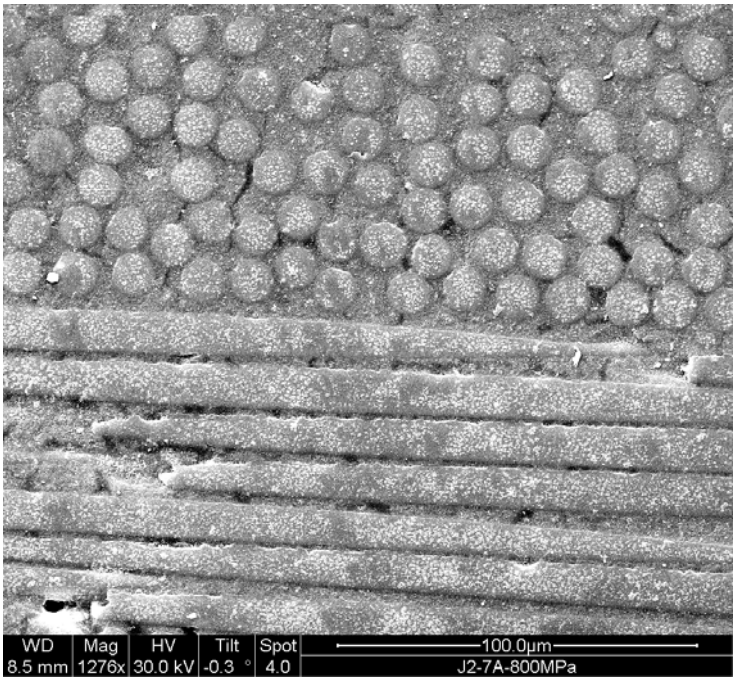

Figure 47. Virgin N720/AM specimen, 1276X

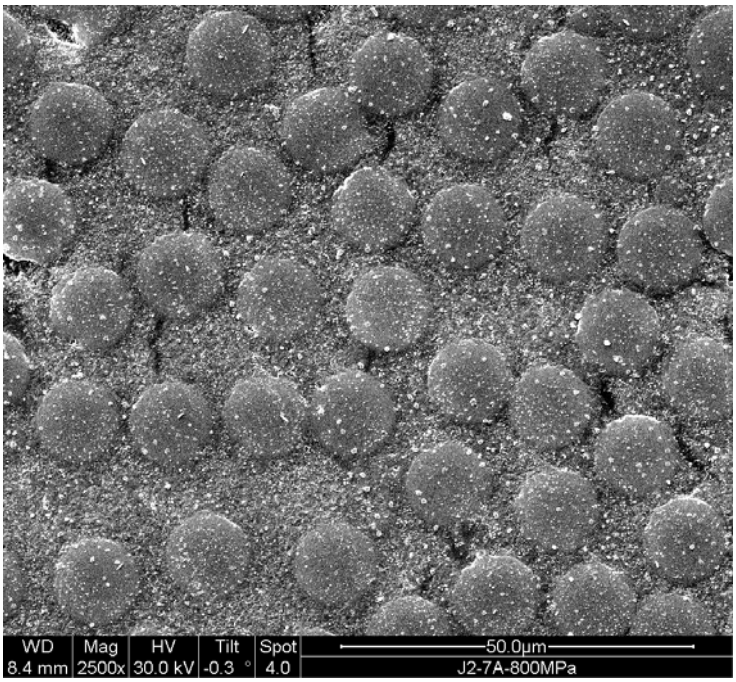

Figure 48. Virgin N720/AM specimen, 2500X

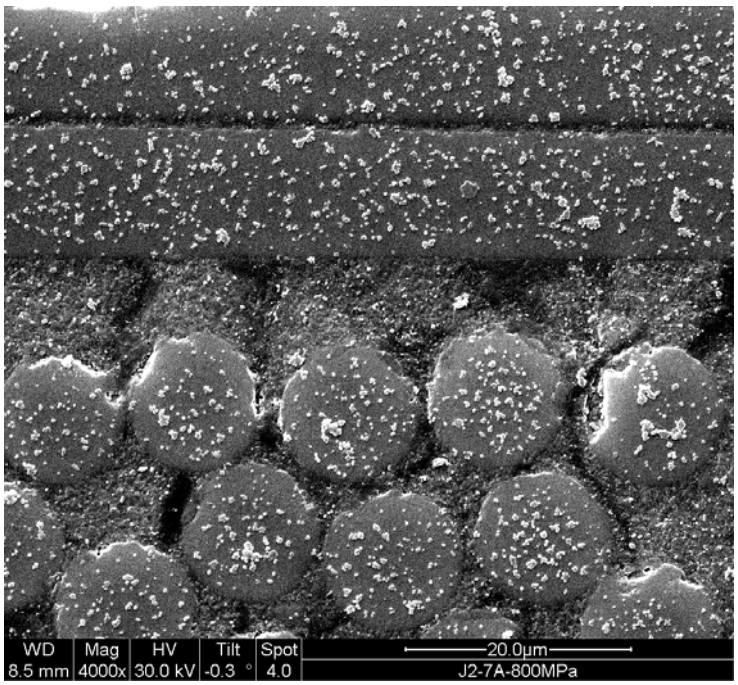

Figure 49. Virgin N720/AM specimen, 4000X

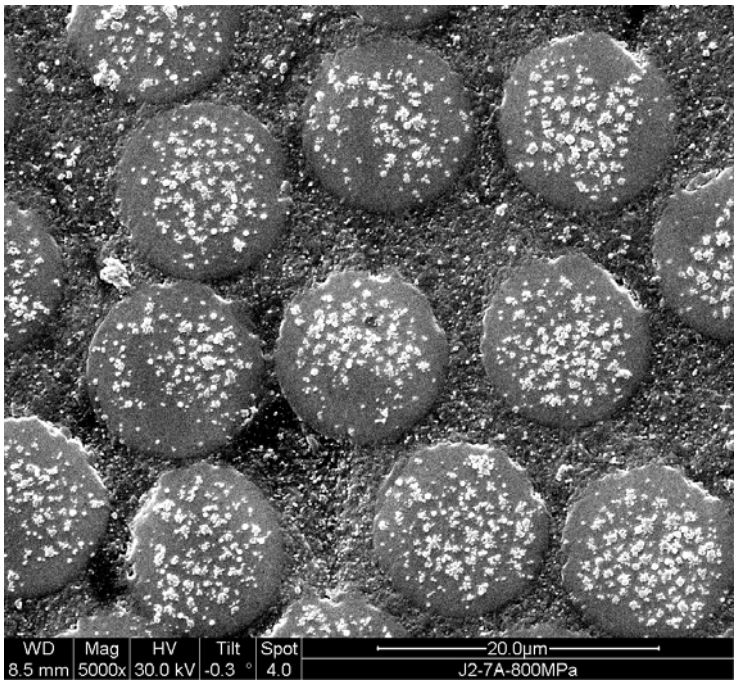

Figure 50. Virgin N720/AM specimen, 5000X

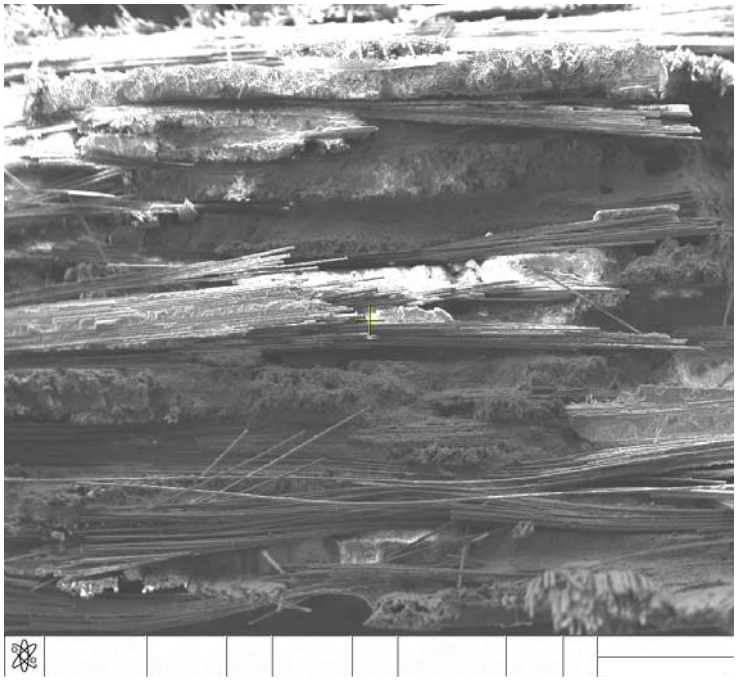

Figure 51. Specimen CG-2 (1200°C, air, tensile), 81X.

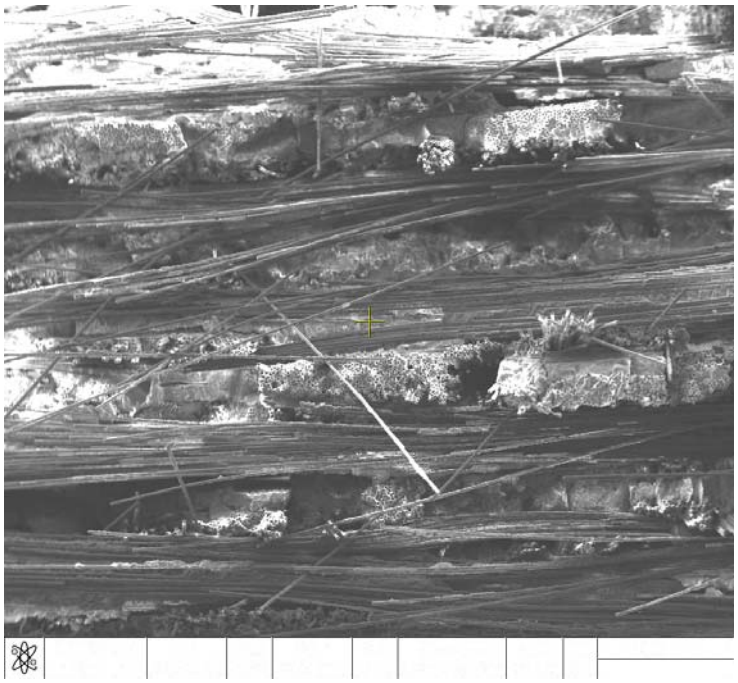

Figure 52. Specimen CG-2 (1200°C, air, tensile), 97X.

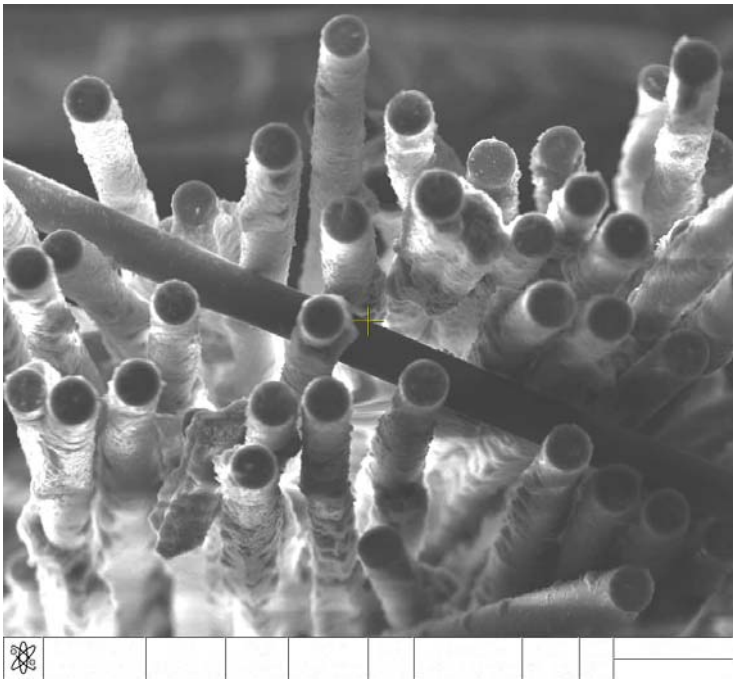

Figure 53. Specimen CG-2 (1200°C, air, tensile), 1545X.

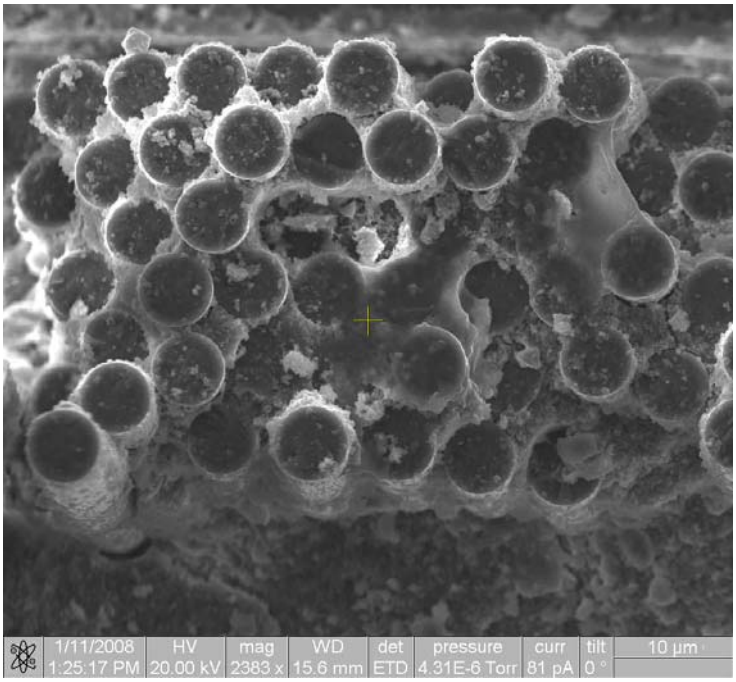

Figure 54. Specimen CG-2 (1200°C, air, tensile), 2383X.

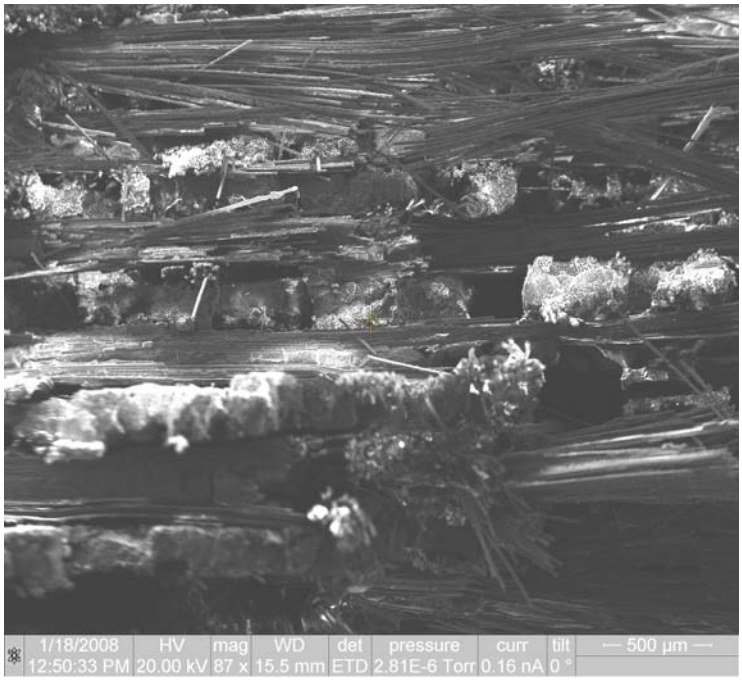

Figure 55. Specimen CG-11 (1200°C, air, 73 MPa, 100 h), 87X.

Figure 56. Specimen CG-11 (1200°C, air, 73 MPa, 100 h), 108X.

Figure 57. Specimen CG-11 (1200°C, air, 73 MPa, 100 h), 280X.

Figure 58. Specimen CG-11 (1200°C, air, 73 MPa, 100 h), 513X.

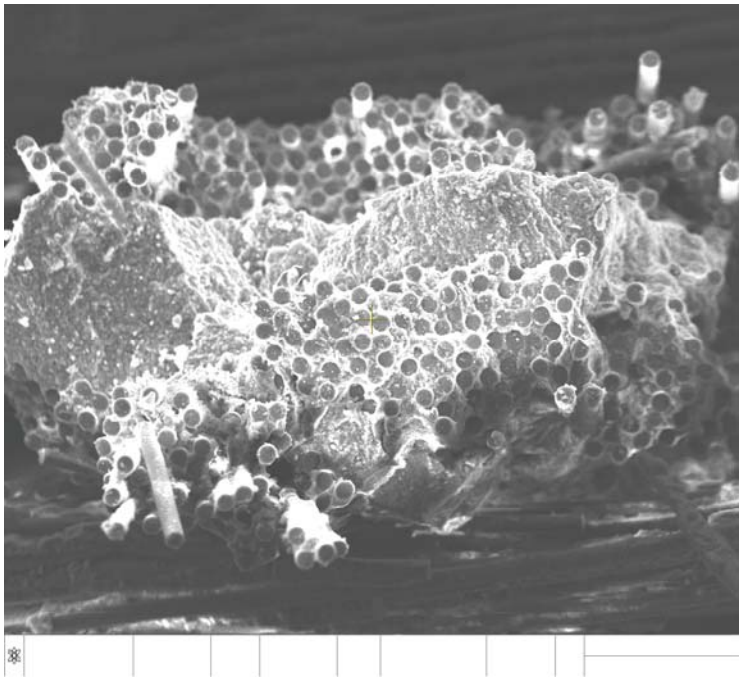

Figure 59. Specimen CG-11 (1200°C, air, 73 MPa, 100 h), 610X.

Figure 60. Specimen CG-11 (1200°C, air, 73 MPa, 100 h), 862X.

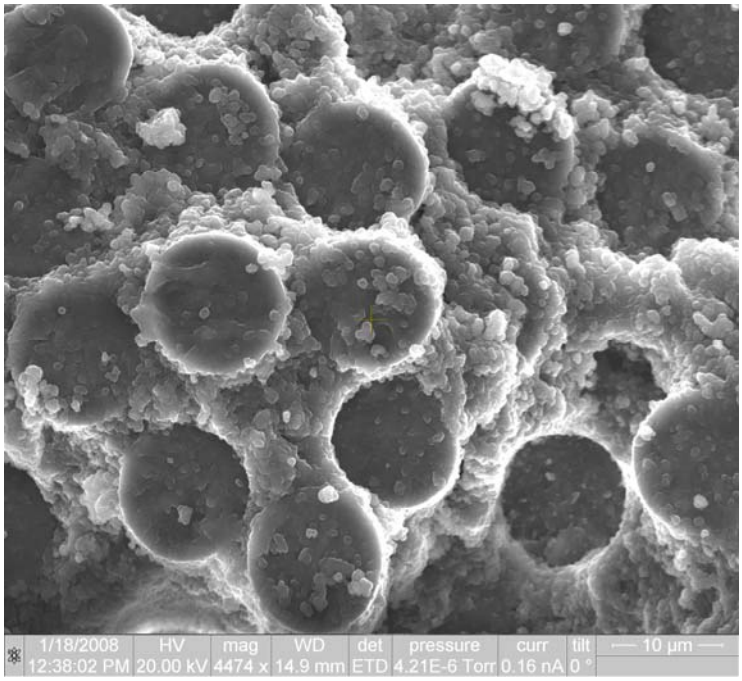

Figure 61. Specimen CG-11 (1200°C, air, 73 MPa, 100 h, 4474X).

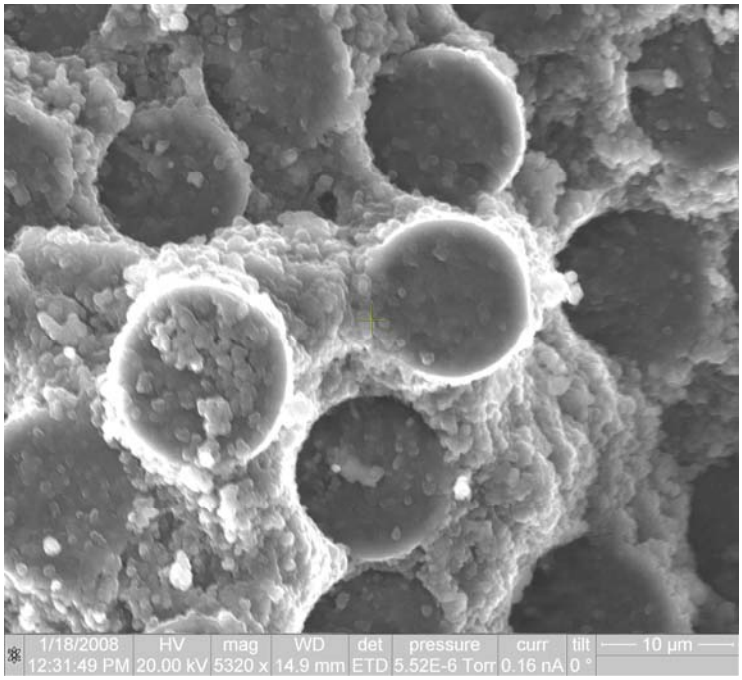

Figure 62. Specimen CG-11 (1200°C, air, 73 MPa, 100 h), 5320X.

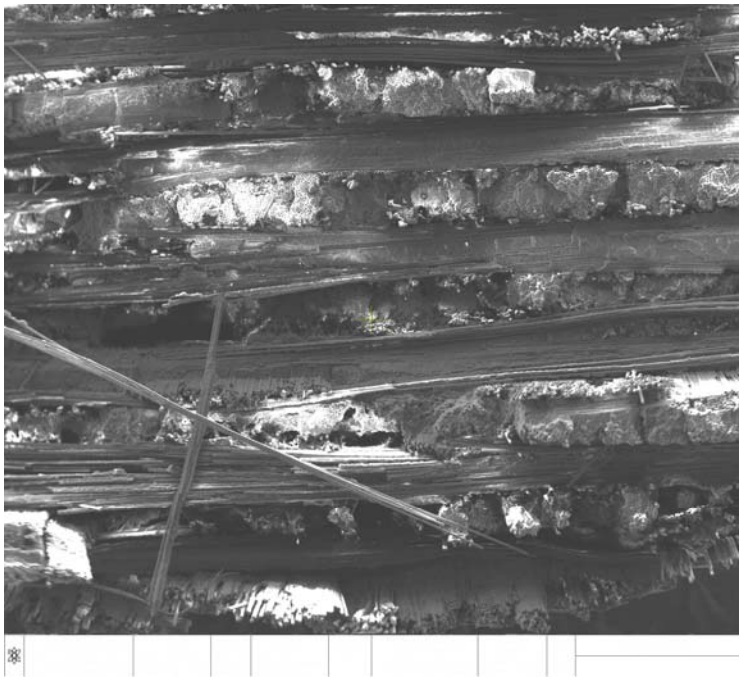

Figure 63. Specimen CG-10 (1200°C, air, 136 MPa, 0.59 h), 80X.

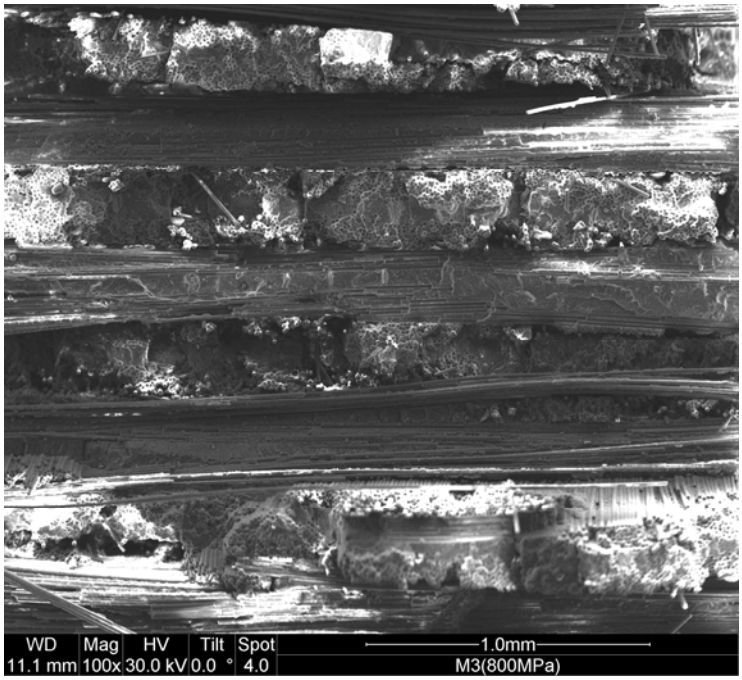

Figure 64. Specimen CG-10 (1200°C, air, 136 MPa, 0.59 h), 100X.

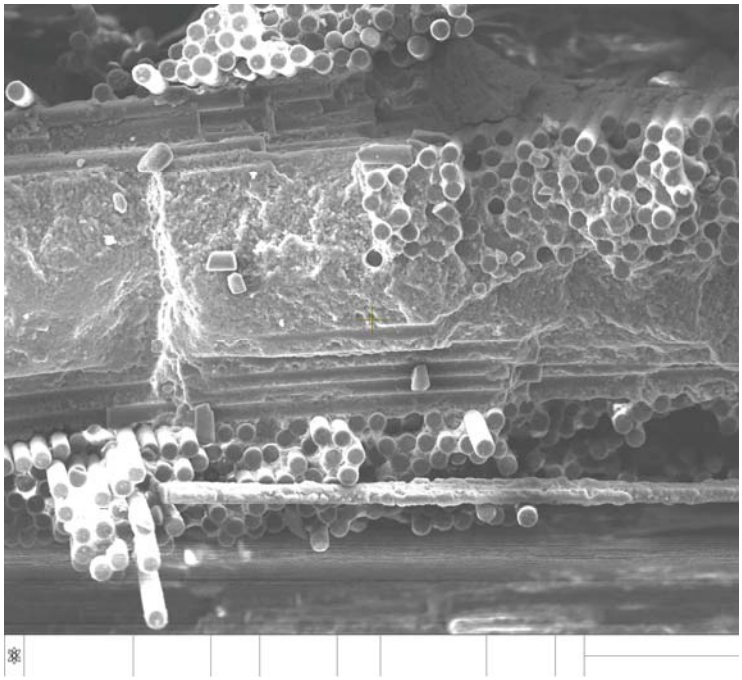

Figure 65. Specimen CG-10 (1200°C, air, 136 MPa, 0.59 h), 611X.

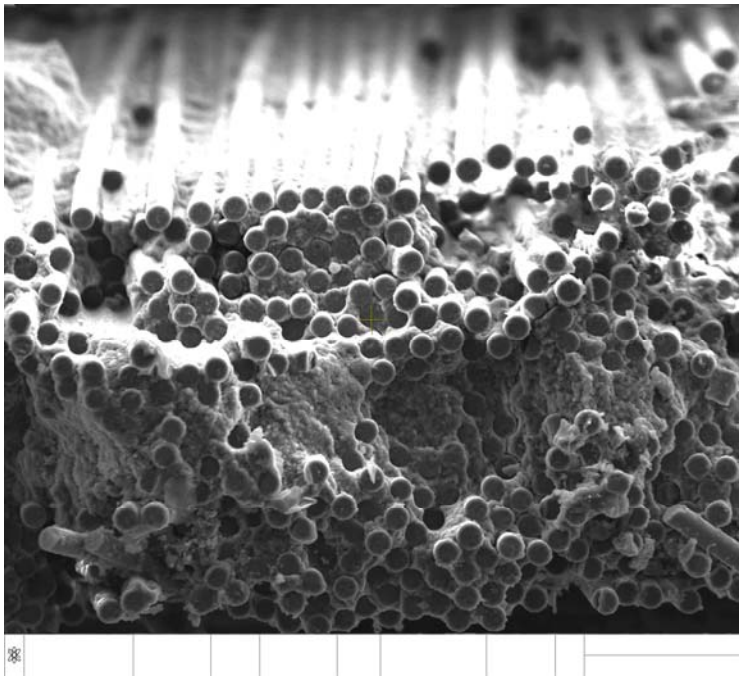

Figure 66. Specimen CG-10 (1200°C, air, 136 MPa, 0.59 h), 784X.

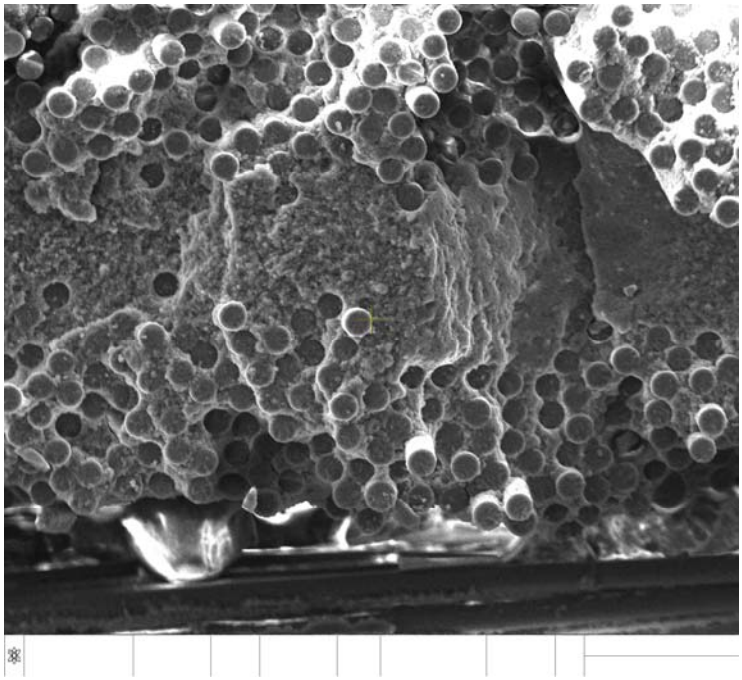

Figure 67. Specimen CG-10 (1200°C, air, 136 MPa, 0.59 h), 905X.

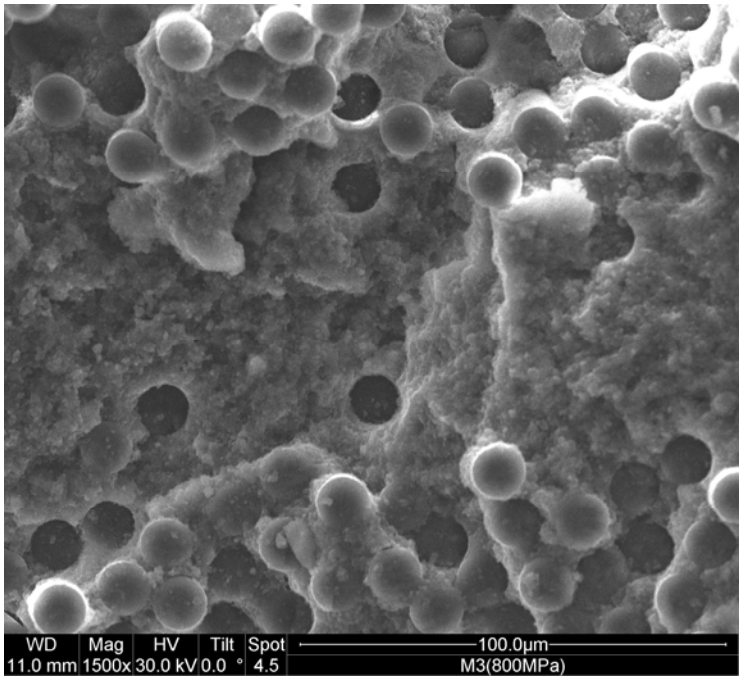

Figure 68. Specimen CG-10 (1200°C, air, 136 MPa, 0.59 h), 1500X.

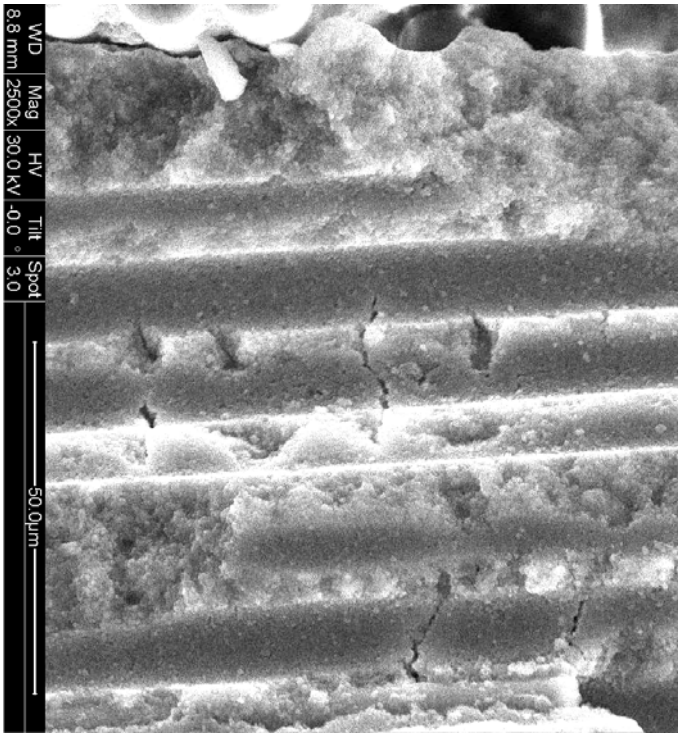

Figure 69. Specimen CG-10 (1200°C, air, 136 MPa, 0.59 h), 2500X.

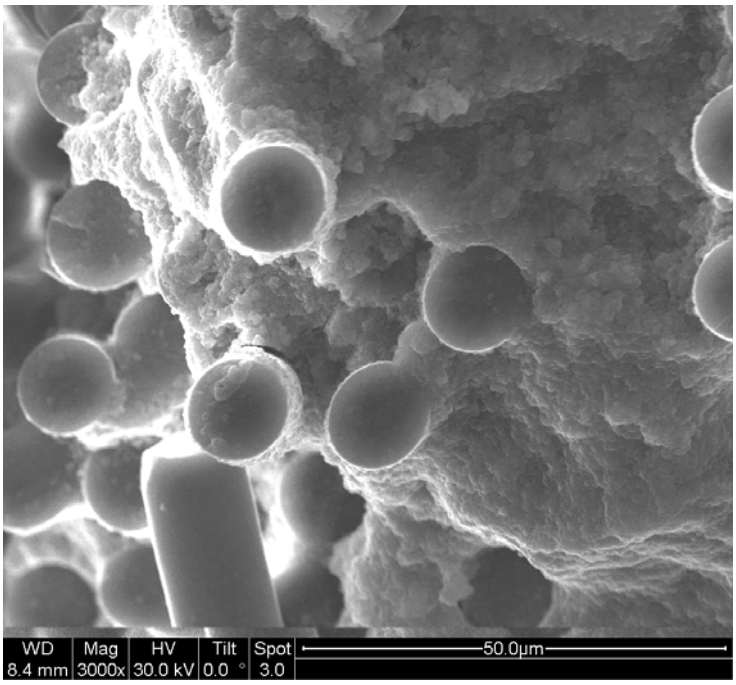

Figure 70. Specimen CG-10 (1200°C, air, 136 MPa, 0.59 h), 3000X.

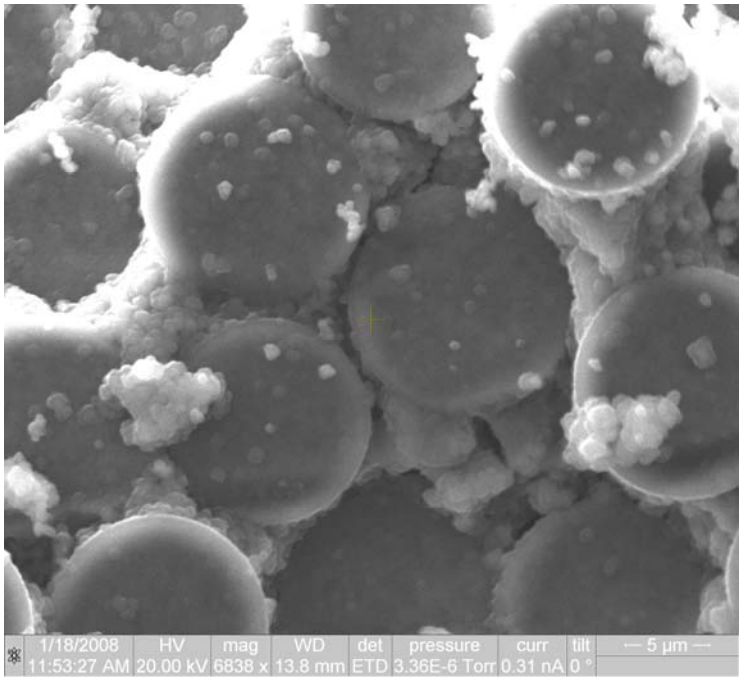

Figure 71. Specimen CG-10 (1200°C, air, 136 MPa, 0.59 h), 6838X.

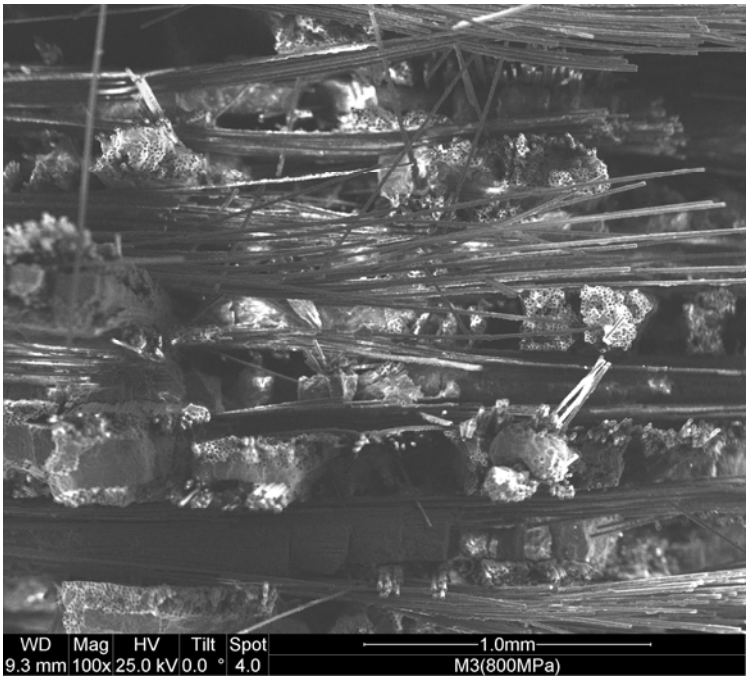

Figure 72. Specimen CG-24 (1200°C, argon, 73 MPa, 92.8 h), 100X.

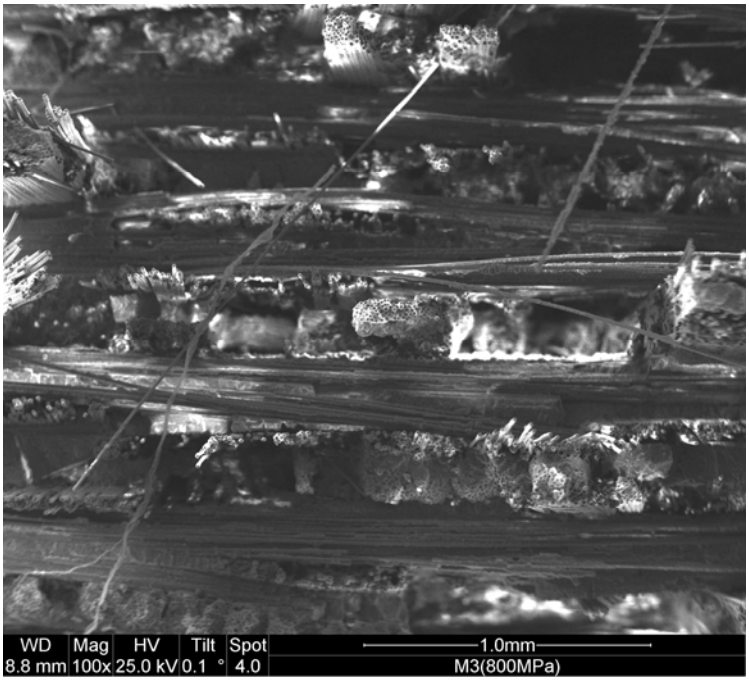

Figure 73. Specimen CG-24 (1200°C, argon, 73 MPa, 92.8 h), 100X.

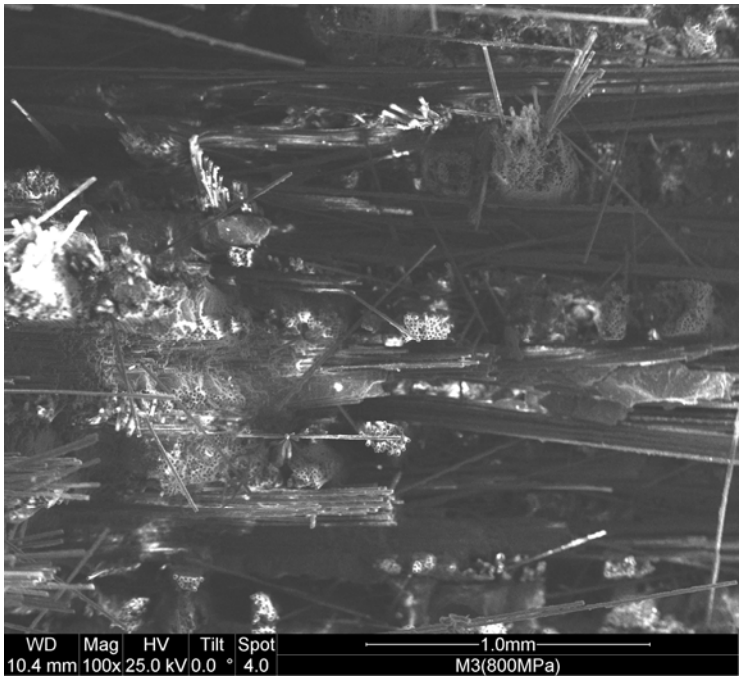

Figure 74. Specimen CG-24 (1200°C, argon, 73 MPa, 92.8 h), 100X.

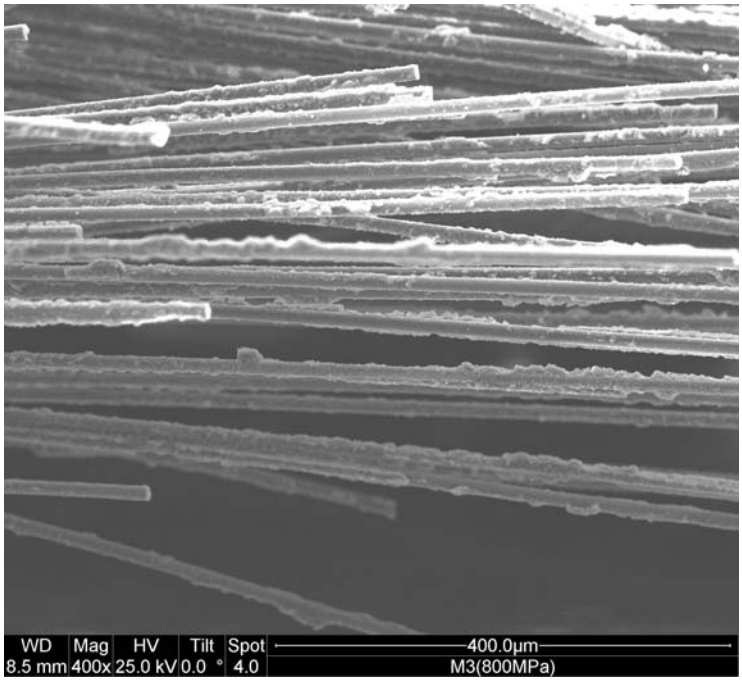

Figure 75. Specimen CG-24 (1200°C, argon, 73 MPa, 92.8 h), 400X.

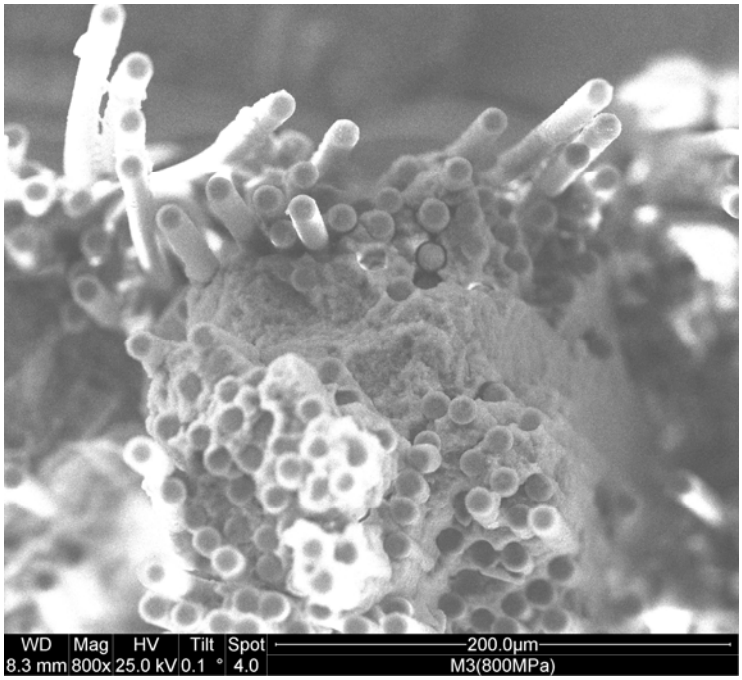

Figure 76. Specimen CG-24 (1200°C, argon, 73 MPa, 92.8 h), 800X.

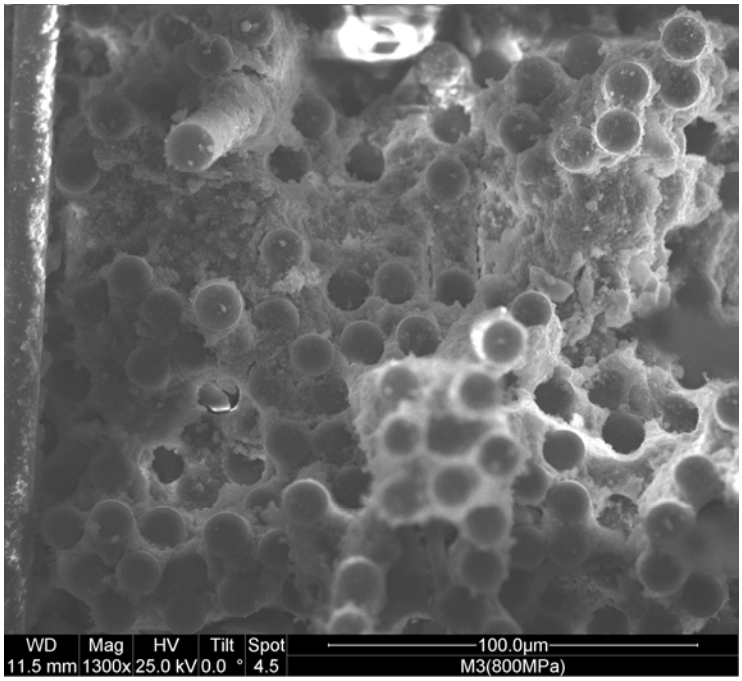

Figure 77. Specimen CG-24 (1200°C, argon, 73 MPa, 92.8 h), 1300X.

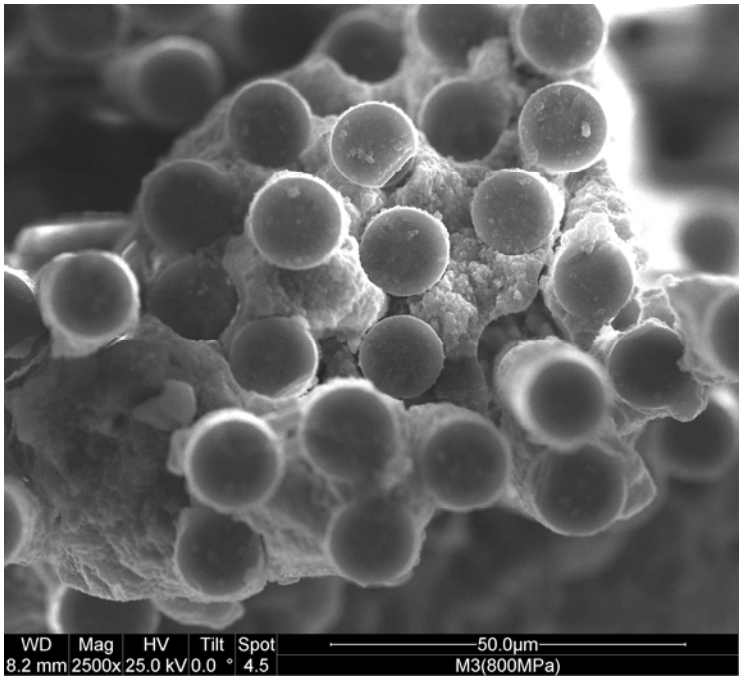

Figure 78. Specimen CG-24 (1200°C, argon, 73 MPa, 92.8 h), 2500X.

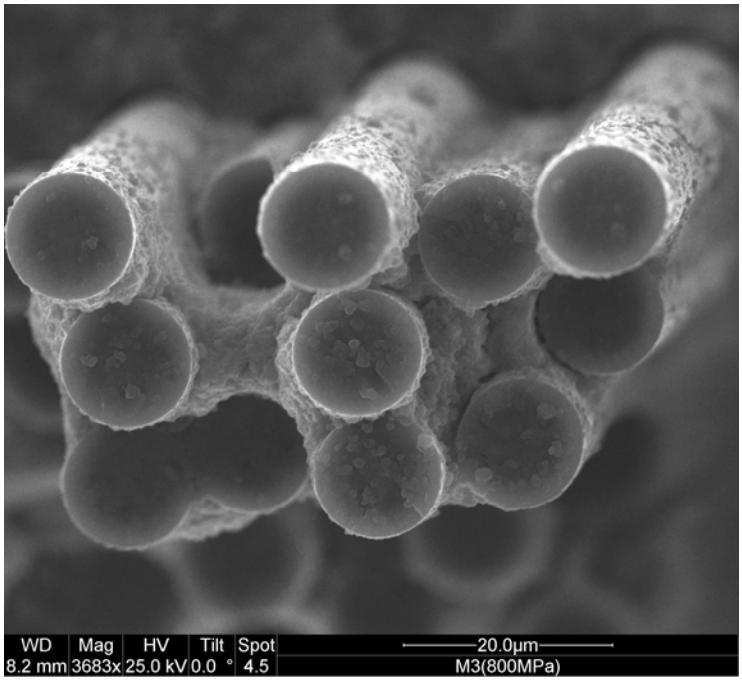

Figure 79. Specimen CG-24 (1200°C, argon, 73 MPa, 92.8 h), 3683X.

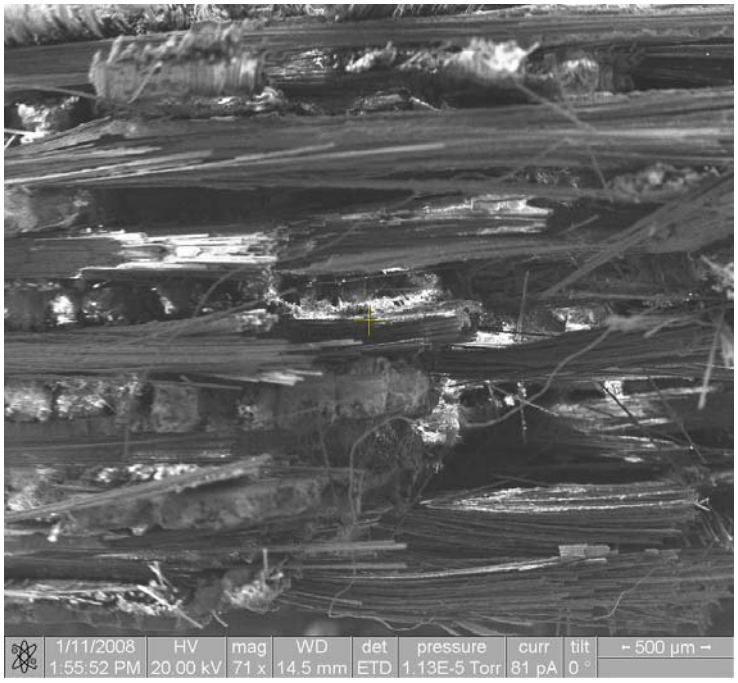

Figure 80. Specimen CG-23 (1200°C, argon, 136 MPa, 0.071 h), 71X.

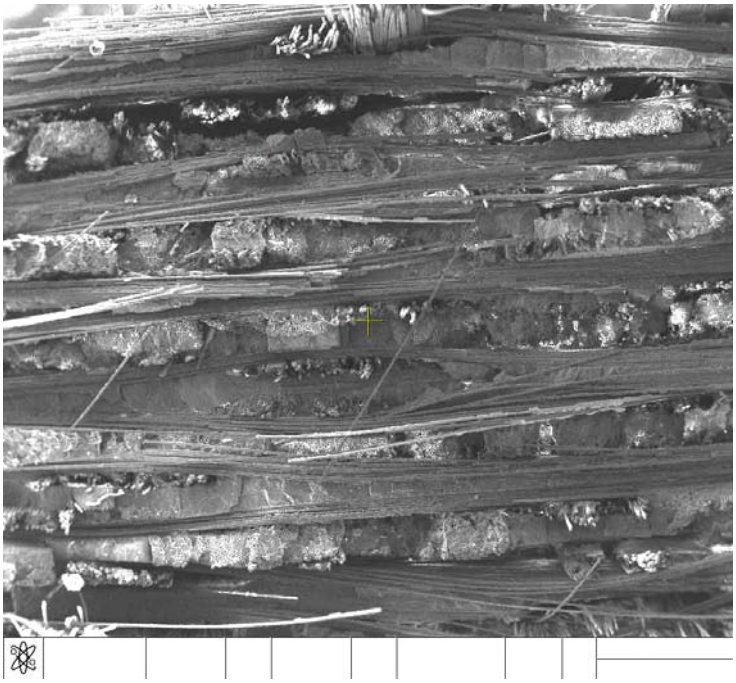

Figure 81. Specimen CG-23 (1200°C, argon, 136 MPa, 0.071 h), 77X.

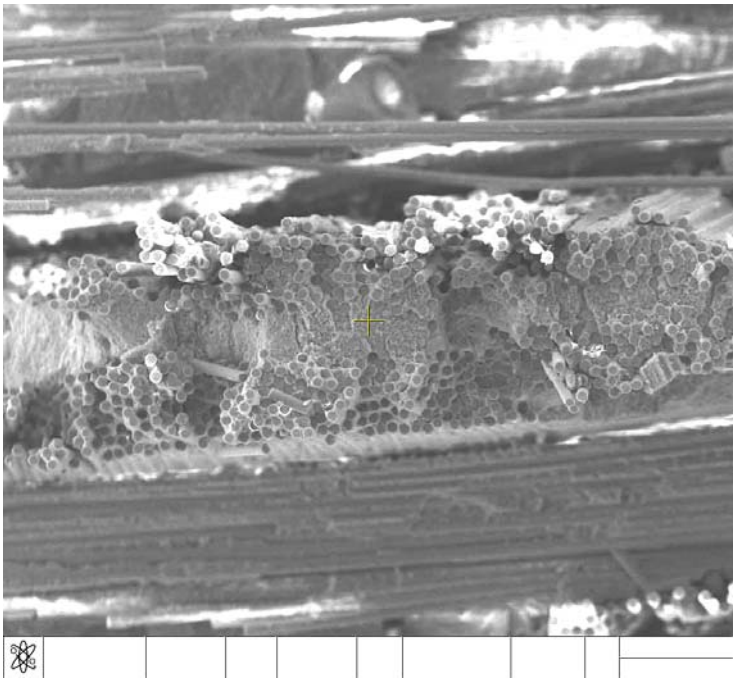

Figure 82. Specimen CG-23 (1200°C, argon, 136 MPa, 0.071 h), 367X.

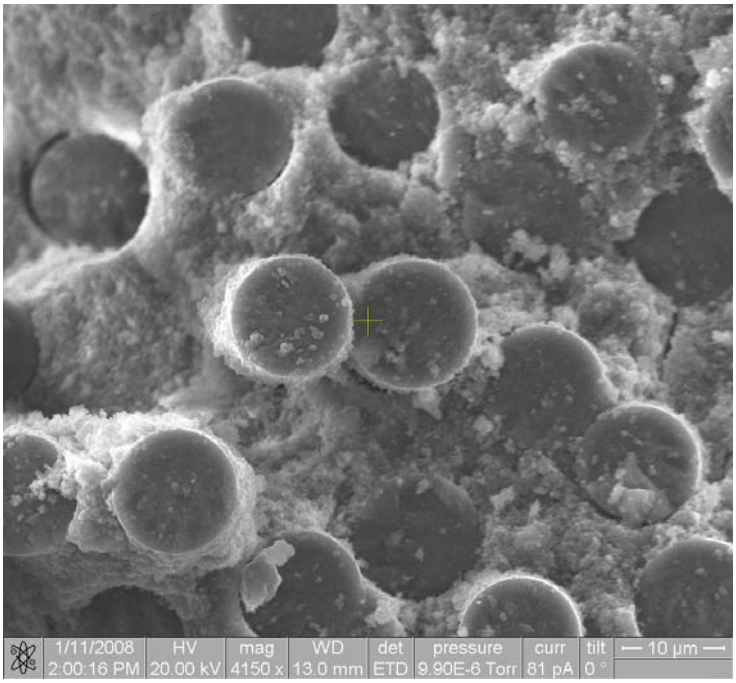

Figure 83. Specimen CG-23 (1200°C, argon, 136 MPa, 0.071 h), 4150X.

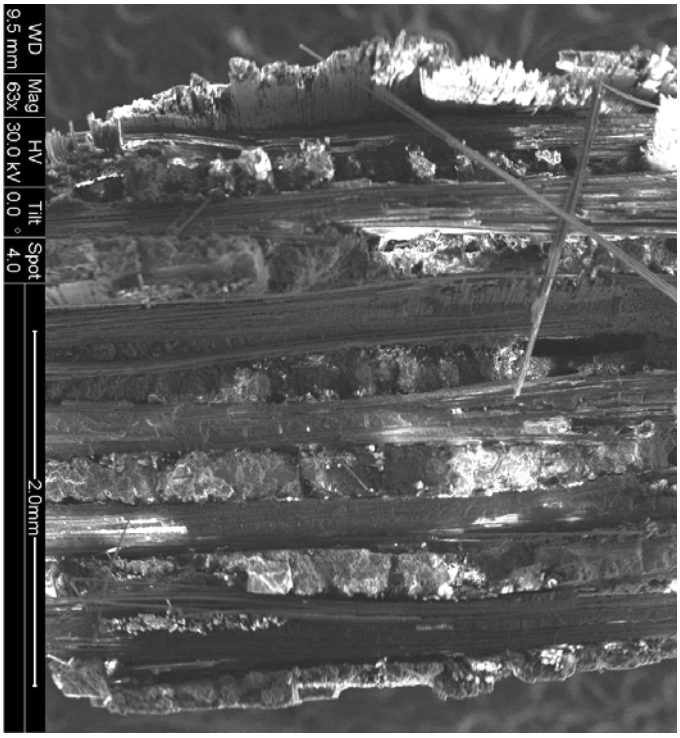

Figure 84. Specimen CG-16 (1200°C, steam, 73 MPa, 37 h), 63X.

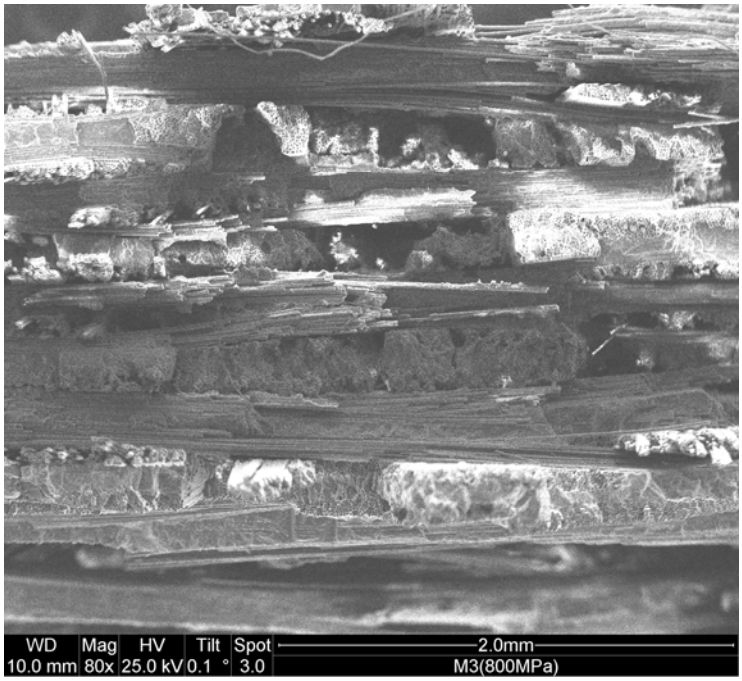

Figure 85. Specimen CG-16 (1200°C, steam, 73 MPa, 37 h), 80X.

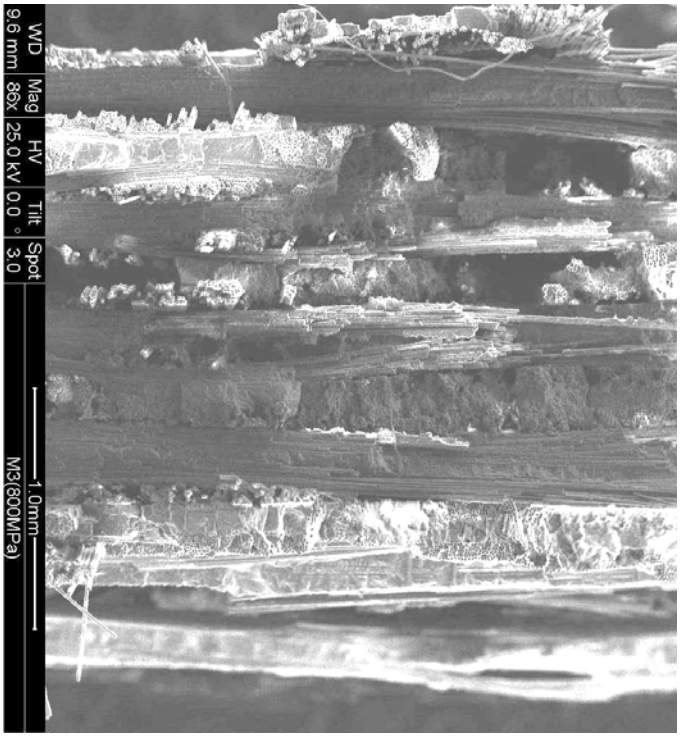

Figure 86. Specimen CG-16 (1200°C, steam, 73 MPa, 37 h), 86X.

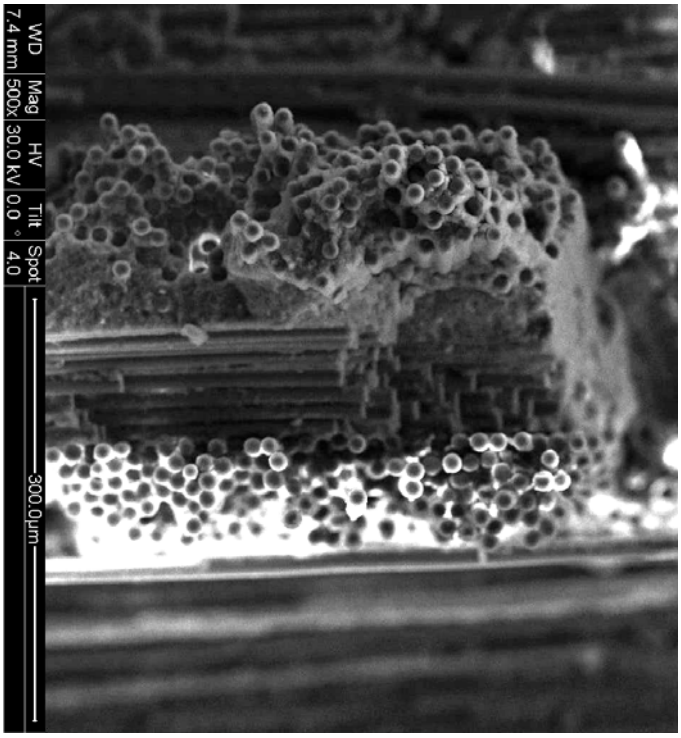

Figure 87. Specimen CG-16 (1200°C, steam, 73 MPa, 37 h), 500X.

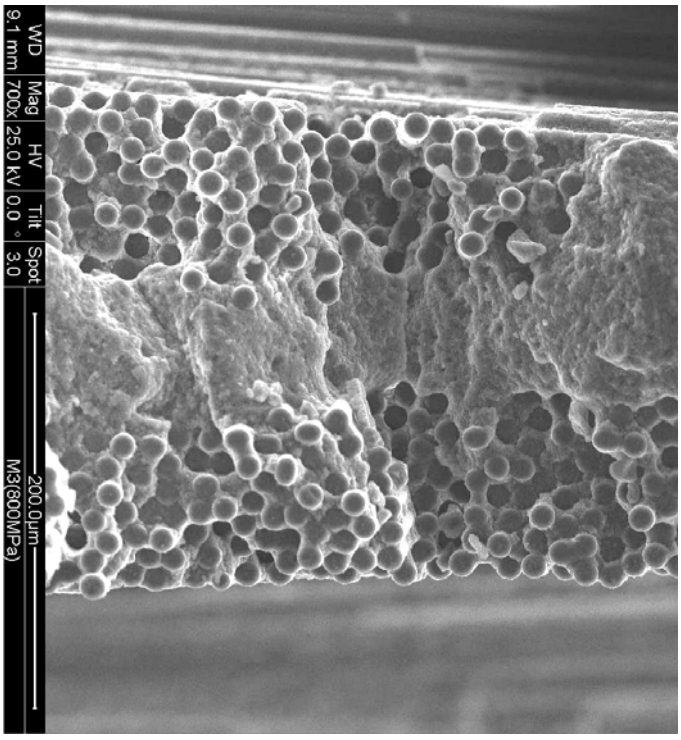

Figure 88. Specimen CG-16 (1200°C, steam, 73 MPa, 37 h), 700X.

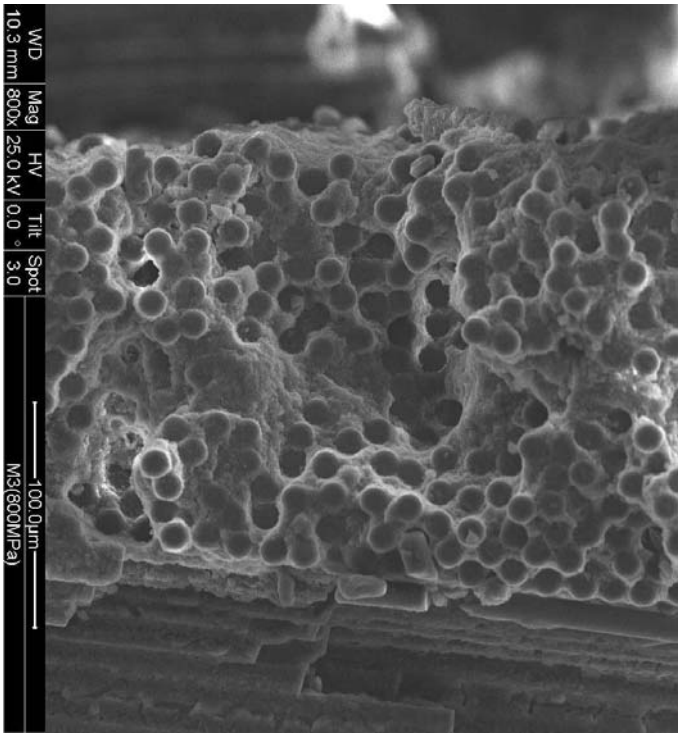

Figure 89. Specimen CG-16 (1200°C, steam, 73 MPa, 37 h), 800X.

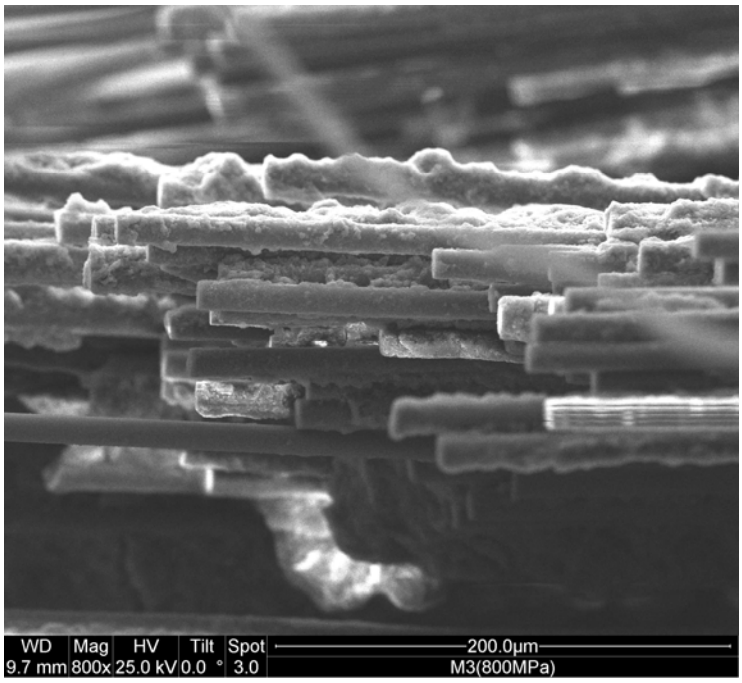

Figure 90. Specimen CG-16 (1200°C, steam, 73 MPa, 37 h), 800X.

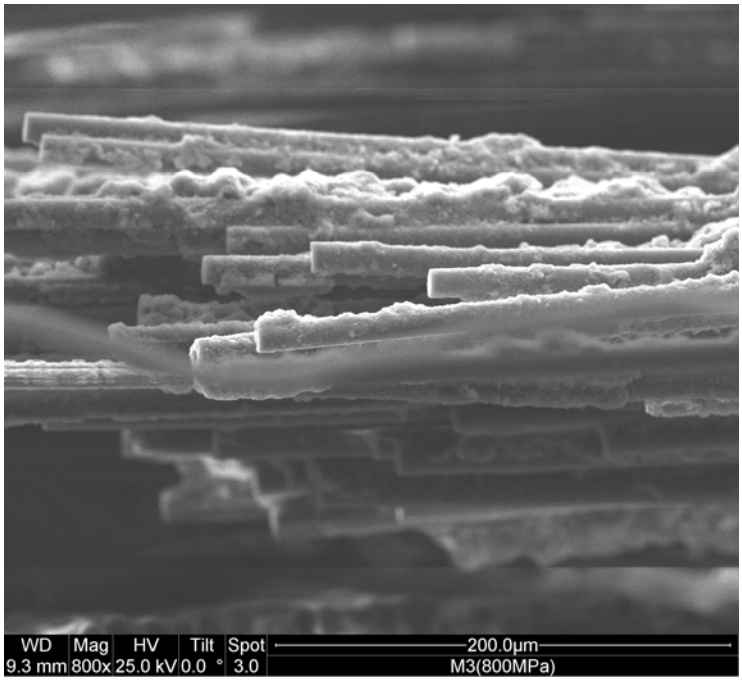

Figure 91. Specimen CG-16 (1200°C, steam, 73 MPa, 37 h), 800X.

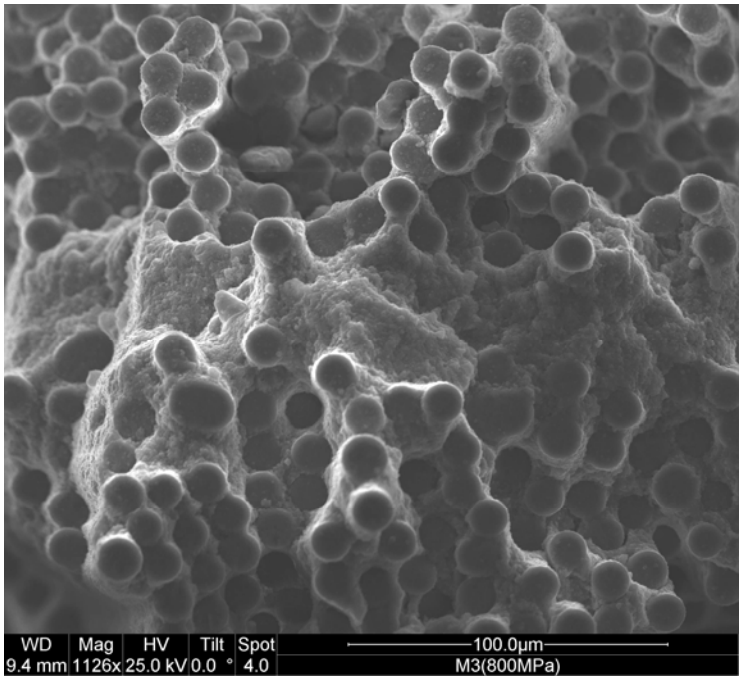

Figure 92. Specimen CG-16 (1200°C, steam, 73 MPa, 37 h), 1126X.

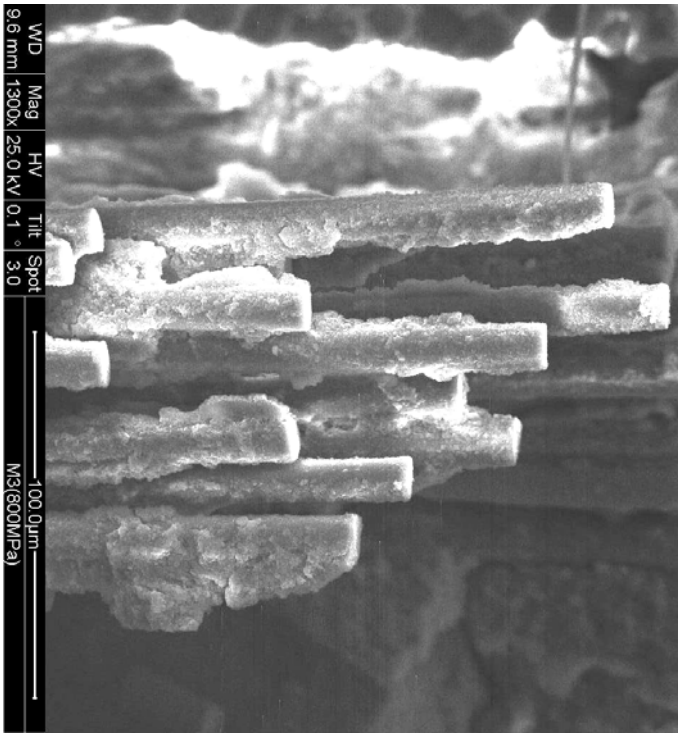

Figure 93. Specimen CG-16 (1200°C, steam, 73 MPa, 37 h), 1300X.

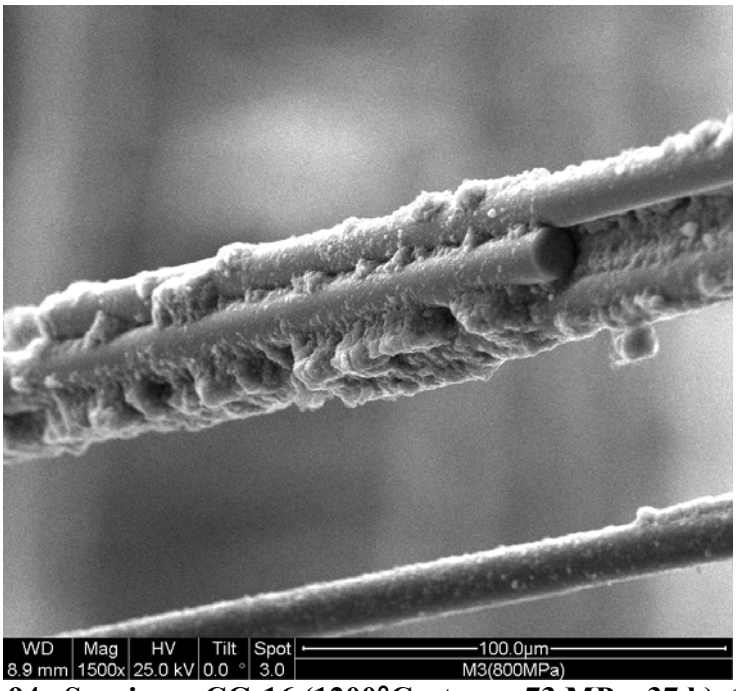

Figure 94. Specimen CG-16 (1200°C, steam, 73 MPa, 37 h), 1500X.

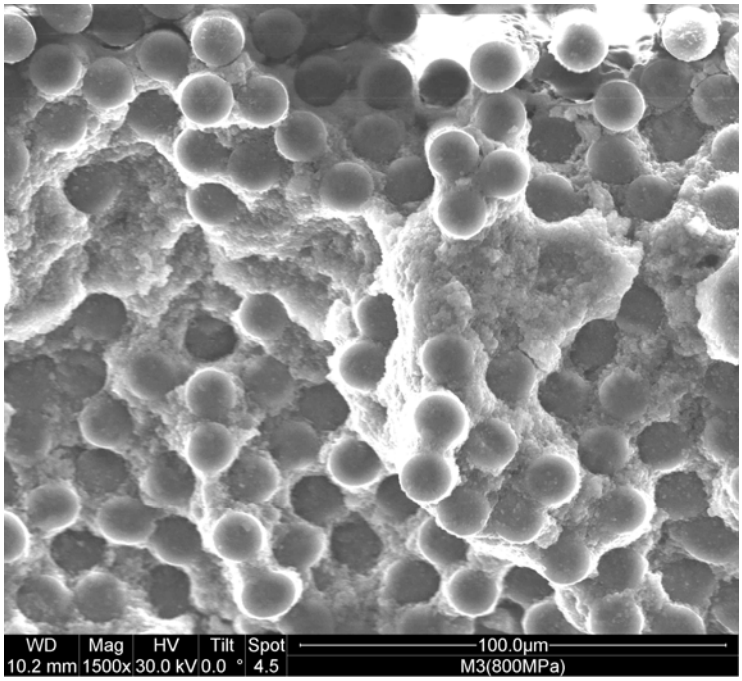

Figure 95. Specimen CG-16 (1200°C, steam, 73 MPa, 37 h), 1500X.

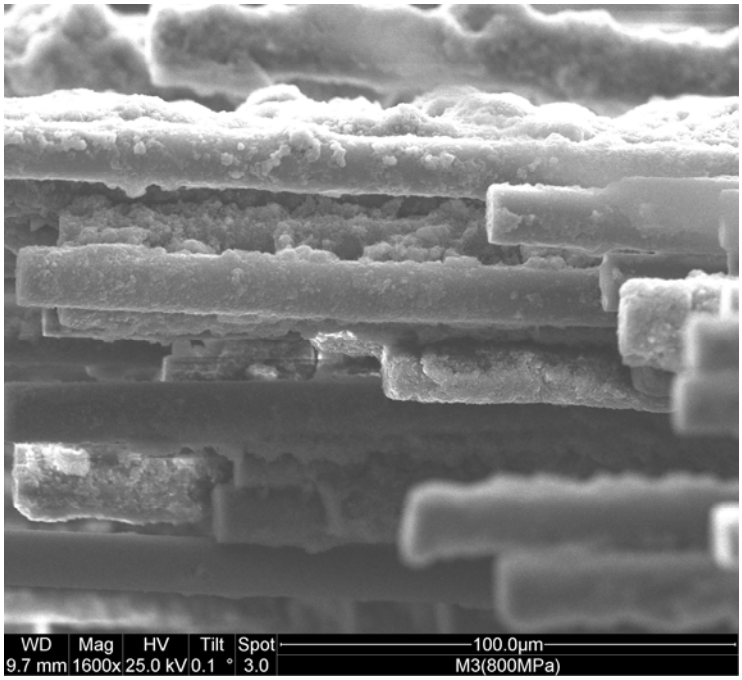

Figure 96. Specimen CG-16 (1200°C, steam, 73 MPa, 37 h), 1600X.

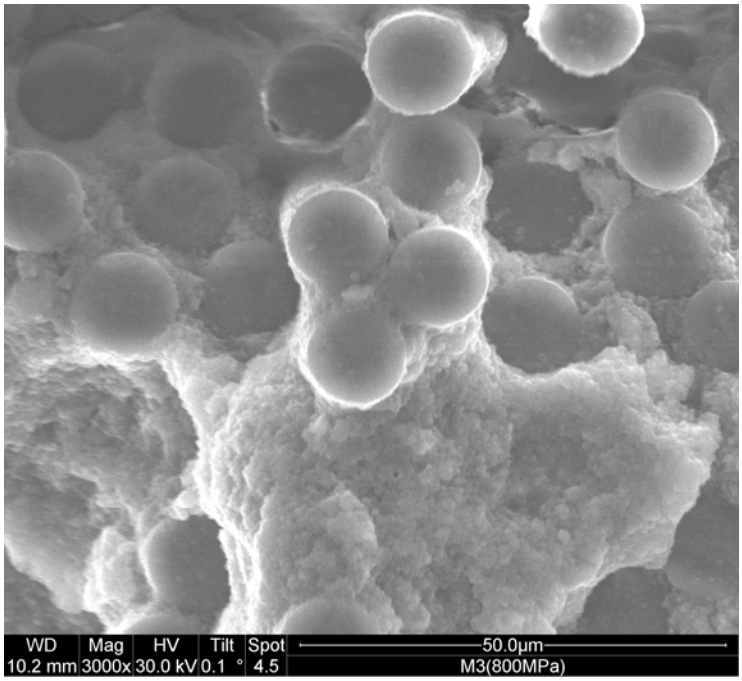

Figure 97. Specimen CG-16 (1200°C, steam, 73 MPa, 37 h), 3000X.

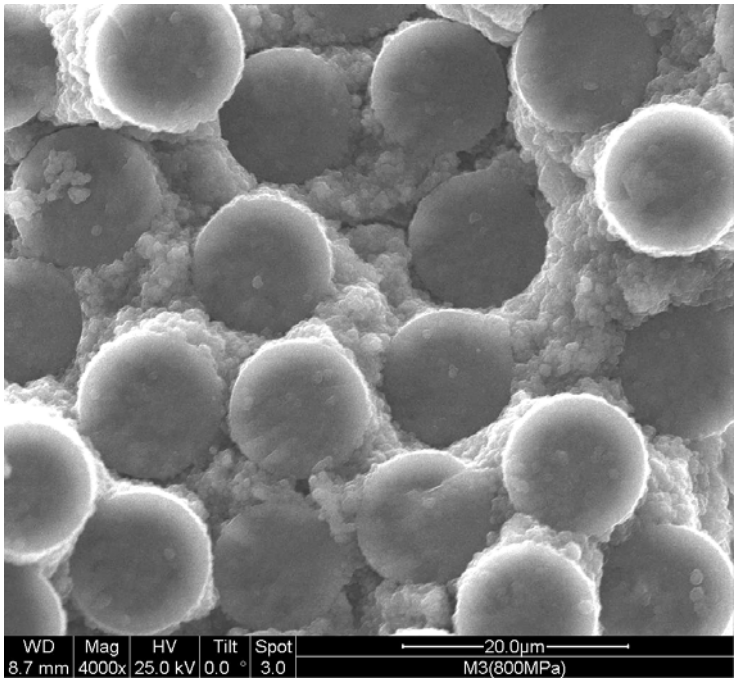

Figure 98. Specimen CG-16 (1200°C, steam, 73 MPa, 37 h), 4000X.

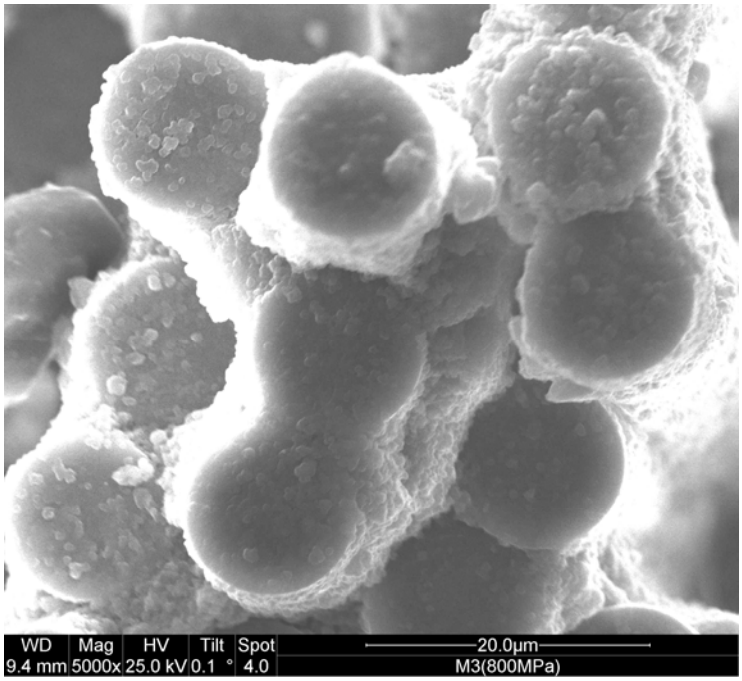

Figure 99. Specimen CG-16 (1200°C, steam, 73 MPa, 37 h), 5000X.

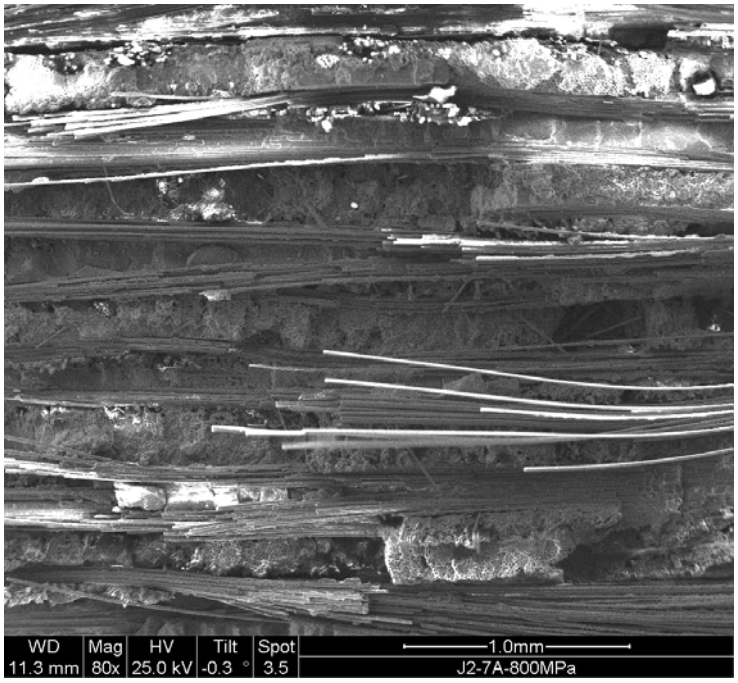

Figure 100. Specimen CG-12 (1200°C, steam, 136 MPa, 0.012 h), 80X.

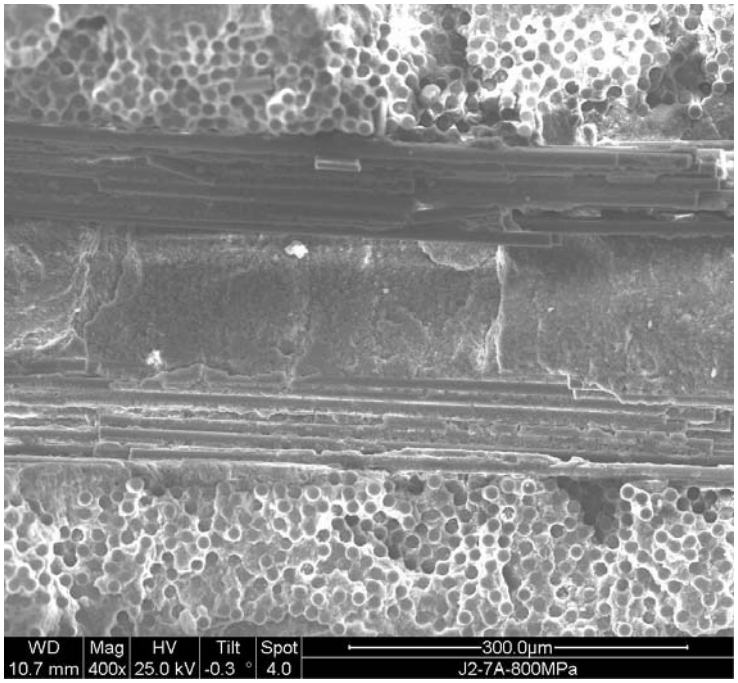

Figure 101. Specimen CG-12 (1200°C, steam, 136 MPa, 0.012 h), 400X.

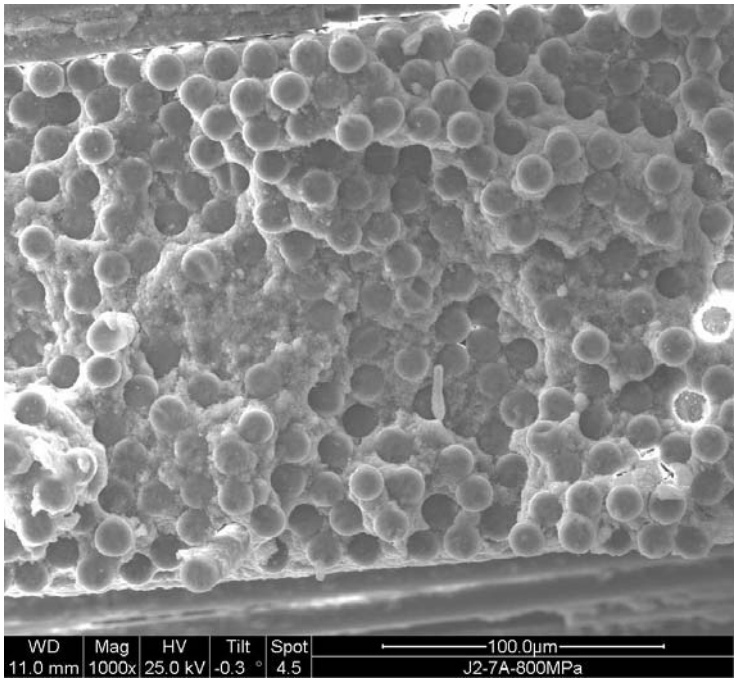

Figure 102. Specimen CG-12 (1200°C, steam, 136 MPa, 0.012 h), 1000X.

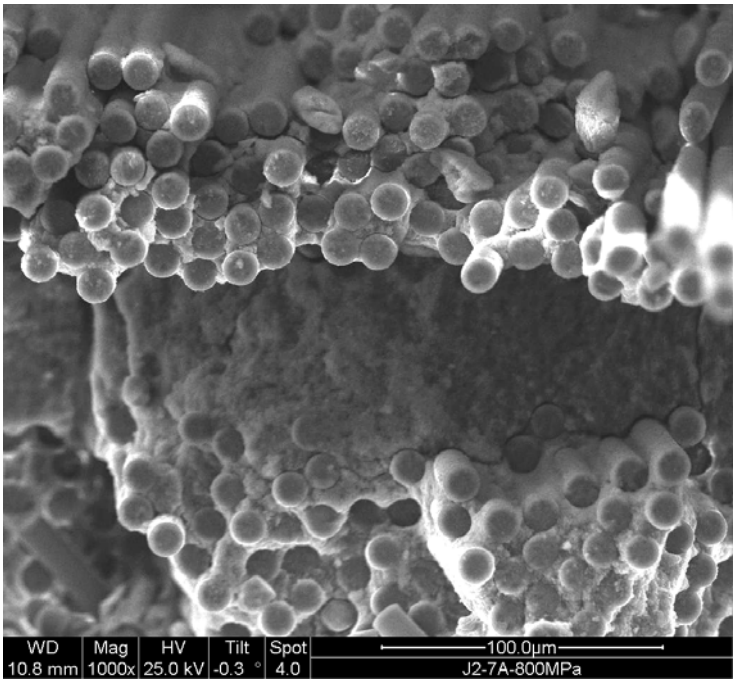

Figure 103. Specimen CG-12 (1200°C, steam, 136 MPa, 0.012 h), 1000X.

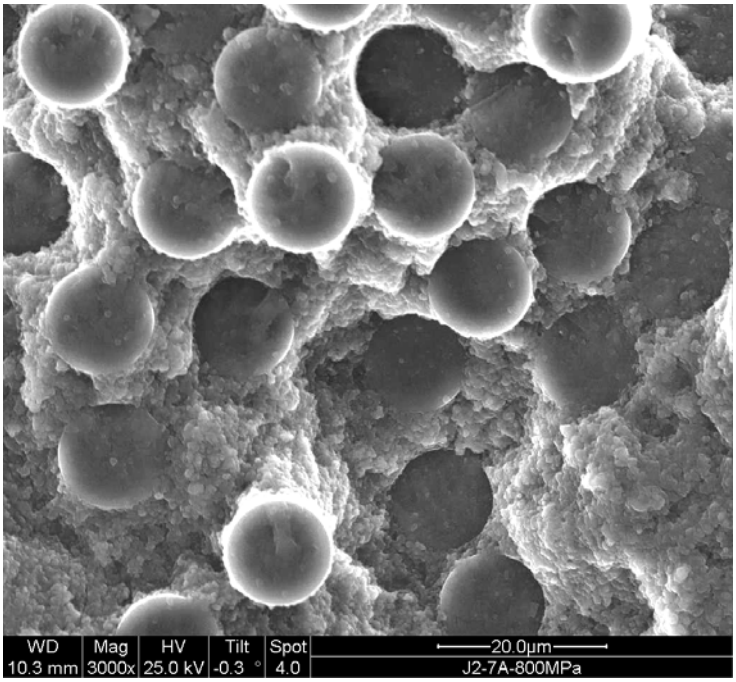

Figure 104. Specimen CG-12 (1200°C, steam, 136 MPa, 0.012 h), 3000X.

Bibliography

1. ASTM C1368. *Standard Test Method for Determination of Slow Crack Growth Parameters of Advanced Ceramics by Constant Stress-Rate Flexural Testing at Ambient Temperature*. American Society for Testing and Materials, 2001.

2. ASTM C1465. Standard Test Method for Determination of Slow Crack Growth Parameters of Advanced Ceramics by Constant Stress-Rate Flexural Testing at Elevated Temperatures. American Society for Testing and Materials, 2000.

3. Braun, Jason C. *Effects of Temperature and Environment on Creep Behavior of an Oxide-Oxide Ceramic Matrix Composite*. MS thesis, AFIT/GAE/ENY/07-M04, School of Engineering and Management, Air Force Institute of Technology (AU), Wright-Patterson AFB, OH, March 2007.

4. Braun, J.C., Ruggles-Wrenn, M.B. "Effects of Temperature and Environment on Creep Behavior of an Oxide-Oxide Ceramic Composite," 32nd *International Conference and Exposition on Advanced Ceramics and Composites Proceedings*, CACC-S1-079-2008.

5. Callister, W.D. *Materials Science and Engineering an Introduction*. New York: John Wiley & Sons Inc, 2000.

6. Chawla, K. K. *Ceramic Matrix Composites*. Boston: Kluwer Academic Publishers, 2003.

7. Choi, S.R., Bansal, N.P., Verrilli, M.J. "Delayed Failure of Ceramic Matrix Composites in Tension at Elevated Temperatures," *Journal of the European Ceramic Society,* 25:1629-36 (2005).

8. Choi, S.R., Gyekenyese, J.P. "Load-Rate Dependency of Ultimate Tensile Strength in Ceramic Matrix Composites at Elevated Temperatures," *Journal of Fatigue*, 27:503-10 (2005).

9. Daniel, I.M., Ishai, O. *Engineering Mechanics of Composite Materials*. New York: Oxford University Press, 2006.

10. Deleglise, F., Berger, M.H., Bunsell, A.R. "Microstructural evolution under load and high temperature deformation mechanisms of a mullite/alumina fibre," *Journal of the European Ceramic Society*, 22:1501-1512 (2002).

11. Evans, A.G. "Slow Crack Growth in Brittle Materials under Dynamic Loading Conditions," *Journal of Fracture Mechanics,* 10(2):251-59 (1974).

12. Fujita, H., Jefferson, G., McMeeking, R.M., Zok, F.W. "Mullite/Alumina Mixtures for Use as Porous Matrices in Oxide Fiber Composites," *Journal of the American Ceramic Society*, 87[2]:261-67 (2004).

13. Harlan, Lee B. *Creep-Rupture Behavior of an Oxide/Oxide Ceramic Matrix Composite at Elevated Temperatures in Air and Steam Environments*. MS thesis, AFIT/GAE/ENY/05-M05, School of Engineering and Management, Air Force Institute of Technology (AU), Wright-Patterson AFB, OH, March 2005.

14. Hetrick, Griffin. *Effects of Frequency and Environment on Fatigue Behavior of an Oxide-Oxide Ceramic Matrix Composite at 1200°C*. MS thesis, AFIT/GAE/ENY/07-J05, School of Engineering and Management, Air Force Institute of Technology (AU), Wright-Patterson AFB, OH, June 2006.

15. Koutsoukos, Pavlos A. *Effects of Environment on Creep Behavior of Two Oxide-Oxide Ceramic Matrix Composites at 1200°C*. MS thesis, AFIT/GAE/ENY/06-S05, School of Engineering and Management, Air Force Institute of Technology (AU), Wright-Patterson AFB, OH, September 2006.

16. Mattoni, M.A., Yang, J.Y., Levi, C.G., Zok, F.W., Zawada, L.P. "Effects of Combustor Rig Exposure on a Porous-Matrix Oxide Composite," *International Journal of Applied Ceramic Technology*, 2(2):133-140 (2005).

17. Mattoni, M.A., Yang, J.Y., Levi, C.G., Zok, F.W. "Effects of Matrix Porosity on the Mechanical Properties of a Porous-Matrix, All-Oxide Ceramic Composite," *Journal of the American Ceramic Society*, 84[11]:2594-602 (2001).

18. Mehrman, John M. Effects of Hold Times on Fatigue Behavior on Nextel™ 720/Alumina Ceramic Matrix Composite at 1200°C in Air and in Steam Environment. MS thesis, AFIT/GAE/ENY/06-M23, School of Engineering and Management, Air Force Institute of Technology (AU), Wright-Patterson AFB, OH, March 2006.

19. Parlier, M., Ritti, M.H. "State of the art and perspectives for oxide/oxide composites," *Aerospace Science and Technology*, 7:211-221 (2003).

20. Parthasarathy, T.A., Zawada, L.P., John, R., Cinibulk, M.K., Zelina, J. "Evaluation of Oxide-Oxide Composites in a Novel Combustor Wall

Application," *International Journal of Applied Ceramic Technology*, 2(2):122-132 (2005).

21. Raymer, D.P. *Aircraft Design: A Conceptual Approach*. Blacksburg Virginia: AIAA, 2006.

22. Ritter, J.E. Engineering Design and Fatigue Failure of Brittle Materials. Fracture Mechanics of Ceramics. New York: Plenum Press, 1978.

23. Ruggles-Wrenn, M.B., Koutsoukos, P., Baek, S.S. "Effects of Environment on Creep Behavior of Two Oxide-Oxide Ceramic Matrix Composites at 1200°C," *Journal of Materials Science*, In Press.

24. Ruggles-Wrenn, M.B., Mall, S., Eber, C.A., Harlan, L.B. "Effects of Steam Environment on High Temperature Behavior of Nextel™720/Alumina (N720/A) Continuous Fiber Composite," *Science Direct*, 37(11):2029-2040 (2006).

25. Siegert, Gregory T. *Effect of Environment on Creep Behavior of an Oxide/Oxide CFCC with ±45° Fiber Orientation*. MS thesis, AFIT/GAE/ENY/06-J15, School of Engineering and Management, Air Force Institute of Technology (AU), Wright-Patterson AFB, OH, June 2006.

26. Wiederhorn, S.M. "Moisture assisted Crack Growth in Ceramics," *Journal of Fracture Mechanics,* 4(2):171-77 (1968).

27. Wiederhorn, S.M., Bolz, L.H. "Stress Corrosion and Static Fatigue of Glass," *Journal of the American Ceramic Society,* 53(10):543-48 (1970).

28. Wiederhorn, S.M. *Subcritical Crack Growth in Ceramics. Fracture Mechanics of Ceramics.* New York: Plenum Press, 1974.

29. Zok, F.W. "Developments in Oxide Fiber Composites," *Journal of the American Ceramic Society*, 89[11]:3309-3324 (2006).

30. Zok, F.W., Levi, C.G., McMeeking, R.M. "Matrix-Enabled Damage Tolerance in Oxide CFFFs," AFOSR Contract F49620-02-1-0128.

31. Zok, F.W., Levi, C.G. "Mechanical Properties of Porous-Matrix Ceramic Composites," *Advanced Engineering Materials*, 3(1-2):15-23 (2001).

Vita

Captain Christopher L. Genelin graduated from Le Sueur-Henderson High School in Le Sueur, Minnesota. He entered undergraduate studies at the University of St. Thomas in St. Paul, Minnesota where he graduated with a Bachelor of Science Degree in Mechanical Engineering as well as minors in Mathematics and Aerospace Studies. He was commissioned through Detachment 410 AFROTC at the University of St. Thomas.

His first assignment was to the 28th Test and Evaluation Squadron, Eglin AFB, Florida. While stationed at Eglin, he served as a Bomber Systems Test Engineer, Special Projects Test Engineer and finally an F-16 Operational Flight Program (OFP) Flight Test Engineer. In August of 2006, he entered the Graduate School of Engineering and Management, Air Force Institute of Technology. Upon graduation, he will be stationed at the Air Force Research Laboratory Airbase Technologies Division Tyndall AFB, Florida.

REPORT DOCUMENTATION PAGE

Form Approved
OMB No. 074-0188

The public reporting burden for this collection of information is estimated to average 1 hour per response, including the time for reviewing instructions, searching existing data sources, gathering and maintaining the data needed, and completing and reviewing the collection of information. Send comments regarding this burden estimate or any other aspect of the collection of information, including suggestions for reducing this burden to Department of Defense, Washington Headquarters Services, Directorate for Information Operations and Reports (0704-0188), 1215 Jefferson Davis Highway, Suite 1204, Arlington, VA 22202-4302. Respondents should be aware that notwithstanding any other provision of law, no person shall be subject to a penalty for failing to comply with a collection of information if it does not display a currently valid OMB control number.
PLEASE DO NOT RETURN YOUR FORM TO THE ABOVE ADDRESS.

1. REPORT DATE *(DD-MM-YYYY)*	2. REPORT TYPE	3. DATES COVERED *(From – To)*
27-03-2008	Master's Thesis	June 2007 – March 2008

4. TITLE AND SUBTITLE

Effects of Environment on Creep Behavior of Nextel 720/Alumina-Mullite Ceramic Composite at 1200°C

5a. CONTRACT NUMBER

5b. GRANT NUMBER

5c. PROGRAM ELEMENT NUMBER

6. AUTHOR(S)

Genelin, Christopher L., Captain, USAF

5d. PROJECT NUMBER
2006-097

5e. TASK NUMBER

5f. WORK UNIT NUMBER

7. PERFORMING ORGANIZATION NAMES(S) AND ADDRESS(S)
Air Force Institute of Technology
Graduate School of Engineering and Management (AFIT/EN)
2950 Hobson Way, Building 640
WPAFB OH 45433-8865

8. PERFORMING ORGANIZATION REPORT NUMBER
AFIT/GAE/ENY/08-M11

9. SPONSORING/MONITORING AGENCY NAME(S) AND ADDRESS(ES)
AFRL/RZTS
Attn: Dr. Ruth Sikorski
1950 5th Street
WPAFB OH 45433-7251

10. SPONSOR/MONITOR'S ACRONYM(S)

11. SPONSOR/MONITOR'S REPORT NUMBER(S)

12. DISTRIBUTION/AVAILABILITY STATEMENT

APPROVED FOR PUBLIC RELEASE; DISTRIBUTION UNLIMITED.

13. SUPPLEMENTARY NOTES

14. ABSTRACT

The creep behavior of an oxide-oxide ceramic matrix composite (CMC) was investigated at 1200°C in laboratory air, in steam and in argon. The composite consisted of a porous alumina-mullite matrix reinforced with laminated, woven mullite/alumina (Nextel/720) fibers. The composite had no fiber coating and relied on its porous alumina/mullite matrix for flaw tolerance. Tensile stress-strain behavior was investigated and the tensile properties were measured at 1200°C in laboratory air. Tensile creep behavior of the CMCs was examined for creep stress level of 73, 91, 114 and 136 MPa. Creep run-out, set to 100 h, was achieved for stress levels ≤ 91 MPa in air. The presence of steam or argon accelerated the creep rates the N720/AM composite. Optical and scanning electron microscope (SEM) micrographs were used to examine fracture surfaces and to evaluate failure mechanisms. Fracture surfaces of the N720/AM composite were predominately planar. Limited areas of short fiber pull-out were observed for specimens tested at low creep stress levels in air.

15. SUBJECT TERMS

Ceramic Matrix Composite (CMC), Oxide-Oxide, Nextel 720, Creep, Air, Argon, Steam

16. SECURITY CLASSIFICATION OF:			17. LIMITATION OF ABSTRACT	18. NUMBER OF PAGES	19a. NAME OF RESPONSIBLE PERSON
a. REPORT	b. ABSTRACT	c. THIS PAGE			Dr. Marina B. Ruggles-Wrenn
U	U	U	UU	116	19b. TELEPHONE NUMBER *(Include area code)* (937) 255-6565, ext 4641 (marina.ruggles-wrenn@afit.edu)